COSMIC RAYS AT HIGH HELIOLATITUDES

B. HEBER[1,*] and M. S. POTGIETER[2]
[1]*Institut für Experimentelle und Angewandte Physik, Christian-Albrechts-Universität Kiel, Leibnizstr. 11, 24118 Kiel, Germany*
[2]*School of Physics, North-West University, Potchefstroom. 2520, South Africa*
*(*Author for correspondence: E-mail: heber@physik.uni-kiel.de)*

(Received 11 August 2006; Accepted in final form 24 October 2006)

Abstract. The Ulysses spacecraft has been the first to orbit the Sun over its poles and to explore the heliosphere at these high heliolatitudes. It has now completed two fast latitude scans, one at solar minimum and one at solar maximum. Since its launch in October 1990, this mission has led to several surprising discoveries concerning energetic particles, cosmic rays, Jovian electrons, the solar wind, the heliospheric magnetic field and the global features of the heliosphere. This review addresses mainly the propagation and modulation of cosmic rays and other charged particles, from both an observational and theoretical point of view, with emphasis on what has been learned from exploring the inner heliosphere to high heliolatitudes. This is done for solar minimum and maximum conditions. The review is concluded with a summary of the main scientific discoveries and insights gained so far from the Ulysses mission.

Keywords: cosmic rays, modulation, planetary particles, particle propagation, heliosphere, diffusion

1. Introduction

Cosmic ray research began in 1912 when Victor Hess measured the intensity of the ionizing radiation with an electroscope in a balloon to an altitude of about 5000 m. He discovered evidence of a very penetrating radiation, later called cosmic rays, coming from outside the atmosphere.

The systematic experimental study of cosmic rays began in the 1930s, using ground-based and balloon borne ionization chambers. In the 1950's it expanded on a much larger scale with neutron monitors, coordinated world-wide during the International Geophysical Year (IGY) in 1957. For a review, see Simpson (2000). When Parker (1958) described the solar wind, the theoretical research of cosmic rays began, stimulated by the beginning of in situ space observations that have led over four decades to important space missions, including the Ulysses mission to high heliolatitudes after its launch in 1990.

Presently, we know that at energies below several GeV the solar modulation of cosmic rays (energy spectra) becomes increasingly important. Measurements by various particle detectors have shown that the intensity varies on different time scales. The short term variations observed at Earth and at various spacecraft are

Space Science Reviews (2006) 127: 117–194
DOI: 10.1007/s11214-006-9085-y

mostly correlated with disturbances originating at the Sun e.g. coronal mass ejections (Cane, 2000) and the interaction of solar wind streams with different speeds forming corotating interaction regions beyond the Earth's orbit (Richardson, 2004). On longer time scales the cosmic ray flux is varying in anti-correlation with the 11-year and 22-year solar activity cycle. Thus, cosmic rays entering the region surrounding the Sun are increasingly modulated as they traverse space dominated by the Sun, called the heliosphere. In 2007, the 50th anniversary of the IGY will be celebrated by an internationally coordinated program, called the International Heliophysical Year (IHY 2007). The main objective will focus on advancing our understanding of the fundamental heliophysical processes, emphasizing the relevance of heliospheric research (http://www.ihy2007.org/).

Of the many interesting problems waiting to be solved within heliospheric physics, only those concerned with propagation and modulation of cosmic rays at high heliolatitudes are selected here. The main question to pose, is:

How do energetic charged particles propagate through the three-dimensional heliosphere and how do their transport and propagation vary with the solar cycle?

Problems related to this main question can be addressed according to the scale of the propagation phenomena, varying from the micro-scale through intermediate to the large-scale, which in this context is the global heliosphere. Examples are:

- What are the time, spatial and rigidity dependence of the elements of the diffusion tensor?
- What is the relative importance of these elements compared to global gradient, curvature and current sheet drifts?
- How are these diffusion coefficients (diffusion theory) related to the heliospheric plasma and magnetic properties (turbulence theory), at solar minimum and maximum activity?
- What can we learn from observations at high heliolatitude over a solar cycle about these propagation parameters, and how they affect the distribution of cosmic rays in the inner heliosphere, especially with latitude?
- Can cosmic rays and other charged energetic particles, also Jovian electrons, transport information from low to high heliolatitudes, and vice versa?
- Can cosmic ray observations at high heliolatitudes in the inner heliosphere contribute to the improved determination of local interstellar cosmic ray spectra?
- How sensitive is particle modulation in the inner heliosphere to global solar wind regimes?
- Can cosmic rays be used to effectively probe the large scale structure of the heliospheric magnetic field and its reversal during extreme solar maximum activity?

These issues are addressed in the following sections by reviewing relevant observations and the corresponding theory.

2. Extended Background

2.1. The Sun and The Solar Wind

The Sun, an "ordinary G2V star", is the largest object in the solar system and at present consists of about 70% hydrogen and 28% helium by mass, everything else amounts to less than 2%. Figure 1 displays the Sun observed in different wavelengths with instruments aboard the Solar and Heliospheric Observatory (http://soho.esac.esa.int/data/).

The photosphere, displayed in the upper left two images, is the region on the Sun that has been observed by astronomers for several centuries. Its temperature is at about 5800 K. Sunspots are "cool" regions of about 3800 K, clearly seen in the first two images, caused by the Sun's complicated magnetic field. The next images show the Sun in the light of ionized helium at 30.4 nm corresponding to temperatures of 60,000 K. This emission comes from the chromosphere which is a small region above the photosphere. The lower three images taken in the extreme ultraviolet

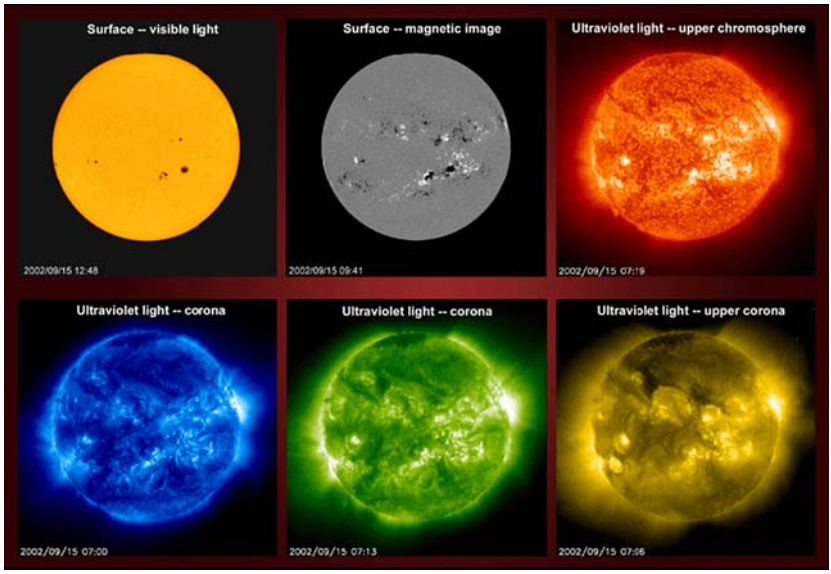

Figure 1. The Sun observed in different wavelengths (http://sohowww.estec.esa.nl/pickoftheweek/old/17sep2002/). Note the sunspots in the first panel, with corresponding features in the other panels. The last four images can be taken only from space. The dark areas at polar latitudes are called coronal holes.

display a plasma of several million Kelvin. The light is emitted from a region above the chromosphere, called the corona, that extends millions of kilometers into space. The concept of the corona's supersonic expansion, the solar wind, was described formally by Parker (1958). Its existence was confirmed with Mariner 2 in 1962 by Snyder and Neugebauer (1963).

Presently, essentially two solar wind speed regimes have been observed (Schwenn, 1990), discussed in detail in Section 2.6.3. They are the:

Fast solar wind: The observed speed is typically ∼800 km/s and the temperature is close to 10^6 K. The fluctuation of these quantities are ∼10%. The areas emitting the fast solar wind can be associated with dark areas in e.g. images of the Sun in the emission of the Fe XII line. During low solar activity the polar region of each hemisphere is covered by "coronal holes". As shown by the lower panels in Figure 1, these coronal holes can extend even to the heliographic equator and beyond.

Slow solar wind: The typical wind speeds varies around ∼400 km/s, and the temperatures fall within $(1.5 - 2) \times 10^6$ K. The slow wind is significantly more variable. Located near the heliospheric equator, above the solar streamer belt, closed magnetic fields are observed.

2.2. The Heliospheric Magnetic Field

The electric currents within the Sun generate a complex magnetic field that extends far out into the heliosphere. The hot coronal plasma and the solar wind possess an extremely high electrical conductivity, so that the concept of frozen-in magnetic field-lines is applicable. The plasma β, defined as the ratio of the thermal energy density nkT to the magnetic energy density $B^2/2\mu_0$, is an important parameter: well inside the Alfvén radius $r \ll r_A \sim 0.1$ AU ($\beta < 1$), the solar wind is not able to modify the structure of the solar magnetic field. In this region the solar magnetic field forces the solar wind to co-rotate with the Sun. Beyond the Alfvén radius $r \gg r_A$ ($\beta > 1$) the continuous flow of coronal material into interplanetary space results in the transport of the solar magnetic field into the heliosphere. Although the solar wind moves out almost radially from the Sun, the rotation of the Sun gives the magnetic field the form of an Archimedian spiral that became known as the Parker spiral (Parker, 1963). The angle ψ at a certain heliographic latitude θ is the angle between the field line and the radial direction and is given by:

$$\Gamma = \tan(\psi) = \frac{\Omega \cdot (r - r_A)}{V} \cos(\theta) . \tag{1}$$

Here Ω is the angular velocity of the Sun, r the radial distance and r_A the Alfvén radius. At the orbit of the Earth the angle between the field lines and the radial line is about 45 degrees. Typical magnetic field lines based on this simplified approach

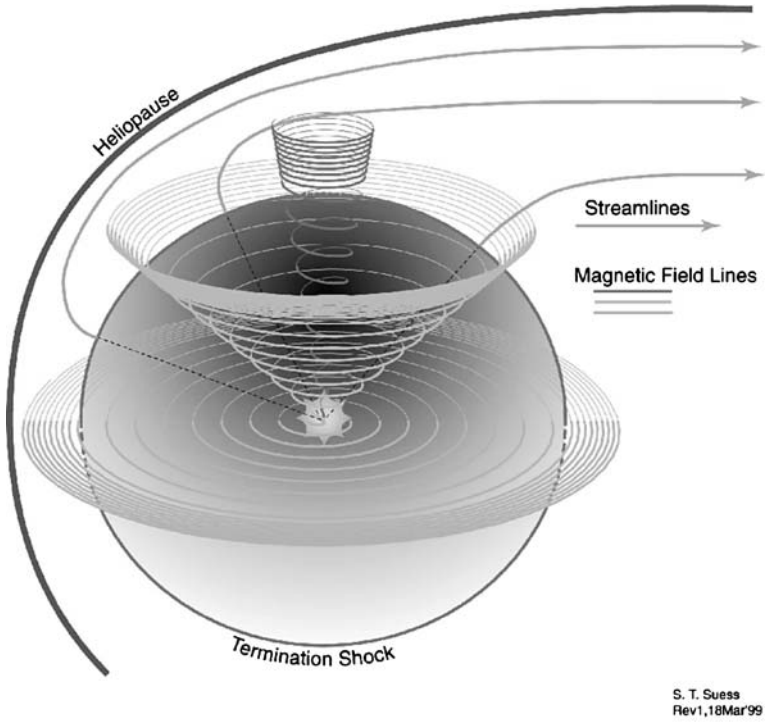

Figure 2. Illustration of the Parker spiral magnetic field lines at different heliographic latitudes without taking into account the latitudinal dependence of the solar wind at solar minimum, and shear in the outer heliosphere. (http://science.nasa.gov/ssl/pad/solar/suess/Interstellar_Probe/IMF/IMF.html).

are displayed in Figure 2. Obviously, this magnetic field does not have a component in the θ-direction. Close to the Sun the field is nearly radial, while it is tangential in the outer heliosphere:

$$\mathbf{B} = \frac{B_0}{r^2}(\mathbf{e_r} - \tan\psi\,\mathbf{e}_\varphi) \cdot [1 - 2H(\theta - \theta')] \; . \tag{2}$$

From this equation follows that the radial component and the tangential components fall off as $1/r^2$ and $1/r$, respectively. The heliospheric magnetic field originates in regions on the Sun where the magnetic field is "open"– that is, where field lines emerging from one region do not return to a conjugate region but extend virtually indefinitely into space. The direction (polarity) of the field is represented by the Heaviside step function and is in the Sun's northern hemisphere opposite to that of the field in the southern hemisphere. The polarities reverse at solar maximum with each solar cycle (see also Section 3.4).

Along the plane of the Sun's magnetic equator, the oppositely directed open field lines run anti-parallel to each other and are separated by a thin current sheet, known as the "heliospheric current sheet", when expanded into

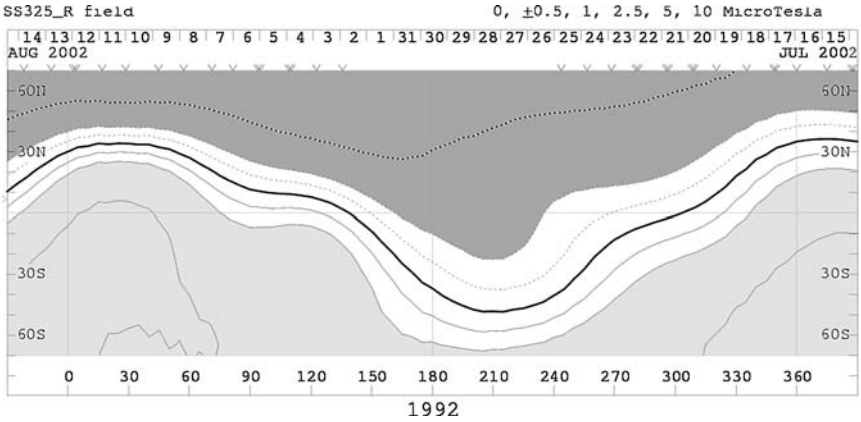

Figure 3. The magnetic source surface field at 3.25 solar radii, as calculated by Hoeksema (http://quake.Stanford.EDU:80/∼wso/). The thick line separating the inward (dark) and outward polarity is the origin of the wavy heliospheric current sheet.

interplanetary space. Figure 3 displays the computed heliospheric magnetic field at a radial distance of 3.25 solar radii from the Sun in July to August 2002 (http://quake.Stanford.EDU:80/∼wso/). The reference frame in this figure was introduced by Carrington in 1863: The mean period for a single rotation of the Sun as seen from the Earth is 27.2753 days. Carrington started to count the number of rotations of the Sun's surface since November 9, 1853. The corresponding Carrington longitude is the heliographic longitude of the Sun's disk center.

The thick line, separating the inward (dark) and outward polarities in Figure 3, is the origin of the heliospheric current sheet. It is tilted because of an offset between the Sun's rotational and magnetic axes. An additional quadrupole contribution of the solar magnetic field leads to a warped current sheet. Thus, the heliospheric current sheet has a wavy, "ballerina skirt"-like structure as it extends into interplanetary space as displayed in Figure 4 (Schwenn, 1990). Because the Earth is located sometimes above and sometimes below the rotating current sheet, it experiences regular, periodic changes in the polarity of the heliospheric magnetic field. These periods of alternating positive (away from the Sun) and negative (toward the Sun) polarity are known as magnetic sectors (see also Smith, 2001).

The shape of the current sheet usually evolves slowly – over months – as the large-scale pattern of the Sun's field changes in response to the emergence and decay of solar active regions. Figure 5 displays the evolution of the heliospheric magnetic field source surface during solar cycles 22 and 23: coronal mass ejections often disrupt the background pattern temporarily, but sometimes they cause a long-term reconfiguration of the solar source field. Near solar maximum the dipole decays, leaving a much more complicated structure with an asymmetrical polarity reversal during this period.

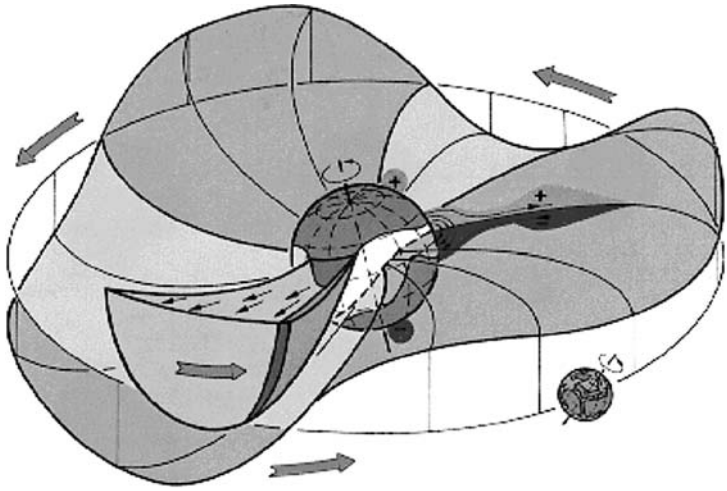

Figure 4. Illustration of the sector structure of the heliospheric magnetic field due to the inclination of the wavy heliospheric current sheet (Schwenn, 1990).

2.3. The Heliosphere

The region around the Sun, filled by the solar wind and its embedded magnetic field, is called the heliosphere. Its geometry and structure, resulting from axial-symmetric hydromagnetic models models (e.g. Fahr *et al.* 2000; Zank and Pauls, 1996 and Malama *et al.*, 2006) is displayed in Figure 6. The interaction of the supersonic solar wind with the local interstellar medium leads to a transition from supersonic to subsonic speeds at the heliospheric termination shock. Such a transition might also occur when the interstellar wind is slowed down at the heliospheric bow shock. In this picture the heliopause is defined as the boundary layer between the local interstellar medium and the solar wind. The exact geometry as well as the dimensions of the heliosphere are still uncertain, but several models have been used to compute the modulation volume: it may extend over 500 AU in the equatorial plane and to about 250 AU in the polar regions; see e.g. the review by Fichtner *et al.* (2001). The Voyager 1 spacecraft reached 94 AU in December 2004 when it encountered the relatively weak termination shock (as predicted) at a heliolatitude of $\sim 30^{\circ}$(Stone *et al.*, 2005; Burlaga *et al.*, 2005; Decker *et al.*, 2005). Hence, Voyager 1 has entered the unknown region between the termination shock and the heliopause, known as the heliosheath.

2.4. Particle Population in the Heliosphere

Within the heliosphere, energetic charged particles of different origin can be identified, as sketched in Figure 7 (Dröge, 1994). Note that the different particle populations can be grouped by their origin.

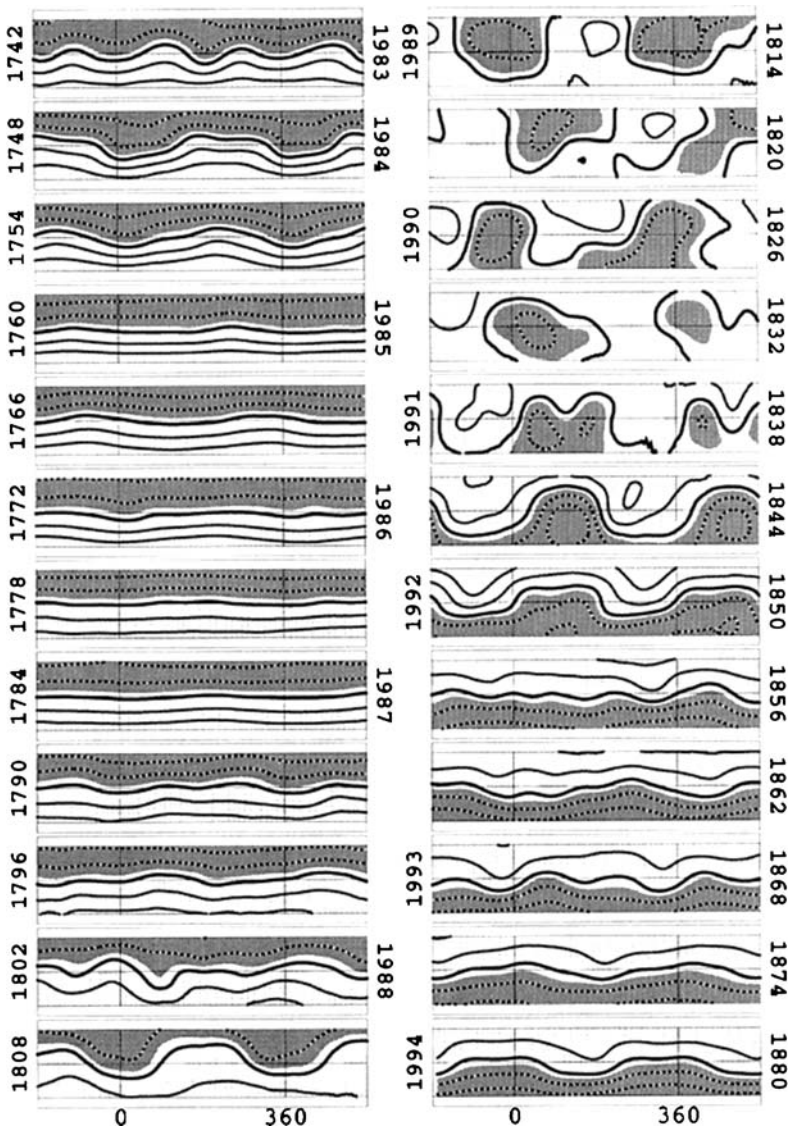

Figure 5. Evolution of the heliospheric magnetic source surface field as a function of heliolongitude and time during solar cycles 22 and 23. Carrington rotations are indicated on the left and year numbers on the right of each panel (Hoeksema, 1995).

2.4.1. *Solar Energetic Particles*

The first evidence of high-energy particles from the Sun was obtained more than 50 years ago when Forbush (1946) studied the large solar events of February and March 1942. Observation of solar energetic particle events with neutron monitors, riometers and later with detectors on balloons and spacecraft, led to extensive

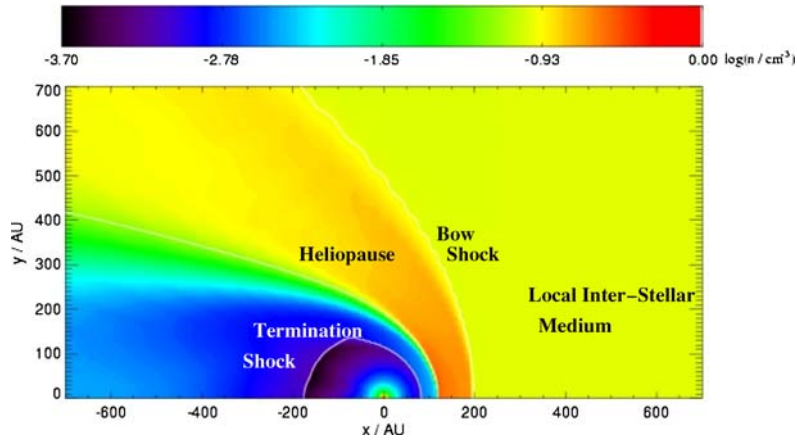

Figure 6. The structure of the heliosphere resulting from an axial symmetric model (Fahr *et al.*, 2000). The proton number density that is seen in the rest frame of the Sun equals the neutral gas number density of the local interstellar medium ($n_p = n_H = 0.1$ cm^{-3}, Scherer *et al.*, 2001).

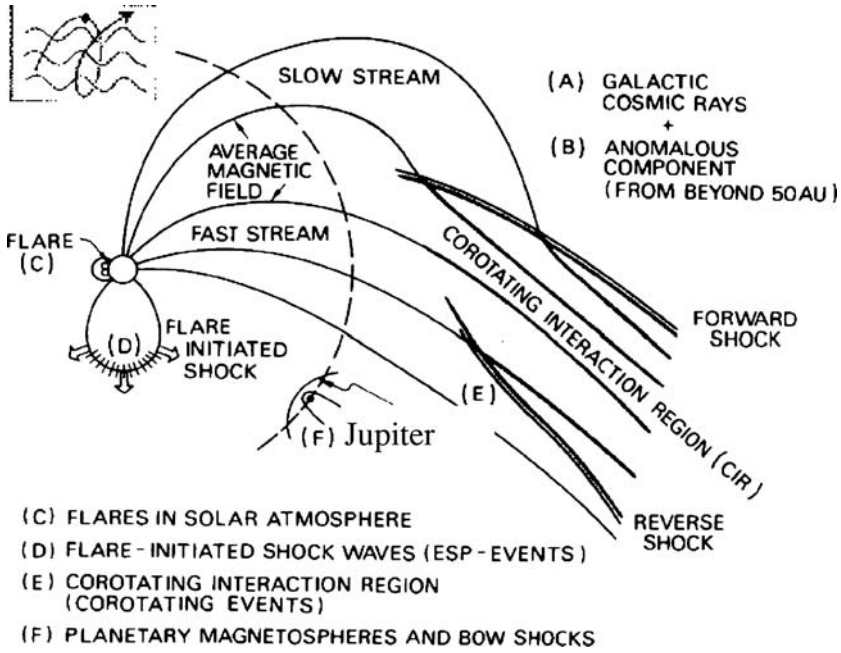

Figure 7. Sketch of different particle populations in the inner heliosphere (Kunow *et al.*, 1991).

knowledge of their time profiles, spectra and abundance. Today, it is still an open question whether the particle acceleration which occurs in spatial and temporal conjunction with a solar event, is caused by a solar flare or due to shock waves driven by coronal mass ejections (for a review see e.g. Reames, 1999).

2.4.2. *Jovian Electrons*

Historically, it became clear that Jupiter is a continuous source of MeV electrons in the solar system when Pioneer 10 came within 1 AU of the planet (Teegarden *et al.*, 1974; Simpson, 1974; Simpson *et al.*, 1974). Eighteen years later, when Ulysses approached the giant planet, the intensity-time profiles showed the same characteristics as the Pioneer measurements: the averaged intensity is increasing with decreasing distance to the planet. After the Jovian flyby by Ulysses in February 1992 a continuous decrease had been observed, indicating that Jupiter is indeed a strong source of up to about 30 MeV electrons. The location of Jupiter with respect to the structure of the heliospheric magnetic field is precisely determined and non-central. This makes Jovian electrons very interesting, and complementary to e.g. solar flare electrons for the modeling of their interplanetary propagation.

Jovian electron studies resulted in the first strong observational evidence for a diffusive transport of electrons perpendicular to the mean heliospheric magnetic field (Chenette *et al.*, 1974; Hamilton and Simpson, 1979).

Teegarden *et al.* (1974) further identified Jupiter as the source of "quiet time" electron increases previously observed at 1 AU (e.g. McDonald *et al.*, 1972, and L'Heureux *et al.*, 1972). This variability is caused mainly by varying heliospheric conditions, e.g. by corotating interaction regions (Rastoin, 1995;, Conlon and Simpson, 1977; Conlon, 1978, Fichtner *et al.*, 2001).

2.4.3. *Particles Accelerated by Interplanetary Shock Waves*

A coronal mass ejection propagating out from the Sun might drive a shock wave. Such a shock wave is able to accelerate particles. Desai *et al.*, (2003) investigated different possible sources of these particles, which may come from the solar wind distribution or suprathermal remnants from prior solar energetic particle events. Observations of energetic particles provide information about the structure of the coronal mass ejections and its topology (Richardson, 1997). Figure 8 from Cane and Lario (2005) shows as an example, the energetic particle response at 1 AU to the passage of a coronal mass ejection in September 1998.

A strong interplanetary shock (solid vertical line) locally accelerated ions to at least ∼60 MeV and electrons to at least ∼50 keV on its arrival at 1 AU. Panels [B] and [C] show the 1.9–4.8 MeV first-order parallel (A_1) and second-order (A_2) anisotropy coefficients, respectively. A_1 changes its sign at the passage of the shock indicating that these particles were flowing away from the shock. The entry of the spacecraft into the coronal mass ejection is accompanied by an abrupt decrease in the low-energy ion intensities, and the occurrence of bidirectional ion flows. After exiting from the coronal mass ejection, low-energy ions recovered to nearly similar intensities as before. The recovery of cosmic ray intensities, as shown in panel [D], was more gradual and extended for several days. A recent review on the influence of coronal mass ejections on energetic particles was given by Cane and Lario (2005).

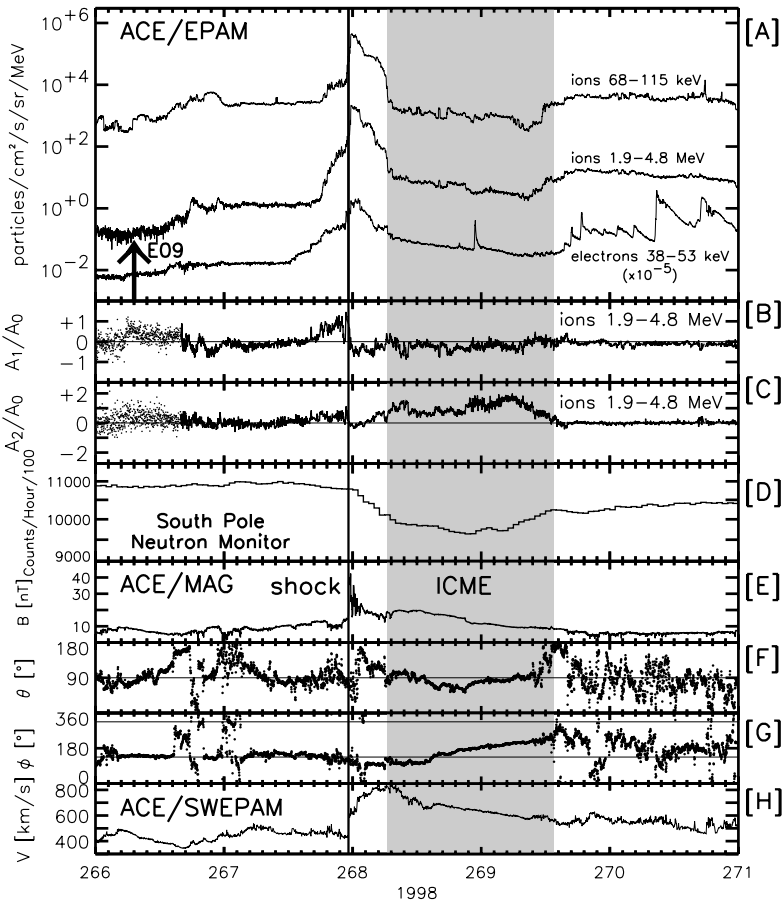

Figure 8. From top to bottom. [A] The 96-second averages of the ion and electron intensities as measured by the ACE spacecraft. [B] and [C] 1.9–4.8 MeV ion first- and second-order anisotropy. [D] Count rates measured by the South Pole cosmic ray monitor. [E-H] Magnetic field magnitude and direction, and solar wind speed measured by the ACE spacecraft (Cane and Lario, 2005).

2.4.4. *Particles Accelerated by Corotating Interaction Regions*

Corotating interaction regions result from the interaction of fast solar wind, from a polar coronal hole extending to low heliographic latitudes, with accompanying slow solar wind (see Figure 9 A). A stationary observer close to the Sun will note recurrent fast and slow wind streams. If the pressure gradient becomes sufficiently strong and the speed difference exceeds the local magnetosonic speed, shocks can be formed. This typically happens at a distance of $\gtrsim$1.5 AU. As shown in Figure 9 B, adapted from Heber *et al.* (1999), an observer at such distances (2–6 AU) close to the ecliptic will measure:

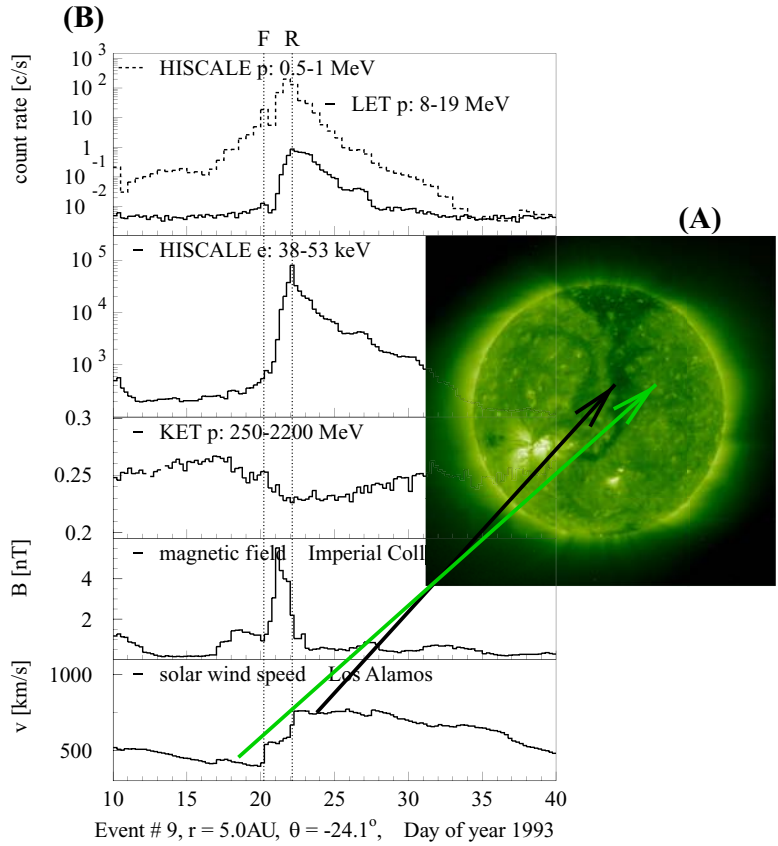

Figure 9. (A) Image at 195Å from the Extreme Ultraviolet Imager onboard the Solar and Heliospheric Observatory spacecraft. (B) From top to bottom: count rate of 0.5–1 MeV (dashed line) and 8–19 MeV protons, ∼50 keV electrons, ∼1 GeV galactic cosmic ray protons, magnetic field strength and solar wind speed (Heber *et al.*, 1999).

A forward shock, moving into the slow wind ahead, indicated by F in Figure 9. Typical signatures are step-like increases of the solar wind velocity, density, and magnetic field strength.

A stream interface, the surface along the two solar wind streams that interact with each other. Typical signatures are the change in entropy, density and abundance ratio of different solar wind elements (Wimmer-Schweingruber *et al.*, 1997).

A reverse shock, moving backward into the fast stream, indicated by R in Figure 9. Typical signatures are a step-like increase of the solar wind velocity and decrease of magnetic field strength.

Figure 9 B displays the count rates from two particle sensors (Simpson *et al.*, 1992 and Lanzerotti *et al.*, 1992), the magnetic field strength from the magnetometer

(Balogh *et al.*, 1992), and solar wind speed measurements from the solar plasma instrument (Bame *et al.*, 1992) on board Ulysses. The figure shows, from top to bottom, the count rate of several hundred keV protons, ∼10 MeV protons, ∼50 keV electrons and ∼1 GeV cosmic ray protons as well as the magnetic field strength and solar wind speed from 10-Jan-1993 to 9-Feb-1993. The dotted lines mark the times when the forward shock and reverse shock were identified (Kunow *et al.*, 1999). For accelerated electrons and protons the times of maximum are correlated with the reverse shock passage. The forward shock has a much smaller efficiency on accelerating particles, hardly any peak is seen at the forward shock for ∼50 keV electrons (Scholer *et al.*, 1999). Anti-correlated to these events recurrent galactic cosmic ray decreases occur. All ready in the 1930's, Van Allen (1998) and in the 1960's Bryant *et al.* (1963) and Fan *et al.* (1965) pointed out a correlation of recurrent cosmic ray decreases and recurrent energetic particle events with coronal holes. Reviews on the influence of corotating interaction regions on energetic particles were given by Heber *et al.* (1999) and Richardson (2004).

2.4.5. *Anomalous Cosmic Rays*

Anomalous cosmic rays have been identified by their characteristic energy spectra (Garcia-Munoz *et al.*, 1973). In Figure 10 A and B the characteristic upturn in the oxygen and helium spectra at energies of a few MeV/nucleon are shown, respectively. In contrast to helium and oxygen the 'all particle' spectrum has a positive slope at these energies, as displayed in Figure 10 A. Anomalous cosmic rays are postulated to be of heliospheric origin. The principal ideas were developed by Vasyliunas and Siscoe (1976), discussed in detail by Moraal (2001) and le Roux (2001), leading to the current paradigm as reviewed by Fichtner (2001): Neutral interstellar particles enter the heliosphere and are ionized by the interaction with the solar wind and/or solar radiation. They are picked up by the solar wind and these pickup ions are then convected out to the solar wind termination shock, where they are accelerated to cosmic ray energies. The process of anomalous cosmic ray shock acceleration was theoretically described by Pesses *et al.* (1981) and Lee and Fisk (1982). Interstellar neutral helium and the hydrogen and helium pickup ions were measured with instruments on board the AMPTE (Möbius *et al.*, 1985) and the Ulysses spacecraft (Witte *et al.*, 1993; Gloeckler *et al.*, 1993). Anomalous cosmic rays, like galactic cosmic rays, are modulated by the turbulent heliospheric magnetic field.

In apparent contradiction to many predictions, the recent Voyager 1 observations of the intensity of anomalous cosmic rays (e.g. Helium) did not peak at the termination shock, implying that the anomalous cosmic ray source may not be in the shock region local to Voyager 1. The intensities of 10 MeV electrons, anomalous cosmic rays, and galactic cosmic rays have steadily increased since late 2004 as the effects of solar modulation have decreased (Stone *et al.*, 2005).

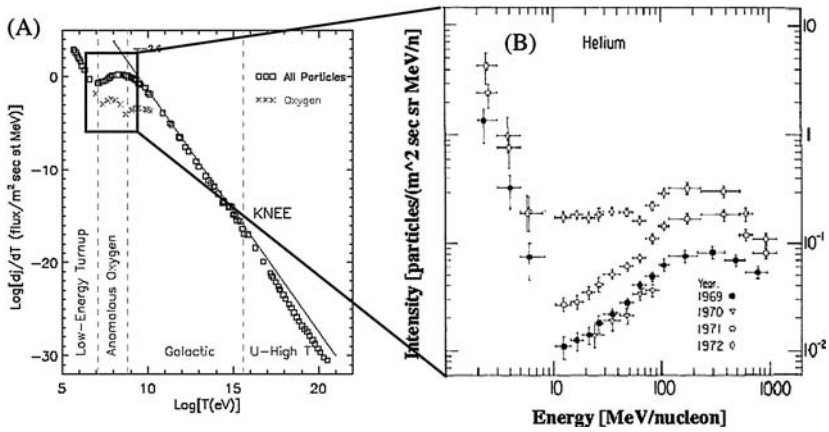

Figure 10. (A) Energy spectrum of cosmic rays measured in the vicinity of Earth, over some 10 orders of magnitude, showing a relatively featureless power-law distribution (Jokipii, 1989). However, at the lowest indicated energies the effects of solar modulation become evident for galactic and anomalous particles. (B) Helium energy spectra showing the peculiar variation between 10 to 50 MeV/nucleon of anomalous cosmic ray intensities with the solar cycle (Garcia-Munoz *et al.*, 1973).

2.4.6. *Galactic Cosmic Rays*

The remarkable feature of cosmic rays are their energy spectra, displayed in Figure 10. From $\sim 10^6$ eV to 10^{20} eV these spectra, over some 10 orders of magnitude variation in intensity, show a relatively featureless power-law distribution but with at least two 'breaks' in the power-law. At energies below a few GeV the influence of solar modulation on the galactic cosmic ray and anomalous spectra becomes important.

Figure 11 shows the proton and helium intensities at the top of the Earth atmosphere as observed during BESS balloon flights in 1997 at solar minimum, in 1998 and 1999 during the rising phase of the solar cycle, and in 2000 during solar maximum. Thus the figure shows clearly solar modulation of the proton and helium intensities.

2.5. Selected Cosmic Ray Observations

In order to put high latitude observations of cosmic rays into perspective, we will first briefly review measurements made by space probes at or near 1 AU and by the Pioneer and Voyager spacecraft in the outer heliosphere. Figure 12 displays the heliographic latitude as a function of the heliocentric distance of the two Voyager, the Pioneer 10 and the Ulysses spacecraft. The latter is discussed in detail in the next section. The inner heliosphere paths are omitted for Pioneer 10 and the Voyagers. The logarithmic scale for the radial distance was chosen to put the outer and inner heliospheric space probes in one figure, putting a strong emphasize on the inner heliosphere.

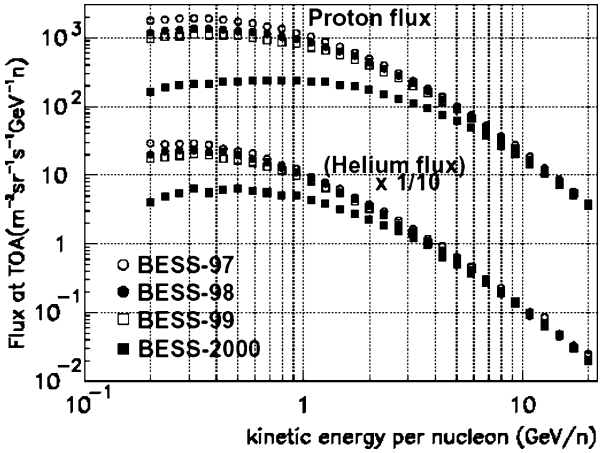

Figure 11. Proton and helium intensities at the top of the atmosphere in 1997, 1998, 1999 and 2000 measured with the BESS instrument on different balloon flights. During these four years solar activity changed from minimum to maximum conditions (Shikaze *et al.*, 2003).

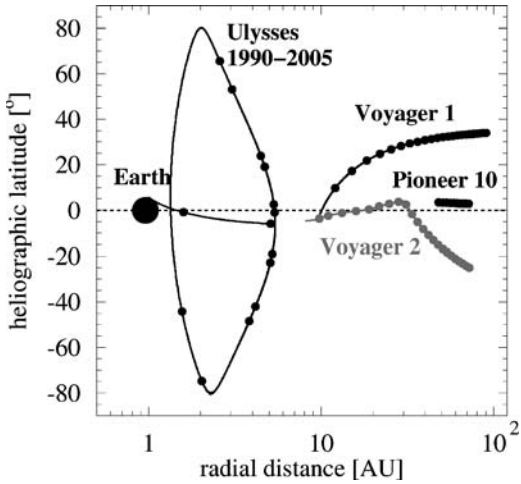

Figure 12. Ulysses, Pioneer 10, and Voyager heliographic latitude as a function of radial distance from the Sun. Marked by the shaded dot is the region close to Earth where a fleet of spacecraft is located, such as the Advanced Composition Explorer, the Solar and Heliospheric Observatory, the WIND and IMP spacecraft. Distances are plotted on a logarithmic scale.

Pioneer 10 and Pioneer 11 launched in 1972 and 1973 ran out of power in 2003 and 1995 at a distance of about 80 AU and 44.7 AU, respectively. The instruments aboard the Pioneer spacecraft provided important and very useful information on cosmic ray nuclei and electrons (McKibben *et al.*, 1973; Lopate, 1991). The two Voyager spacecraft launched in 1978 left the outer planets in the 1980's to begin their mission to the termination shock, heliosheath and interstellar space. Today,

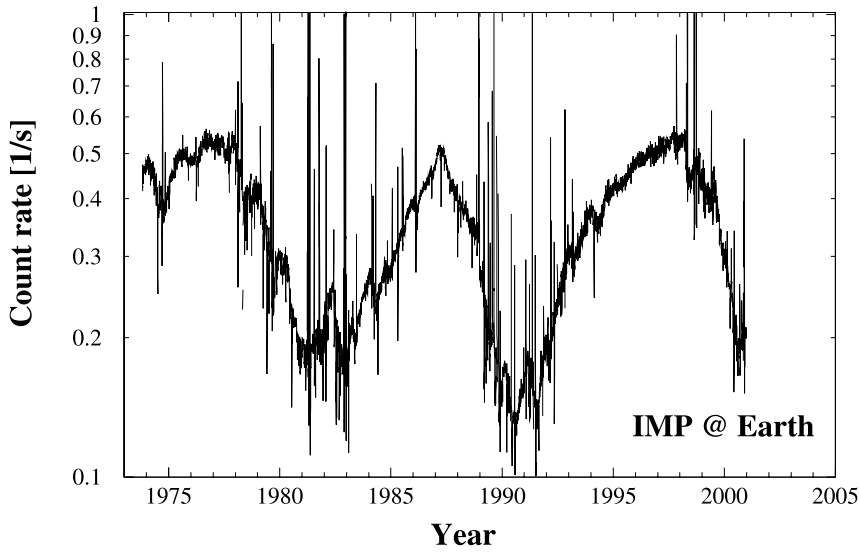

Figure 13. Count rate of >70 MeV protons measured by the University of Chicago instrument aboard the IMP 8 spacecraft at Earth. The intensity spikes are solar energetic particle events.

Voyager 1 is the most distant man made object at about 100 AU from the Sun, moving towards the nose regions of the heliosphere (the direction it is moving) at a latitude of about 30°. Marked by the shaded dot is the region close to Earth, where a fleet of spacecraft, such as the Advanced Composition Explorer, the Solar and Heliospheric Observatory, the WIND and IMP spacecraft, has been exploring the inner heliosphere using advanced instrumentations. From the figure it is evident that the decade of the 1990's was unique to investigate radial and latitudinal gradients in the inner as well as in the outer heliosphere.

Figure 13 displays the count rates of >70 MeV/n particles as measured at Earth (IMP 8) from 1973 to 2001. They have a modulation pattern with a sharp maximum in the 1980's (also in the 1960's and predicted for the 2000's) but much flatter maxima in the 1970's and 1990's. Several short term increases caused by solar energetic particle events were observed. Figure 14 is similar to Figure 13 but differs by taking quiet time counting rates into consideration. The second grey curve starting in 1978 displays the 27-day averaged count rate on Voyager 2. Like the 1 AU count rate, the Voyager count rates are modulated with the solar cycle, but with an amplitude, depending on the spacecraft distance from the Sun. This and the fact that the modulation is delayed in the outer heliosphere demonstrates that the Sun is the source of the modulation. By comparing Voyager and IMP measurements it is evident that the intensity of cosmic rays is higher in the outer heliosphere, with the modulation amplitude smaller in the outer heliosphere. The radial gradient depends on this spatial and time-dependent effect.

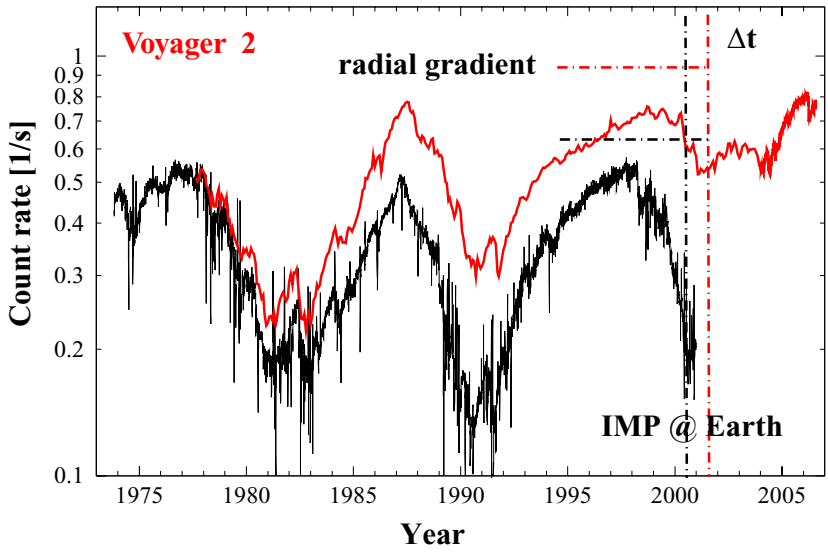

Figure 14. As an illustration of the positive radial gradient, the count rate of >70 MeV protons as measured by the Goddard Spaceflight Center instrument on board Voyager 2, is compared to the University of Chicago instrument on board IMP 8. Obviously, the intensity is always higher in the outer heliosphere.

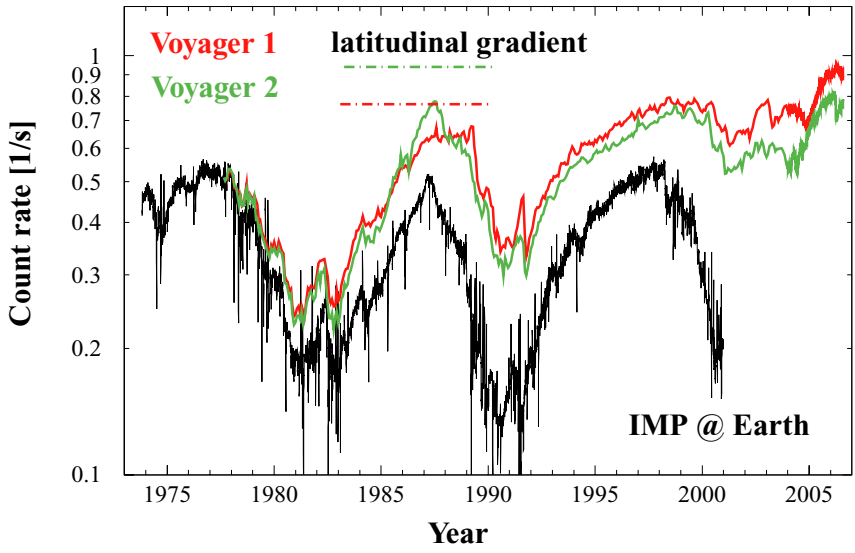

Figure 15. In comparison to Figure 13, the count rate of >70 MeV protons on board Voyager 1 is inserted. Although Voyager 1 was further away from the Sun than Voyager 2 in 1987, the intensity is higher at Voyager 2. Since Voyager 1 was at about 30°N and Voyager 2 still close to the ecliptic, the figure illustrates the existence of a negative latitudinal gradient from 1985 to 1987.

In Figure 15 observations from IMP and Voyager 1 (grey curves) are shown together with Voyager 2 measurements (dark curve). For most time periods the intensity measured at Voyager 1 is larger than at Voyager 2 and at Earth, indicating measurable positive radial gradients also in the outer heliosphere. In the solar minimum of the 1980's however the Voyager 2 intensity exceeded the intensity at Voyager 1, although Voyager 1 was further out in the heliosphere. At that time Voyager 2 was still close to the ecliptic while Voyager 1 was already at 30°N. This was interpreted by Cummings *et al.* (1987) and others as the first direct measurement of a (negative) latitudinal gradient.

Observations of Voyager 1 close to 90 AU had been recognized as the first in-situ 'signals' from the approaching heliospheric termination shock (Krimigis *et al.*, 2003; McDonald *et al.*, 2003). This interpretation was confirmed in December 2004 with the actual crossing of the shock by Voyager 1 as mentioned above.

2.6. The Out-of-Ecliptic Ulysses Mission

The main scientific goal of the joint ESA-NASA Ulysses deep-space mission was to make the first-ever measurements of the unexplored region of space above the solar poles. The Ulysses scientific investigations encompass studies of the heliospheric magnetic field, radio and plasma waves, the solar wind including its minor heavy ion constituents, solar and interplanetary energetic particles, galactic and Jovian electrons, galactic cosmic rays and the anomalous cosmic ray component.

2.6.1. *Ulysses Trajectory*

The characteristics of the Ulysses trajectory are displayed in Figure 16: Ulysses was launched towards Jupiter in October 1990 in the declining solar cycle 22. Following the fly-by of Jupiter in February 1992, the spacecraft has been traveling in an elliptical, Sun-focused orbit inclined at 80.2 degrees to the solar equator. Marked by shading in Figure 16 are the Ulysses polar passes, defined to be those periods during which the spacecraft is above 70 degrees heliographic latitude in either hemisphere. The first polar pass took place in the southern hemisphere. Beginning with 26 June 1994, Ulysses spent 132 days at southern heliographic latitudes greater than 70 degrees, reaching a maximum latitude of 80.2 degrees in mid-September. The first polar pass ended on 5 November 1994. The second (northern) polar pass took place almost exactly one year after the first, and was somewhat shorter in duration (102 days). Although the end of the second pass, on 29 September 1995, marked the completion of the first phase of the mission, Ulysses' exploratory journey continues as described below.

2.6.2. *The Space Environment of Ulysses*

The phenomena being studied with the Ulysses mission are strongly influenced by the 11-year solar activity cycle. The first phase of the mission, ending in September

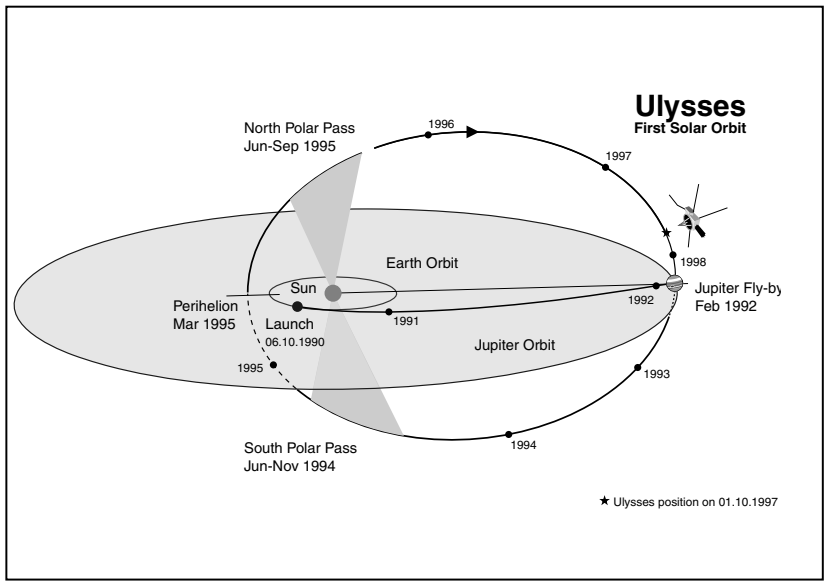

Figure 16. The first orbit of Ulysses around the Sun viewed from a perspective of 15 degrees above the ecliptic plane. The first fast latitude scan occurred from the end of 1994 to about mid-1995.

1995, extended over about half of the solar cycle. Since the orbital period of the Sun-focused, out-of-ecliptic orbit is 6.2 years, continuing the mission for another orbit made coverage of the second half of a solar activity cycle possible. The first and second polar passes occurred during the descending phase of solar cycle 22, close to solar minimum. The polar passes during the second orbit, on the other hand, happened in 2000 and 2001, close to solar maximum. Solar activity parameters, such as sunspot number, the maximum latitudinal extent of the heliospheric current sheet α, are shown in Figure 17 together with Ulysses' heliographic latitude. The upper three panels display the dipole axis direction, the quadrupole and dipole magnetic field strength, compiled from the Wilcox Solar Observatory model with a magnetic source surface at 2.5 solar radii (Hoeksema, 1995).

The four polar passes of Ulysses from Table. I are indicated by the vertical lines. The two solar minimum polar passes occurred during low sunspot number, characterized by a strong dipole component and the dipole axis at low latitudes. The heliospheric current sheet was almost flat at the heliographic equator.

As solar activity increased, the quadrupole magnetic strength increased and the dipole axis slowly tilted away from the Sun's rotation axis, so that the heliospheric current sheet became highly inclined. During the second southern polar pass the quadrupole strength was stronger than the dipolar component. From these calculations one would have expected that Ulysses should have observed a unipolar field. This, however, was not measured (Jones *et al.*, 2003). A year later, when

TABLE I
Key dates of the Ulysses mission.

Event		Year	Month	Day
Launch		1990	10	6
Jupiter flyby		1992	02	08
1st polar pass (S)				
	Start	1994	06	26
	Max. latitude (80.2 S)	1994	09	13
	End	1994	11	05
Perihelion (1.3 AU)		1995	03	12
2nd polar pass (N)				
	Start	1995	06	19
	Max. latitude (80.2 N)	1995	07	31
	End	1995	09	29
Start of 2nd solar orbit		1995	10	01
Aphelion (5.4 AU)		1998	04	17
3rd polar pass (S)				
	Start	2000	09	08
	Max. latitude (80.2 S)	2000	11	27
	End	2001	01	16
Perihelion (1.3 AU)		2001	05	26
4th polar pass (N)				
	Start	2001	09	03
	Max. latitude (80.2 N)	2001	10	13
	End	2001	12	12
Jupiter close approach 2 (0.8 AU)		2004	02	04
Aphelion (5.4 AU)		2004	06	30
5th polar pass (S)				
	Start	2006	11	17
	Max. latitude (80.2°)	2007	02	07
	End	2007	04	03
Perihelion		2007	08	18
6th polar pass (N)				
	Start	2007	11	30
	Max. latitude (80.2°)	2008	01	12
	End	2008	03	15

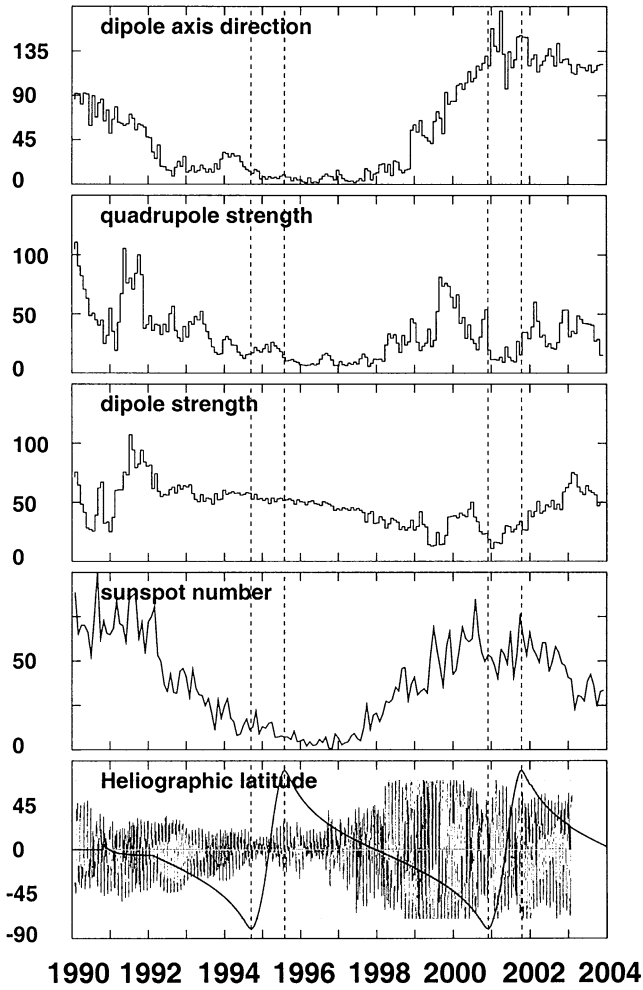

Figure 17. From top to bottom: As a function of time, the latitude of the dipole axis direction, the quadrupole and dipole strength from the Wilcox Solar Observatory source surface model, as well as sunspot number, tilt angle and Ulysses' heliographic latitude (solid line) from launch to the end of 2004 (Sanderson, 2005).

Ulysses was at northern polar latitudes the situation was different. While the tilt of the heliospheric current sheet stayed high, the dipole configuration became the important component.

2.6.3. *The Solar Wind in Three-Dimensions*

The latitudinal and radial dependence of the solar wind velocity around solar minimum and maximum, displayed in Figure 18, is by now well-established (see, e.g.,

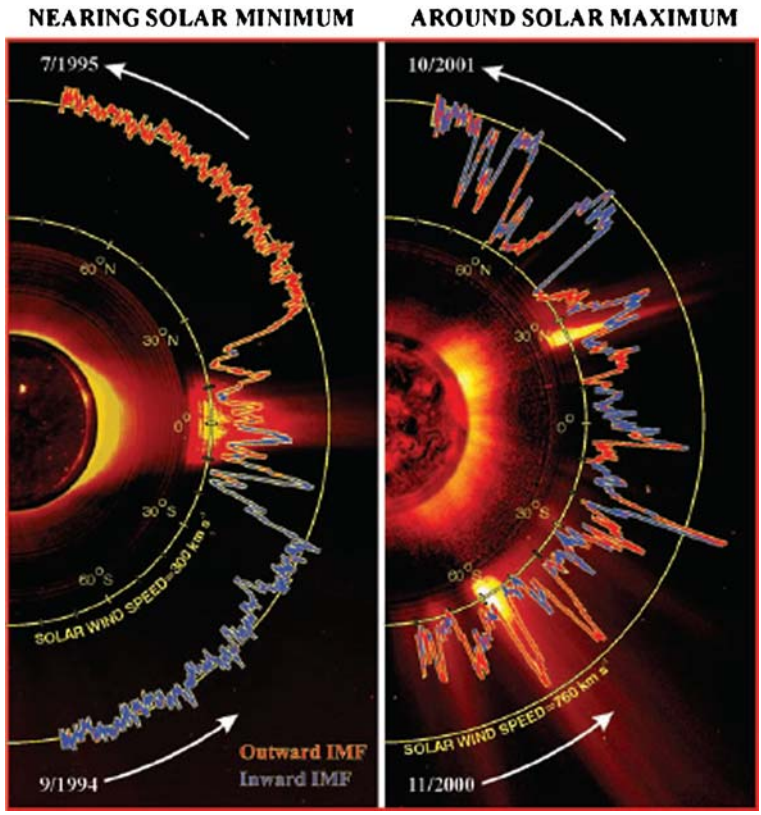

Figure 18. Ulysses solar wind observations during two separate polar orbits of the Sun, six years apart. On the left, the data show the Sun around solar minimum. The data on the right, collected near solar maximum, show that the solar wind speed is slower but more 'chaotic', with fluctuating magnetic fields (McComas *et al.*, 2002).

McComas *et al.*, 2001). The Ulysses spacecraft completed one orbit through the inner solar system during which it had passed over the Sun's south and north poles. Measurements of the solar wind speed and its composition have provided us with a new view of the solar wind.

At solar minimum (Figure 18, left hand side) the solar wind velocity is not uniform. Although it is always directed away from the Sun, it changes speed and carries with it disturbances and interacting regions. The solar wind speed is high (800 km/s) above coronal holes and low (300 km/s) above the streamer belt. During most of the solar cycle, the solar wind at high latitudes is almost uniformly fast, while lower latitudes emit a wind of varying speed.

At solar maximum, the data (Figure 18, right hand side) exhibit a remarkably different and more complicated solar wind structure than observed throughout

most of the solar cycle. The polar solar wind speed at maximum is slower but much gustier than at other times (McComas *et al.*, 2001).

3. Particle Propagation and Modulation

Particles moving along magnetic field lines undergo pitch angle scattering caused by magnetic field fluctuations (see inset of Figure 7). This process appears to operate in many astrophysical environments and is often assumed to be the basic physical process behind diffusive propagation of cosmic ray particles in space plasmas (Dröge, 2000, and references therein). The diffusion tensor has elements (components) parallel and perpendicular to the mean heliospheric magnetic field. A typical power spectrum of the variations is displayed in Figure 19. From magnetometer and plasma wave observations in the solar wind (Denskat *et al.*, 1983) it became evident that the magnetic fluctuations typically exhibit a dissipation range with a steepening of the spectrum above the ion gyrofrequency. For such magnetic field fluctuations, quasi-linear theory predicts larger mean free paths, than observed (Dröge, 2000). This problem can be solved when assuming that a significant fraction of the total wave power cannot lead to particle scattering (Dröge, 2003). Because of gradients and curvatures in the magnetic field, gradient, curvature and current sheet drifts play a fundamental role in particle propagation too.

At energies below a few GeV/nucleon the influence of solar modulation on the galactic cosmic ray energy spectra becomes important. The variation of several GeV particles with the solar cycle is shown in Figure 20. It displays in the lower

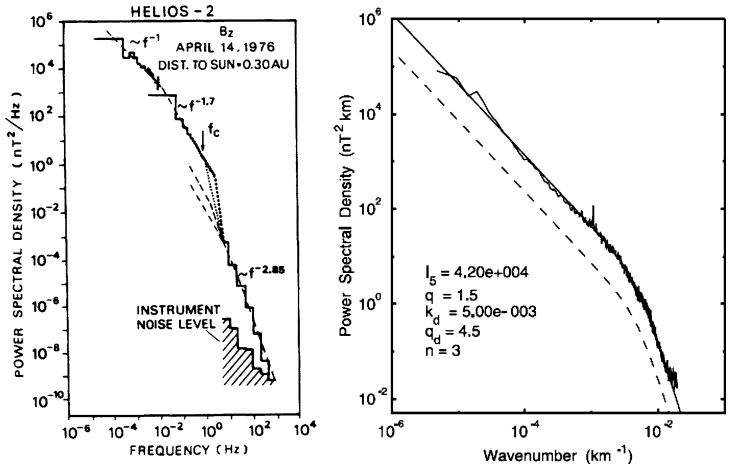

Figure 19. Left: Power spectrum of the heliospheric magnetic field observed by Helios 2 at 0.33 AU from the Sun (Denskat *et al.*, 1983). Right: Power spectrum of the magnetic field normal component in the radial tangential normal system (Dröge, 2003).

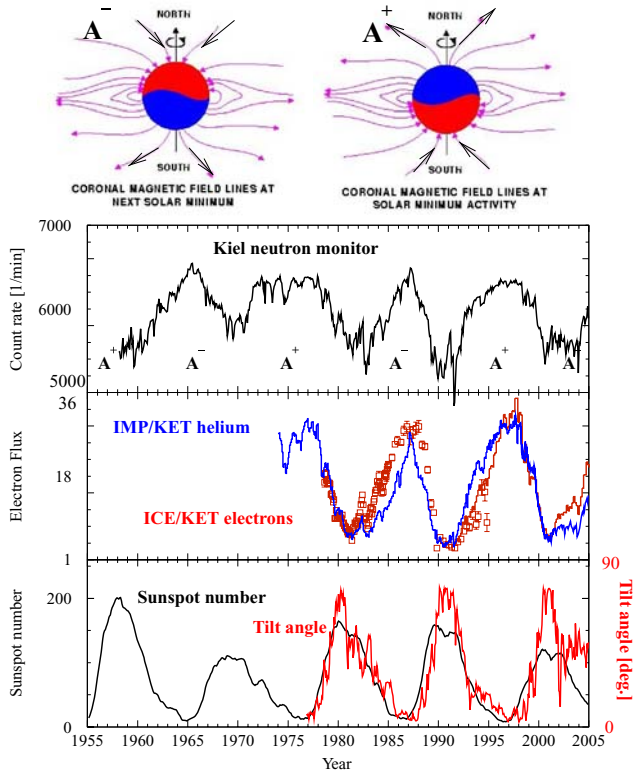

Figure 20. Solar modulation of galactic cosmic rays of both charge signs, monthly sunspot number and tilt angle α of the heliospheric current sheet. Marked by A^+ (A^-) are times when the solar magnetic field is directed inward (outward) from the Sun in the northern polar and outward (inward) in the southern polar region, as sketched on top.

panel the monthly sunspot number (black line) and the evolution of the maximum latitudinal extension of the heliospheric current sheet (tilt angle, grey line). The upper two panels give the cosmic ray variation close to Earth at neutron monitor energies (Kiel neutron monitor, http://www.ieap.uni-kiel.de) and of galactic cosmic ray helium and electrons, measured by the IMP, ICE and Ulysses spacecraft. From the figure three characteristic features of the cosmic ray intensity history are evident:

1. The cosmic ray flux is varying in anti-correlation with the 11-year solar activity cycle, leading to the conclusion that galactic cosmic rays are modulated as they traverse the heliosphere.
2. In the 1960's and 1980's (A^-), when the solar magnetic field is pointing towards the Sun in the northern hemisphere, the time profiles of positively charged particles are peaked, whereas they are more or less flat in the 1970's and 1990's (A^+) during the opposite solar magnetic epoch. The electrons, however, have the

opposite behavior showing clearly the close correlation with the 22 year solar magnetic cycle.

3. Cosmic ray modulation during increased solar activity is characterized by several large steps that are easily recognized from observations at Earth and beyond, as shown in Figure 20. These large steps are correlated with long-lasting intense magnetic fields in the outer heliosphere, called global merged interaction regions (Burlaga *et al.*, 1993).

3.1. The Transport Equation

The transport of cosmic rays in the heliosphere can be described by Parker's (1965) transport equation as discussed in detail by Potgieter (1998): If $f(\mathbf{r}, P, t)$ is the cosmic ray distribution function with respect to the particle rigidity P, then the cosmic ray variation with time t and position $\mathbf{r}$ is given by:

$$\frac{\partial f}{\partial t} = -\Big(\underbrace{\mathbf{V}}_{a} + \underbrace{\langle \mathbf{v}_D \rangle}_{d} \Big) \cdot \nabla f + \underbrace{\nabla \cdot (\kappa_{(s)} \cdot \nabla f)}_{c} + \underbrace{\frac{1}{3}(\nabla \cdot \mathbf{V}) \frac{\partial f}{\partial \ln P}}_{b} + \underbrace{Q}_{e}, \tag{3}$$

where terms on the right-hand side represent the following mechanisms:

a. Outward convection caused by the radially directed solar wind velocity $\mathbf{V}$.
b. Adiabatic deceleration or acceleration depending on the sign of the divergence of $\mathbf{V}$.
c. Diffusion caused by the irregular heliospheric magnetic field. The symmetric part of the diffusion tensor $\kappa_{(s)}$ consists of a diffusion coefficient parallel to the background magnetic field ($\kappa_{\parallel}$) and a perpendicular diffusion coefficient for the radial ($\kappa_{\perp r}$) and polar direction ($\kappa_{\perp \theta}$) as displayed in the left hand side of Figure 21. From this figure follows that the value of the three diffusion coefficients depend on one's position in the heliosphere, also on rigidity (or energy) and on solar activity (time).
d. Gradient and curvature drifts in the global heliospheric magnetic field. The averaged guiding center drift velocity ($\langle \mathbf{v}_D \rangle$) for a near isotropic galactic cosmic ray distribution is given by:

$$\langle \mathbf{v}_D \rangle = \frac{P v}{3} \nabla \times \frac{\mathbf{B}}{B^2},$$

where P and v are the particle rigidity and speed, and B is the magnitude of the background heliospheric magnetic field $\mathbf{B}$. With the solar magnetic field directed outward from the Sun in the northern polar region and inward in the southern polar region, as displayed in Figure 21 (right hand side), positively charged

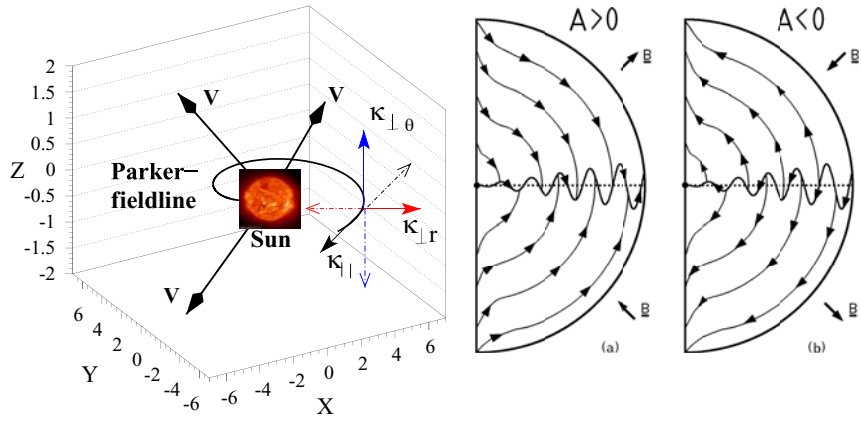

Figure 21. The different elements of the diffusion tensor with respect to the Parker-spiral (left). The arrows V indicate the radially expanding solar wind velocity. The global drift pattern of positively charged particles in an A > 0 and A < 0-solar magnetic epoch, together with a wavy current sheet, are shown in the right panels.

particles are expected to drift into the inner heliosphere over the solar poles and out along the heliospheric current sheet. This period is known as the A > 0 magnetic polarity epoch (cf. Figure 20). In this phase of the solar cycle the drift pattern of negatively charged particles is in the opposite direction. The intensity of negatively charged particles is expected to depend on the latitudinal excursion of the heliospheric current sheet in an A > 0 cycle, whereas the intensity of positively charged particles should vary significantly less (Potgieter and le Roux, 1992). The situation reverses in an A < 0 magnetic cycle (Figure 21b).

e. This part represents possible additional sources e.g., for anomalous cosmic ray particles being accelerated at the solar wind termination or a source of Jovian electrons which can make a major contribution to the particle distribution in the inner heliosphere relatively close to the ecliptic at energies of a few-MeV (Ferreira *et al.*, 2001c). The location of the Jovian magnetosphere with respect to the mean heliospheric magnetic field provides therefore ideal test particles to study heliospheric particle propagation.

Rewriting Equation (3) in heliocentric spherical coordinates (r, θ, ϕ) gives:

$$\frac{\partial f}{\partial t} = \left[\frac{1}{r^2}\frac{\partial}{\partial r}(r^2 K_{rr}) + \frac{1}{r\sin\theta}\frac{\partial}{\partial\theta}(K_{\theta r}\sin\theta) + \frac{1}{r\sin\theta}\frac{\partial K_{\phi r}}{\partial\phi} - V\right]\frac{\partial f}{\partial r}$$
$$+\left[\frac{1}{r^2}\frac{\partial}{\partial r}(rK_{r\theta}) + \frac{1}{r^2\sin\theta}\frac{\partial}{\partial\theta}(K_{\theta\theta}\sin\theta) + \frac{1}{r^2\sin\theta}\frac{\partial K_{\phi\theta}}{\partial\phi}\right]\frac{\partial f}{\partial\theta}$$
$$+\left[\frac{1}{r^2\sin\theta}\frac{\partial}{\partial r}(rK_{r\phi}) + \frac{1}{r^2\sin\theta}\frac{\partial K_{\theta\phi}}{\partial\theta} + \frac{1}{r^2\sin^2\theta}\frac{\partial K_{\phi\phi}}{\partial\phi}\right]\frac{\partial f}{\partial\phi}$$

$$+ K_{rr}\frac{\partial^2 f}{\partial r^2} + \frac{K_{\theta\theta}}{r^2}\frac{\partial^2 f}{\partial \theta^2} + \frac{K_{\phi\phi}}{r^2 \sin^2\theta}\frac{\partial^2 f}{\partial \phi^2} + \frac{2K_{r\phi}}{r\sin\theta}\frac{\partial^2 f}{\partial r \partial \phi}$$
$$+ \frac{1}{3r^2}\frac{\partial}{\partial r}(r^2 V)\frac{\partial f}{\partial \ln p} + Q_{\text{source}}(r, \theta, \phi, p, t)\,. \tag{4}$$

The diffusion tensor can then be written as:

$$\begin{bmatrix} K_{rr} & K_{r\theta} & K_{r\phi} \\ K_{\theta r} & K_{\theta\theta} & K_{\theta\phi} \\ K_{\phi r} & K_{\phi\theta} & K_{\phi\phi} \end{bmatrix}$$
$$= \begin{bmatrix} \kappa_\parallel \cos^2\psi + \kappa_{\perp r}\sin^2\psi & -\kappa_A \sin\psi & \left(\kappa_{\perp r} - \kappa_\parallel\right)\cos\psi\sin\psi \\ \kappa_A \sin\psi & \kappa_{\perp\theta} & \kappa_A \cos\psi \\ \left(\kappa_{\perp r} - \kappa_\parallel\right)\cos\psi\sin\psi & -\kappa_A\cos\psi & \kappa_\parallel \sin^2\psi + \kappa_{\perp r}\cos^2\psi \end{bmatrix}, \tag{5}$$

with ψ the spiral angle of the magnetic field with respect to the radial direction.

The components of the gradient and curvature drift velocity are:

$$\langle \mathbf{v}_d \rangle_r = -\frac{\mathrm{A}}{r\sin\theta}\frac{\partial}{\partial\theta}(\sin\theta K_{\theta r}),$$
$$\langle \mathbf{v}_d \rangle_\theta = -\frac{\mathrm{A}}{r}\left[\frac{1}{\sin\theta}\frac{\partial}{\partial\phi}(K_{\phi\theta}) + \frac{\partial}{\partial r}(rK_{r\theta})\right],$$
$$\langle \mathbf{v}_d \rangle_\phi = -\frac{\mathrm{A}}{r}\frac{\partial}{\partial\theta}(K_{\theta\phi}), \tag{6}$$

with $\mathrm{A} = sign(qB)$ determining the drift direction of particles with charge q in the heliosphere, with magnetic field B, as shown in Figure 21.

The present understanding of the mechanisms of global modulation in the heliosphere, as described above is generally believed to be essentially correct (see the review by (Fisk, 1999)). However, the main obstacle in solving Equation (3) is insufficient knowledge of the spatial, rigidity and temporal dependence of the diffusion coefficients, as well as some other features such as the magnetic field turbulence and structure at high latitudes, the size and geometry of heliosphere, and the values of the local interstellar spectra for different cosmic ray species.

3.2. Modulation Models

Significant progress has been made over the past three decades solving the transport equation with increasing sophistication and complexity. In the late 1960's the force-field approximation was developed (Gleeson and Axford, 1967) that is still in use today. For a recent appreciation of this approach, see Caballero-Lopez and Moraal, (2004). Fisk (1976, 1979) developed the first numerical solution of the transport equation by assuming a steady-state and spherical symmetry. He then included

a polar angle dependence to form an axisymmetric (spatially two-dimensional, 2D) steady-state model, the first important step in the theoretical study of cosmic ray modulation at high heliolatitudes. Moraal *et al.* (1979) and Jokipii and Kopriva (1979) took the second step when they separately developed 2D steady-state models including gradient and curvature drifts for a flat current sheet. The first 2D models to emulate the waviness of the current sheet were developed by Potgieter and Moraal (1985) and Burger and Potgieter (1989), and improved by Hattingh and Burger (1995). These models emphasized the importance of global particle drifts and how it changes the modulation at high latitudes. A third forward step came when Kóta and Jokipii (1983) developed a three-dimensional (3D) steady-state model including drifts and a full wavy current sheet, improved by Hattingh (1998). Another aspect of the study of high latitude modulation became possible when Fichtner *et al.* (2000) and Ferreira *et al.* (2001c) independently developed 3D steady-state models including the Jovian magnetosphere as a source of low-energy electrons. With these models perpendicular diffusion in the polar direction could be studied in detail.

The first 1D time-dependent model was developed by Perko and Fisk (1983), later extended to include drifts and other off-ecliptic aspects by le Roux and Potgieter (1995) enabling the study of long-term cosmic ray modulation effects and the effect of outwards propagating merged interaction regions. Kota and Jokipii (1991) developed a model that could be used to study corotating interaction regions which proved to be very useful in understanding recurrent modulation at high latitudes.

Another important step in modulation modeling came with the inclusion of the solar wind termination shock in models (Jokipii, 1986) which gave a natural explanation to several observed features of the anomalous component; see e.g., Potgieter and Moraal (1988), Potgieter (1989), Steenberg and Moraal (1996), and Langner *et al.* (2003). These models have also increased in complexity e.g., including the geometrical elongation of the heliosphere by Fichtner *et al.* (1996), and stochastic approaches (Zhang, 1999). However, the practical utilization of a 3D time-dependent termination shock model is still beyond the capabilities of current desktop computers.

Self-consistent, mostly hydrodynamic models of the heliosphere and the heliospheric interface with the interstellar medium have also been done e.g., Washimi and Tanaka (1996), Zank and Pauls (1996), Florinski *et al.* (2003), Zank and Müller (2003), Scherer and Fahr (2003), Malama *et al.* (2006) and references therein. However, these models cannot be primarily devoted to cosmic ray modulation studies and must be used in conjuction with transport models in order to obtain cosmic ray spectra and gradients at all latitudes (Ferreira *et al.*, 2004b; Scherer and Ferreira, 2005). Reviews of the hydrodynamically modeled heliosphere were given by Zank (1999), Fahr (2004), and Fichtner (2005); for magnetohydrodynamic modeling, see e.g. Pogorelov *et al.* (2006).

3.3. The Diffusion Tensor from Fundamental Principles

It was mentioned above that the spatial and rigidity dependence of the elements of the diffusion tensor are not well-known and this is at present one of the major handicaps in numerical modeling. Serious efforts are being made however to improve the situation by working from three directions. (1) Determining the diffusion coefficients fundamentally from basic micro-physics theory (turbulence theory, etc.). (2) Partly based on fundamental theory but constraint by cosmic ray observations; (3) Primarily based on compatibility studies between modulation models and cosmic ray observations, see e.g. Burger (2000). The latter two approaches have already contributed much in limiting the values of the various diffusion coefficients. This is certainly a result of the rather comprehensive numerical models that have been developed and applied over the past 20 years as discussed above, and also the excellent cosmic ray observations from a unique combination of spacecraft in the heliosphere, see Heber *et al.* (1997), McKibben *et al.* (1998), and McDonald (1998). The first approach is more difficult, but progress is been made to come to an 'ab initio' formulation of cosmic ray modulation in the heliosphere, that is one in which the diffusion coefficients are determined on the basis of scattering theory and the underlaying fluctuation parameters are computed from plasma theory and known features of the heliospheric magnetic field. These results must eventually be compared to cosmic ray observations, for example, from the Voyager (Fujii and McDonald, 2001) and Ulysses (Heber *et al.*, 1996a) spacecraft to establish how good the different approaches are.

Scattering theory involves turbulence parameters so that one needs to understand how plasma turbulence evolves throughout the heliosphere. Even in the simplest formalisms, this would involve the specification of the turbulence energy density and a correlation scale length in the heliosphere, also at high latitudes. While in-situ data at 1 AU can be used as boundary conditions, it is necessary to understand the evolution in the heliosphere. As discussed by Parhi *et al.* (2003), developing such an 'ab inition' formulation faces some major challenges: (1) A satisfactory theory of diffusion parallel and perpendicular (radial and latitudinal) to the large-scale magnetic field. Theoretical formulations of diffusion coefficients by e.g. Jokipii and Parker (1969), Forman *et al.* (1974), Bieber and Matthaeus (1997), and numerical simulations by e.g. Giacalone and Jokipii (1999), Mace *et al.* (2000) are not yet converging. (2) Perpendicular diffusion in two-component slab/2D turbulence depends critically on an outer scale termed the 'ultra scale' about which little observational information exists, even in the ecliptic plane. (3) The radial and latitudinal variation of the parallel and perpendicular diffusion coefficients depend on the corresponding variation of the correlation length which is also poorly understood. (4) A formal description of realistic global gradient and curvature drifts over a complete 11-year cycle from advanced fundamental principles is still outstanding.

However, significant progress has been made on all mentioned aspects recently e.g., Dröge (2003, 2005), Matthaeus *et al.* (2003), Minnie *et al.* (2003, 2005), Shalchi *et al.* (2004a, b, c), and Shalchi and Schlickeiser (2004).

3.4. Heliospheric Modulation Parameters

Apart from the diffusion coefficients all cosmic ray transport models also require knowledge of the structure and geometry of heliosphere, the heliospheric magnetic field, the current sheet and the solar wind velocity, introduced in Section 2. Observations by the Pioneer, Voyager and Ulysses spacecraft have contributed significantly to understand the spatial dependence and time evolution of these features. A major step forward was the confirmation that **V** is not uniform over all latitudes but it can be divided into the fast and slow solar wind regions (McComas *et al.*, 2000). The fast solar wind speed with characteristic velocities of up to $V = 800$ km/s is associated with polar coronal holes which are located at the high heliographic latitudes. The latitude dependent radial solar wind speed can be approximated for modeling purposes by

$$V(\theta) = V_0\left(1.5 \mp 0.5 \tanh\left[16.0\left(\theta - \frac{\pi}{2} \pm \varphi\right)\right]\right), \tag{7}$$

with $V_0 = 400$ km/s and with all angles in radians in the northern (top signs) and southern (bottom signs) hemispheres respectively with $\varphi = \alpha + 15\pi/180$, where α is the angle between the Sun's rotation and magnetic axes known as the tilt angle which changes with solar activity (Langner *et al.*, 2003). The role of φ is to determine at which polar angle V starts to increase from 400 km/s towards 800 km/s during solar minimum conditions (Moeketsi *et al.*, 2005). For solar maximum modulation conditions $V(\theta) = V_0$. The radial dependence of $V(r)$ up to the termination shock can be approximated by

$$V(r) = V_0\left\{1 - \exp\left[\frac{40}{3r_0}(r_\odot - r)\right]\right\}, \tag{8}$$

with $r_\odot = 0.005$ AU, and $r_0 = 1$ AU. When a termination shock is included, this equation must be modified as described by e.g. Langner *et al.* (2003). Diffusive shock acceleration is implicity described in the transport equation.

Apart from the convection caused by the solar wind, the divergence of **V** is equally important because it describes the adiabatic energy changes of cosmic rays. If it is positive, like in most of the heliosphere, cosmic rays experience energy loses resulting in characteristic spectral shapes at low energies in the inner heliosphere. At the termination shock it is negative and beyond the shock it may vary between positive and negative, with interesting effects for anomalous cosmic rays such as an increasing intensity (Langner *et al.*, 2006).

One of the most fundamental properties of the heliosphere is that its magnetic field is convected outward with the solar wind (see Section 2.2) causing the

heliosphere to be magnetodynamically embedded in the interstellar medium. The magnetic field features determine to a very large extent the transport of energetic particles. In order to properly understand modulation at high latitudes, the geometry, structure and properties of the magnetic field must be known. With the observation of recurrent cosmic ray variations at high heliolatitudes without corresponding variations in the magnetic field, it became evident that Parker's 1958 description of the heliospheric magnetic field, as summarized in Section 2.2, is an oversimplification, particularly at high latitudes. Therefore these equations are usually modified to account for deviations of the Parker field at high latitudes. Jokipii and Kóta (1989) argued that since the radial field lines at the poles are in a state of unstable equilibrium, the smallest perturbation may cause the 'collapsing' of the field line. The solar surface, where the 'feet' of the field lines occur, is not a smooth surface, but a granular turbulent surface that keeps changing with time, especially in the polar regions. This turbulence may cause the 'footpoints' of the polar field lines to wander randomly, creating transverse components in the field, thus causing deviations from the smooth Parker geometry. The net effect of this is a highly irregular and compressed field line. In other words, the magnitude of the mean magnetic field at the poles is greater than in the case of the smooth magnetic field of a pure Parker spiral. Analytically this is given by

$$\mathbf{B} = B_0\left(\frac{r_e}{r}\right)^2\left[\mathbf{e}_r + \left(\frac{r\delta(\theta,\phi)}{r_\odot}\right)\mathbf{e}_\theta - \tan\psi\,\mathbf{e}_\phi\right][1 - 2H(\theta - \theta')]. \tag{9}$$

The magnitude of this modified field is then given by

$$B = B_0\left(\frac{r_e}{r}\right)^2\sqrt{1 + \Gamma^2 + \left(\frac{r\delta(\theta,\phi)}{r_\odot}\right)^2}. \tag{10}$$

The effect of this modification is to increase the field in the polar regions in such a way that for large r it decreases as $1/r$ instead of $1/r^2$. In the ecliptic region of the outer heliosphere, where $1 + \tan^2\psi \gg 1$, this modification has little effect on the field and it becomes in essence a Parker spiral field. Qualitatively, this modification is supported by measurements made of the magnetic field in the polar regions of the heliosphere by Ulysses (Balogh *et al.*, 1995).

As illustrated in Figure 22, Fisk (1996) pointed out that a different correction needs to be made to the Parker spiral model for the simple reason that the Sun does not rotate rigidly but differentially, with the solar poles rotating ~20% slower than the solar equator. The interplay between the differential rotation of the footprints of the field lines in the photosphere of the Sun, and the subsequent non radial expansion of the field lines with the solar wind from coronal holes, can result in excursions of the field lines with heliographic latitude. This effect accounts for observations from the Ulysses spacecraft of recurrent energetic particle events at higher latitudes. In the Fisk model the magnetic field lines at high latitudes can be connected directly to corotating interaction regions in the solar wind at lower latitudes. When the

footpoint trajectories on the source surface can be approximated by circles offset from the solar rotation axis with an angle β_A, an analytical expression for this field is obtained (Zurbuchen *et al.*, 1997):

$$
\begin{aligned}
B_r &= B_0 \left(\frac{r_e}{r}\right)^2, \\
B_\theta &= B_r \frac{r}{V} \omega \sin\beta_A \sin\left(\phi + \frac{\Omega r}{V}\right), \\
B_\phi &= B_r \frac{r}{V}\left[\omega \sin\beta_A \cos\theta \cos\left(\phi + \frac{\Omega r}{V}\right) + \sin\theta(\omega\cos\beta_A - \Omega)\right]
\end{aligned}
\tag{11}
$$

with ω the differential rotation rate. A field with a meridional component leads to a more complicated form of the transport equation than for a Parker-type field. It is inherently three dimensional and time dependent so that the increase of the number of mixed derivatives results in the numerical codes that are used to solve the transport equation easily becoming unstable (Jokipii and Kóta, 2000, 2001b; Burger and Hattingh, 2001; Burger *et al.*, 2001). The properties of this type of field have been studied extensively (e.g., Burger and Hitge, 2004), but because of its complexity this type of field is not yet fully incorporated in numerical modulation models. Although the Jokipii-Kóta modification is to some extent unsatisfactory, it is still well motivated and the most convenient to apply, see Burger (2005).

A major corotating structure in the heliosphere is the current sheet which divides the heliospheric magnetic field into hemispheres of opposite polarity. Every $\sim$11 years the solar magnetic field changes sign across a current sheet. It has a wavy structure and is rooted in the coronal magnetic field, correlated to the solar activity of the Sun. The waviness is caused by the fact that the magnetic equator of the Sun does not coincide with the heliographic equator, because the magnetic axis of the Sun is tilted relative to the rotational axis. This tilt angle is usually denoted by α. During high levels of activity, the observed tilt angle increases to as much as $\alpha \approx 75^\circ$, beyond that it becomes undetermined. During times of low solar activity the axis of the magnetic equator and the heliographic equator become nearly aligned, causing relative small current sheet waviness with $\alpha \approx 5^\circ$ to 10° (see Figures 5 and 20). The wavy structure of the sheet is carried outwards by the solar wind as is shown in Figure 4 (Forsyth *et al.*, 2002). For periods of high levels of solar activity the dipole-like appearance of the Sun's magnetic field changes. The dipole configuration is replaced by quadrupole moments and therefore even multiple current sheets are possible (Crooker *et al.*, 1993; Kóta and Jokipii, 2001a).

The wavy structure of the current sheet plays an important role in cosmic ray modulation (Thomas and Smith, 1981). For a constant and radial solar wind speed, the current sheet position in spherical coordinates can be approximated according

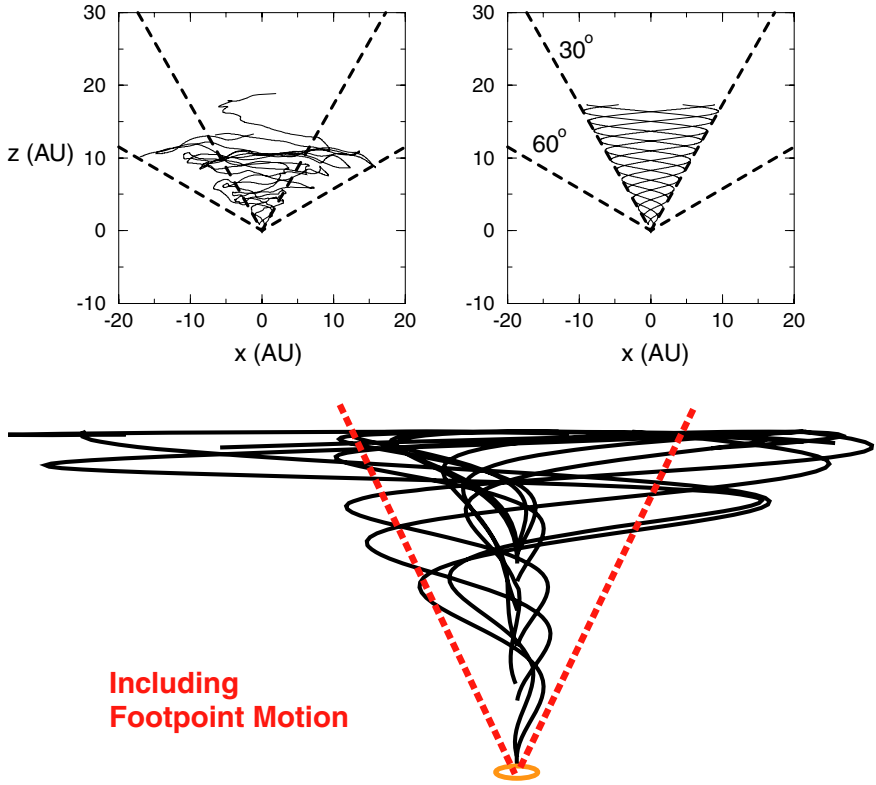

Figure 22. Illustration of the magnetic field lines as projected out into the heliosphere for the stochastically modified heliospheric magnetic field (Giacalone and Jokipii, 1999, upper left panel), the Parker heliospheric magnetic field (upper, right panel), and the modified heliospheric magnetic field using the foot-point motion, as suggested by Fisk (1996). Adapted from Fisk and Jokipii (1999).

to Jokipii and Thomas (1981) by

$$\theta' = \frac{\pi}{2} + \sin^{-1}\left\{\sin\alpha \sin\left[\phi + \frac{\Omega(r - r_\odot)}{V}\right]\right\}. \tag{12}$$

For small tilt angles it becomes

$$\theta' = \frac{\pi}{2} + \alpha \sin\left[\phi + \frac{\Omega(r - r_\odot)}{V}\right]. \tag{13}$$

This approximation is still widely used in numerical modeling. For a review on the wavy current sheet, see Smith (2001).

Figure 6 illustrates schematically the four relevant spatial regions of the heliosphere (the modulation volume). They are: (1) the region within the heliospheric termination shock, (2) the heliosheath and the heliopause, (3) a possible bow shock, and (4) the local interstellar medium. Presently, the latter is believed to

be characterized by a proton density of $n_p \sim 0.1$ cm^{-3}, a hydrogen atom number density of $n_p \sim 0.1$ cm^{-3}, a temperature of $T \sim 8000$ K, a speed of $v \sim 25$ km/s, a magnetic field strength of $B \sim 1.4$ μG, and a cosmic ray energy density of $\sim 0.5 - 1$ eV/cm^3 (Fahr *et al.*, 2000), resulting in what is shown in Figure 6.

Until recently, the heliosphere was assumed to be spherical in most modulation models with an 'outer boundary' at radial distances beyond ~100 AU, although it has not always been discussed clearly in the literature to what this 'outer boundary' physically corresponds to. Presently, it is considered to be the heliopause, implying that it is the region where cosmic ray modulation actually starts, although it cannot be excluded that modulation at lower energies may occur beyond the heliopause. Assuming the termination shock to be spherical is still considered the most reasonable assumption (Scherer and Ferreira, 2005; Langner *et al.*, 2006).

The region between the heliopause and termination shock is referred to as the (inner) heliosheath. Studying the role of the termination shock and that of the heliosheath in cosmic ray modulation with numerical models have become most relevant since Voyager 1 crossed the termination shock on 16 December 2004 (Stone *et al.*, 2005; Burlaga *et al.*, 2005; Decker *et al.*, 2005). Voyager 1 and 2 and Pioneer 10 spacecraft observations over 22 years and out to ~100 AU have also shown markedly different behavior for minimum modulation conditions between the radial intensity profiles for periods of opposite magnetic polarities and that most of the residual modulation for these periods took place in the outer heliosphere, near and beyond where the termination shock is expected to be. If the heliosheath is several tens of AU, it should have a noticeable effect on the modulation of low energy galactic and anomalous cosmic rays (see e.g., Langner *et al.*, 2003, 2005, 2006).

The typically assumed heliocentric distances in the upwind (nose) direction are 80–100 AU for the termination shock, 150–200 AU for the heliopause, and 300–400 AU for the bow shock. These distances are much shorter than the corresponding downwind figures (Scherer *et al.*, 2002; Zank and Müller, 2003; Scherer and Ferreira, 2005; Borrmann and Fichtner, 2005; Malama *et al.*, 2006).

3.5. Local Interstellar Spectra

In order to study the transport of cosmic rays in the heliosphere and to find proper diffusion coefficients it is important that the local interstellar spectra of the different particle species are known with adequate accuracy. For this, galactic propagation models are needed and significant progress has been made in computing galactic spectra for all cosmic ray species during the past decade (Moskalenko *et al.*, 2002 and Strong *et al.*, 2000).

In Figure 23, from Heber (2001a), the local interstellar spectrum for anti-protons, protons, positrons and electrons are compiled (see also, Langner *et al.*, 2001; Potgieter *et al.*, 2001b). Using these new local interstellar spectra, the modulation

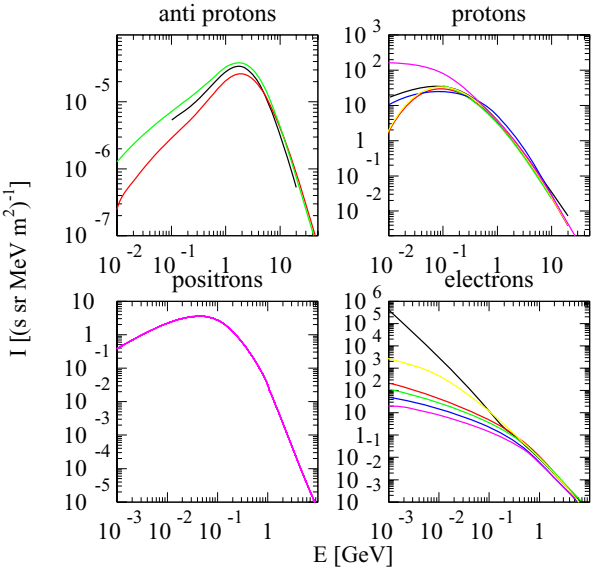

Figure 23. Local interstellar spectra for anti-protons and protons (upper panels) and positrons and electrons (lower panels), respectively. Different colors represent different numerical models (Heber, 2001b).

of protons, anti-protons, positrons, electrons, helium, carbon and boron together with fundamentally based diffusion coefficients has been revisited by Langner *et al.* (2003, 2004a,b) and Potgieter and Langner (2004). They concluded that the local interstellar spectrum for protons may not be known below a few hundred MeV until a spacecraft would actually approach the heliopause because of the strong modulation in the heliosheath, the effects of the termination shock and the consequent presence of the anomalous protons. In the inner heliosphere the modulated proton intensities are dominated by adiabatic energy losses. For anti-protons these effects are less pronounced because their galactic spectrum is predicted to be much lower at low energies than for protons. The shape of the modulated spectra for anti-protons is similar to that for protons but the radial gradients will be radically less than for protons. The situation for galactic helium at lower energies is similar to that for protons because of the presence of anomalous helium.

In contrast to protons, galactic electrons (and positrons but with a completely different spectral shape) do not experience very large adiabatic energy losses and less drifts with decreasing energy. However, in the inner heliosphere they are completely dominated up to about 30 MeV by Jovian electrons out to 10 AU in the ecliptic regions (Ferreira *et al.*, 2001b). In the outer heliosphere electrons (and positrons) below 100 MeV should also experience relatively large modulation in the heliosheath so that as for protons the local interstellar spectrum below a few hundred MeV may not be observed until a spacecraft would reach the heliopause.

4. Ulysses High Heliolatitude Cosmic Ray Observations During Solar Minimum

Because the Ulysses measurements reflect not only the spatial but also the temporal variation of the energetic particle intensities, it is important to know the intensity variations for a stationary observer in the heliosphere. Radial and latitudinal gradients which are directly correlated to particle propagation conditions can be derived from Ulysses and e.g. 1 AU observations, if the following assumptions were satisfied:

1. The variation of the galactic and anomalous cosmic ray intensities with heliolongitude caused by e.g. corotating interaction regions does not alter the determination of the spatial gradients when using averages over heliolongitude-solar rotation (Paizis *et al.*, 1999; Heber *et al.*, 2000).
2. Around solar minimum the radial gradient is nearly constant, so that the latitudinal gradient of cosmic rays can be calculated by taking into account the radial variation of Ulysses.

In addition to galactic and anomalous cosmic rays, Jovian electrons contribute significantly to the measured quiet time intensities in the MeV range. Around solar maximum activity solar energetic particle events become an important ingredient of the cosmic ray flux.

Figure 24 displays in the first two panels the hourly averaged solar wind speed and magnetic field strength. A few MeV protons (black curve) and electrons (grey curve) are shown in panel three. The fourth panel shows the variation of MeV/nucleon helium (black curve) and oxygen (grey curve), that are dominated by anomalous cosmic rays at solar minimum and solar energetic particles at solar maximum. The lower panel combines "quiet time" Ulysses galactic cosmic ray observations of protons (black curve) with electrons (grey curve) at a rigidity of 2.5 GV. "Quiet time" profiles have been determined by using only time periods when the several ten MeV proton channel showed no contribution of solar or interplanetary particles (Heber *et al.*, 1999). The 26-day averaged "quiet time" counting rates are presented as percentage changes with respect to the rates $C_{\max}$ measured in mid-1997 at solar minimum, $(C(t) - C_{\max})/C_{\max}$. It is common to use the particle rigidity – momentum per charge – in addition to its energy, because particles with the same rigidity will have the same Larmor radius in the heliospheric magnetic field, and therefore sample similar field structures. Marked by shading are the Jovian magnetosphere flyby in 1992, the two rapid pole-to-pole passages in 1994/1995 and 2000–2001, and the ecliptic crossing in 1998. The observed variations in the particle intensities are caused by the temporal changes during the solar cycle and by spatial variations along the Ulysses trajectory. Although not shown here, the number of short term decreases (Forbush decreases) is increasing at solar maximum (see e.g., Ahluwalia and Kamide, 2005). These decreases are caused by coronal mass ejections (Cane, 2000). Because the spatial size of a coronal mass ejection

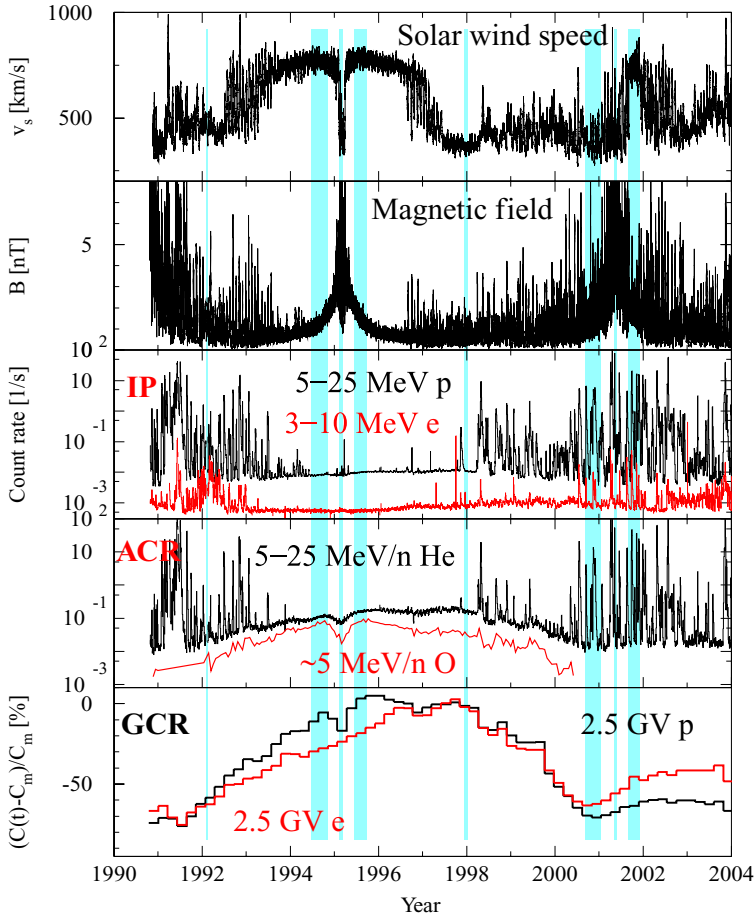

Figure 24. The upper two panels display hourly averages of solar wind speed and magnetic field strength as a function of time along the Ulysses' trajectory. Panel 3 shows daily averaged count rates of 5–25 MeV/nucleon protons and 3–10 MeV electrons. Panel 4 displays the variation of 5–25 MeV/nucleon helium and 2–6 MeV/nucleon oxygen. Normalized 26-day "quiet time" count rates of 2.5 GV protons (black) and electrons (grey) at Ulysses are combined in the lowest panel for the time period from launch in 1990 to 2004.

is restricted, a Forbush decrease might occur at Earth but not at Ulysses' position, making it more difficult to determine spatial gradients at solar maximum than at solar minimum. While the spacecraft remained close to the ecliptic plane it encountered solar maximum conditions until mid-1992 and again from 1999 to 2003, and solar minimum conditions in 1996 and 1997. During these periods galactic cosmic rays showed minimum and maximum intensity, respectively. The variation of the 2.5 GV electron and proton intensities is normalized to the maximum values during solar minimum in 1997. Therefore, Figure 24 shows the modulation amplitude from solar minimum to solar maximum.

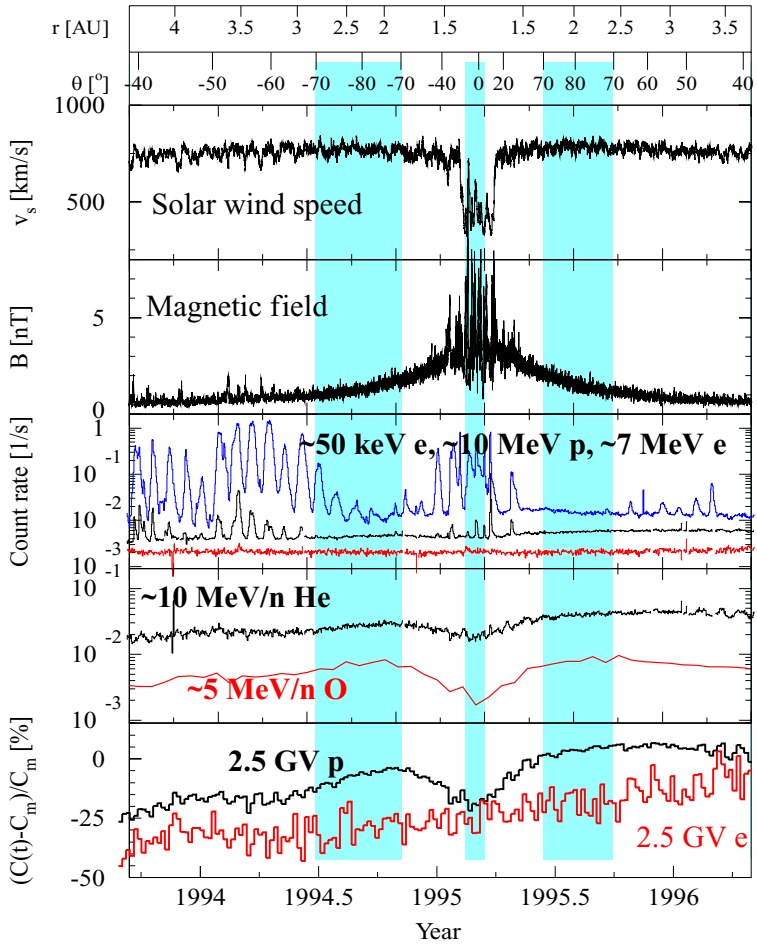

Figure 25. Similar to Figure 24, but only for the first out of ecliptic orbit from late-1993 to mid-1996. The ∼50 keV electrons are inserted in the third panel.

4.1. The Local Interstellar Spectrum in the Inner Heliosphere?

Figure 25 is similar to Figure 24 besides that it displays the period only from mid-1993 to mid-1996. In addition to Figure 24, 50 keV electrons are inserted in panel 3. From this figure it is evident that Ulysses was embedded in the fast solar wind for most of the time. The magnetic field varies with $1/r^2$ and shows less variations in the fast solar wind than in the slow solar wind close to the ecliptic plane. The recurrent intensity increases of ∼10 MeV protons and ∼50 keV electrons are discussed in section 4.3.3. The *v*-shape of galactic and anomalous cosmic ray nuclei are the focus of the following section. Galactic cosmic ray and Jovian electrons are discussed in Section 4.2 and 4.3.4, respectively.

An important prediction from drift-dominated modulation models, as described in Section 3.2, was the expectation that protons would have large positive latitudinal gradients in an A > 0 solar magnetic epoch. Figure 26 therefore illustrates in parts A and B the expected variation of the proton spectrum with latitude. It displays the Ulysses trajectory during the fast latitude scans and the expected proton spectra at 1 AU in the ecliptic and at 80° latitude. The model parameters have been chosen so that the 1 AU spectrum fits typical solar minimum spectra close to Earth. At energies below several 100 MeV an increase by an order of magnitude was expected and the local interstellar spectrum should become almost unmodulated at polar latitudes. Figure 26 shows in part C the observations from Ulysses during solar minimum. The solid symbols and line correspond to the observations and the computation for the heliographic equator, the open symbols are Ulysses measurements above 70°. In contrast to the expectations shown in B, the measured spectrum over the poles was observed to be highly modulated. The fact that Ulysses did not measure the local interstellar spectra during the minimum of solar cycle 22 at high heliolatitudes – with positive particles drifting primarily inwards through the polar regions – leads to the conclusion that it is impossible to determine the local interstellar spectrum in the inner heliosphere. Therefore the local interstellar spectrum will only be measurable by a space probe, like Interstellar Probe (Mewaldt and Liewer, 2001) or the Interstellar Heliopause Probe (Leipold *et al.*, 2003), send far beyond the heliospheric termination shock.

4.2. Spatial Gradients at Solar Minimum

Although Ulysses did not measure local interstellar spectra at polar latitudes, the spatial distribution of galactic and anomalous cosmic rays, which varies with radial distance from the Sun and heliographic latitude, is of large interest. In an ideal situation one would have space probes separated by a few AU (Δr) at the same latitude moving outwards with the same speed and another set of spacecraft moving at the same distance r but at different latitudes. From the measured intensity differences ΔI it would then be possible to calculate the radial and latitudinal gradients G_r, and G_θ. Such an ideal situation, however, does not exist. Since many other processes contribute to the particle transport in the heliosphere too, certain assumptions about the radial and latitudinal gradients have to be made; e.g. the radial gradient is assumed to be constant during an appropriate time. At solar minimum the cosmic ray intensity varies quasi-periodically with a time scale of one solar rotation, caused by corotating interaction regions, as described by Heber *et al.* (1999). Before discussing the latitudinal gradients it is essential to summarize the radial gradients and their modulation importance, based on Ulysses measurements.

4.2.1. *Radial Gradients*

The radial intensity gradient G_r at a location $\mathbf{r}$ in the heliosphere is taken as the variation of the intensity I with radius r. These 'global' gradients, in contrast to the

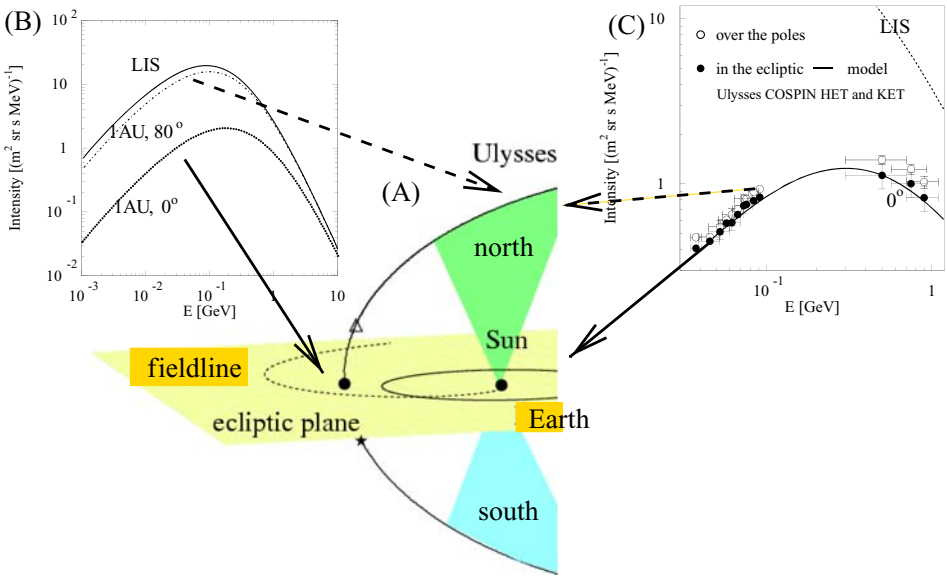

Figure 26. (A) Ulysses and Earth trajectory in 1994 and 1995. (B) Computed proton energy spectra using a drift dominated modulation model with parameters prior to the Ulysses mission (Haasbroek and Potgieter, 1995a); the upper solid line represents the local interstellar spectrum (LIS) at 100 AU, the dashed and lower solid line are the proton spectrum at 1 AU in the polar regions and in the ecliptic plane (0°). Part (C) displays the corresponding Ulysses observations (adapted from Heber *et al.*, 1996a).

theoretical differential gradients (Potgieter *et al.*, 1989), can be measured by space probes separated in radial distance, assuming that the gradients are only slightly varying with distance (Fujii and McDonald, 2001). Belov *et al.* (1999) and Heber *et al.* (2002b) determined the radial gradient around solar minimum for >2 GeV and >250 MeV protons and found values of 0.5%/AU and 2.2%/AU, in agreement with previous studies. (Teegarden *et al.*, 1973).

Clem *et al.* (2002) report the first determination of a radial gradient for cosmic ray electrons in the heliosphere at rigidities of 1.2 GV and 2.5 GV from 1 to 5 AU. In contrast to the expectation, the electron radial gradients appears to be the same as those for positive particles of the same rigidity. Unfortunately, the inability to study time evolution greatly hampers the interpretation of their results.

4.2.2. *Latitudinal Gradients*

Trattner *et al.* (1995, 1996, 1997), Keppler *et al.* (1996), Quenby *et al.* (1996), Heber *et al.* (1996a), McKibben *et al.* (1999), Simpson *et al.* (1996), and Ferrando *et al.* (1996) determined the latitudinal gradient of galactic and anomalous cosmic rays over a wide rigidity range. These gradients G_θ are displayed in Figure 27.

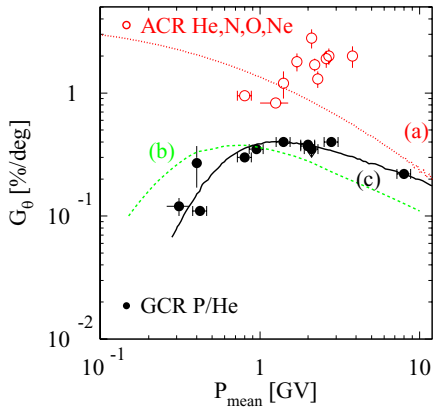

Figure 27. Latitudinal gradient G_θ for galactic (GCR) and anomalous cosmic rays (ACR) as a function of rigidity during the solar minimum fast latitude scan of Ulysses in 1994–1995. Curves (a), (b), and (c) are results of model calculations (Heber and Marsden, 2001).

Curve (a) corresponds to the expectations before the Ulysses mission, discussed above, while curves (b) and (c) take into account several modifications:

(a) The observed G_θ of cosmic ray protons at solar minimum is small. It increases as a function of rigidity up to 2 GV then decreasing for higher rigidities. The dotted line (a) is the computed values done before to the Ulysses mission. Modulation models then predicted much higher latitude gradients than derived from the Ulysses measurements (a factor of ten at 0.2 GV). In contrast to this expectation, galactic cosmic rays had a maximum latitudinal gradient at ∼2GV.

(b) The dashed line curve (b) displays the result of a modulation model $\kappa_\parallel$ (e.g. Burger and Hattingh, 1998). The gradient computed with with $\kappa_{\perp\theta}$ increased but proportional $\kappa_{\perp\theta}$ increased in the polar regions (Potgieter *et al.*, 1997), that is, the implicit decrease of drifts (Potgieter *et al.*, 2001a), describes the observations overall well and exhibits a maximum but at lower rigidities than observed.

(c) In order to obtain the good agreement shown in Figure 27 by curve (c), it turned out that changing the rigidity dependence of $\kappa_{\perp\theta}$ is the most efficient way. Burger *et al.* (2000) found that $\kappa_{\perp\theta}$ must have a flatter rigidity dependence than $\kappa_\parallel$, in particular when $\kappa_{\perp\theta}$ flattens to become almost independent of rigidity.

The determination of the spatial gradients of 2.5 GV electron is less straightforward. It relies on Figure 28 from Heber *et al.* (1999) which displays the 2.5 GV proton to electron ratio from mid-1994 to end of 1995, indicating charge dependent spatial modulation along the Ulysses trajectory at solar minimum (Ferrando *et al.*, 1996). The solid curve in Figure 28 from Heber *et al.* (1999) represents the variation of the temporally detrended 2.5 GV proton count rates only (from Figure 5 in Heber *et al.*, 1996a). With this curve almost a perfect fit to the proton to electron ratio, one

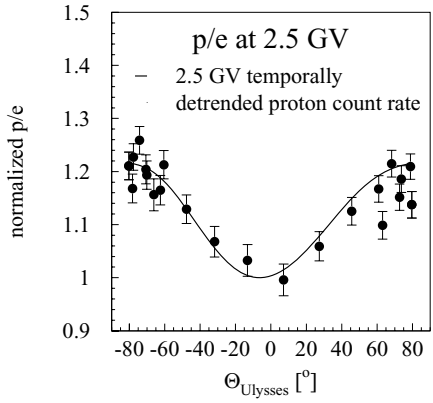

Figure 28. The 2.5 GV proton to electron ratio (p/e) as a function of Ulysses heliographic latitude (Heber *et al.*, 1999). The solid line is the latitudinal variation of 2.5 GV protons as determined by Heber *et al.* (1996a).

has to conclude that the contribution of electron latitudinal gradients to this ratio is negligible. Heber *et al.* (1999) had to assume that electrons and protons recover at approximately the same rate and that the radial gradient is approximately the same for both species (Clem *et al.*, 2002). They found the minimum proton to electron ratio close to the heliographic equator. The same maximum ratio was determined at southern and northern polar latitudes. In contrast to the small latitudinal gradients in the $A > 0$ solar magnetic epoch, McDonald *et al.* (1997) determined relatively large negative latitudinal gradients during the 1987 ($A < 0$) epoch, indicating that the time, rigidity and latitude dependence may be rather complex.

4.2.3. *The Diffusion Tensor Revisited*

Particles moving along magnetic field lines undergo pitch angle scattering because of field fluctuations. This process can be described by using a diffusion tensor with elements parallel and perpendicular to the mean magnetic field as described in Section 3.1.

There are two approaches to determine the diffusion tensor in the heliosphere. The first, the turbulence approach, relies on the determination from plasma and magnetic field observations using either turbulence theory (Bieber *et al.*, 1994) or the theory of particle wave interaction (Dröge, 2000); see also e.g., Lerche and Schlickeiser (2001), Schlickeiser (2002), Dröge (2005), and McKibben (2005). Using a realistic local interstellar spectrum and some assumption about the size of the modulation volume, model calculations lead to cosmic ray distributions that can be directly compared with observations. In the second approach the same information is used, but in contrast to the first a diffusion tensor is derived by finding compatibility between model results and a large set of particle observations in the heliosphere. Because the theory of particle scattering in turbulent magnetic fields is

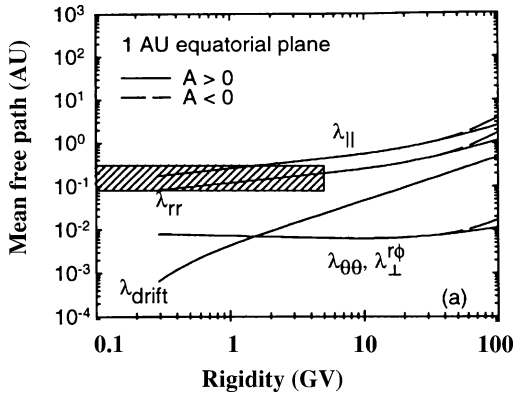

Figure 29. The rigidity dependence of the parallel ($\lambda_\parallel$), perpendicular ($\lambda_{\perp r}$, $\lambda_{\perp\theta}$) and the drift mean free paths in the equatorial plane at 1 AU. The rectangle denotes the Palmer consensus range (Palmer, 1982) for $\lambda_\parallel$. The rigidity dependence is shown for an A > 0 (solid lines) and A < 0-solar magnetic epoch (dashed lines) (adapted from Burger *et al.*, 2000).

still developing, this cosmic ray approach provides useful and important constraints to the diffusion tensor. And, indeed, both methods are linked with each other, e.g. the overall rigidity dependence of the diffusion tensor used in the modeling can be motivated from wave-particle and/or turbulence theory, restricting the number of free parameters in the calculations.

As stated above, a large set of observations is used in the cosmic ray approach to determine the time, spatial and rigidity (energy) dependence of the diffusion coefficients. Presently, most of the modeling research uses information from the turbulence and diffusion theory to restrict the choice in parameter space. Such a combined approach has been very successful in modeling (1) the observed latitudinal gradients (Heber *et al.*, 1996a, 1998; Belov *et al.*, 1999) in the inner heliosphere by Ulysses (Burger *et al.*, 2000; Heber, 2001b; Heber and Potgieter, 2000; Heber and Marsden, 2001), (2) the propagation of Jovian electrons (Heber *et al.*, 2001b, 2002a; Ferreira *et al.*, 2001b, c), and (3) the solar cycle dependence (Heber *et al.*, 2002b, 2003, Potgieter *et al.*, 1999; Paizis *et al.*, 2001).

As an example of a combined approach, the rigidity dependence of the parallel $\lambda_\parallel$, perpendicular ($\lambda_{\perp r}$, $\lambda_{\perp\theta}$) and the drift ($\lambda_{\rm drift}$) mean free paths in the equatorial plane at 1 AU are shown in Figure 29 from Burger *et al.* (2000). They found that $\lambda_{\perp\theta}$ must have a flatter rigidity dependence than $\lambda_\parallel$ in order to describe the rigidity dependence of the latitudinal gradient shown in Figure 27. The rectangle denotes the so-called Palmer consensus range (Palmer, 1982) for $\lambda_\parallel$. See also Section 3.3.

4.3. Cosmic Rays as Probe for Heliospheric Features

As mentioned in the introduction, some stable structures in the heliosphere exist at solar minimum. The inner heliosphere is then separated into two distinct regions, (1)

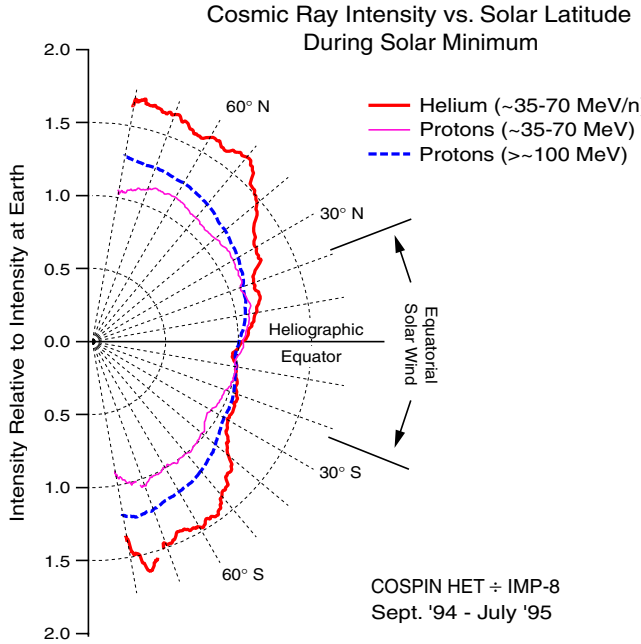

Figure 30. Polar plot of 30–70 MeV and >100 MeV protons, and 30–70 MeV/nucleon helium as Ulysses to IMP 8 intensity ratios, illustrating the North-South-asymmetry of cosmic rays in the inner heliosphere (McKibben *et al.*, 1998).

the streamer belt area, where the solar wind speed varies from ∼400 to >800 km/s and (2) the "coronal hole area," where the wind speed varies from ∼600 to 800 km/s. The interaction of slow and fast solar wind at low latitudes (<40 °) can lead to the formation of corotating interaction regions (see Section 2.4.4). In this section we describe particle observations at high latitudes that colud remotely "sense" low-latitude heliospheric structures.

4.3.1. *The North-South-Asymmetry of Cosmic Rays in the Heliosphere*

For simplicity the modulation models mentioned above assumed that the galactic cosmic rays were symmetrically distributed with respect to the heliographic equator. It was a pleasant surprise when Simpson *et al.* (1996), and Heber *et al.* (1996b, 1997) found that the flux of >100 MeV protons was not symmetric to the heliographic equator. At first, neither the solar wind experiments nor the magnetic field investigations reported corresponding asymmetries (Forsyth *et al.*, 1996; Phillips *et al.*, 1995). Simpson *et al.* (1996) and Heber *et al.* (1996b) found a shift of ∼7–10° of the minimum galactic cosmic ray flux into the southern hemisphere, as illustrated in the Figures 30 and 31. Figure 30 from McKibben *et al.* (1998) displays the Ulysses to 1 AU 35–70 MeV and >100 MeV protons and 30–70 MeV/nucleon helium count rate ratio as a polar plot. The two instruments were normalized to one another during the equator crossing in March 1995. A constant ratio of one

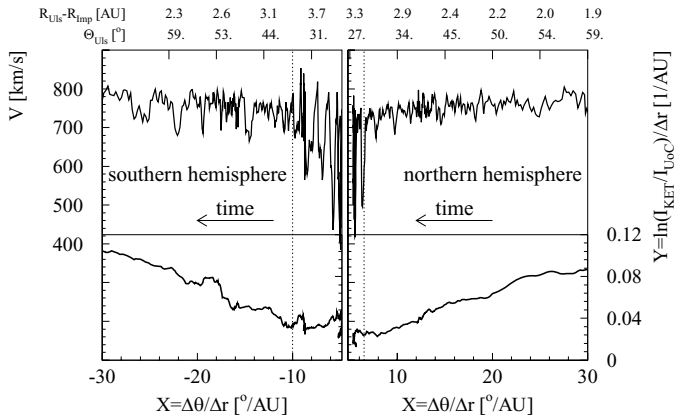

Figure 31. Solar wind speed and $Y = \ln(c_U/c_E)/\Delta r$ as a function of $X = \Delta\theta/\Delta r$ for >106 MeV protons in the southern hemisphere. Ulysses radial distance r and heliographic latitude θ are shown at the top (Heber *et al.*, 1998).

means a spherical symmetric cosmic ray distribution. From this figure it is evident that 35–70 MeV protons do not show any significant latitudinal excess (purple curve), whereas >100 MeV protons (blue curve) and 30–70 MeV/nucleon helium (red curve) do. The helium channel is dominated by anomalous cosmic rays contributing significantly to the variation of the 30–70 MeV/nucleon helium channel. From that figure a North-South-asymmetry in the cosmic ray flux is obvious.

To calculate this offset Heber *et al.* (1998) used the computed latitudinal extension of the heliospheric current sheet into the northern and southern hemisphere. They showed that in a coordinate system using the heliospheric current sheet position, the cosmic ray profiles are a function of this "latitude" only. A full understanding of this effect has not been achieved yet. However, there are several explanations that can account for a North-South-asymmetry (e.g. Hattingh *et al.*, 1997; Heber and Burger, 1999):

- The cosmic ray distribution is symmetric with respect to the current sheet, but the sheet may be displaced by some degrees with respect to the Sun's equatorial plane. Magnetic field observations support the idea of such a 'hanging' heliospheric current sheet (Smith *et al.*, 2000).
- Overwinding of the heliospheric magnetic field, as reported by Forsyth *et al.* (1996), in the southern hemisphere may cause the propagation parameters in one hemisphere to be different than in the other hemisphere.
- Another possibility has been put forward by Heber *et al.* (1998). Figure 31 displays the solar wind speed and $Y = \ln(c_U/c_E)/\Delta r$ as a function of $X = \Delta\theta/\Delta r$. Herein $\Delta r = r_U - r_E$ and $\Delta\theta = |\theta_U| - |\theta_E|$ are the radial and latitudinal distance between Ulysses and an observer at Earth. If G_r and G_θ were independent of time and space, their values would be simply given by the offset and the slope of

a straight line. Comparing the solar wind speed measurements and the particle data, Figure 31 suggests a correlation between latitudinal effects and different solar wind speed domains (Belov *et al.*, 1999).

It is also a matter of much discussion if this observation were an occurrence of events that pertained during the rapid pole to pole passage or if it were correlated to a permanent magnetic flux deposit in the southern heliosphere compared to the northern hemisphere (Smith *et al.*, 2000). These observations are another interesting piece of the puzzle how the Sun is structuring the heliosphere.

4.3.2. *Spectral Variation of the Anomalous Cosmic Ray Spectrum*

Heber *et al.* (2001c) determined the anomalous cosmic ray Oxygen spectra by using data from the Energetic PArticle Composition Experiment (Keppler *et al.*, 1992) and the Low Energy Telescope on board Ulysses (Simpson *et al.*, 1992). They found that the location of the peak energy is depending on the solar wind regime and is decreasing from $E = 4.9 \pm 0.5$ MeV/nucleon in the fast solar wind regime to $E = 3.4 \pm 0.4$ MeV/nucleon in the streamer belt. Because of the propagation in the heliosphere, the observed spectrum is obviously not the same as the source spectrum. It is also confirmed that anomalous protons are very difficult to observe in the inner heliosphere. However, the observations presented by Heber *et al.* (2001c) confirms typical predictions (Steenberg and Moraal, 1999; Potgieter and Langner, 2003, 2004) that can be found in the modulated spectra.

4.3.3. *Recurrent Particle Events and Modulation*

Since measurements with spacecraft in the interplanetary space have become available, it is known that associated with the occurrence of recurrent fast and slow solar wind streams, recurrent variations in the energetic particle intensities can be observed (Simpson, 1998).

At the beginning of 1993 recurrent galactic cosmic ray decreases were correlated with the occurrence of fast streams from corotating interaction regions. An example of an in-ecliptic event is shown in Figure 9. The evolution of the Ulysses observations towards high heliographic latitude is displayed in Figure 32 and 33. Figure 32 shows from top to bottom the solar wind speed, the magnetic field strength, count rate of >92 MeV protons and their long term detrended variation as well as the detrended count rate of the Maui neutron monitor. Figure 33 presents an overview of daily averages of the 40–65 keV electrons (upper panel) 0.5–1.0 MeV protons (lower panel). The latitude θ ranges from 13°S through both polar regions, and finally ends at 10°N:

- Periodic enhancement in the electron intensity have been observed in the 40–65 keV electrons even up to the 80°S latitude of the polar pass.
- For protons up to 3.8 MeV increases are visible for latitudes up to $\sim 70^\circ$ (Sanderson *et al.*, 1995).

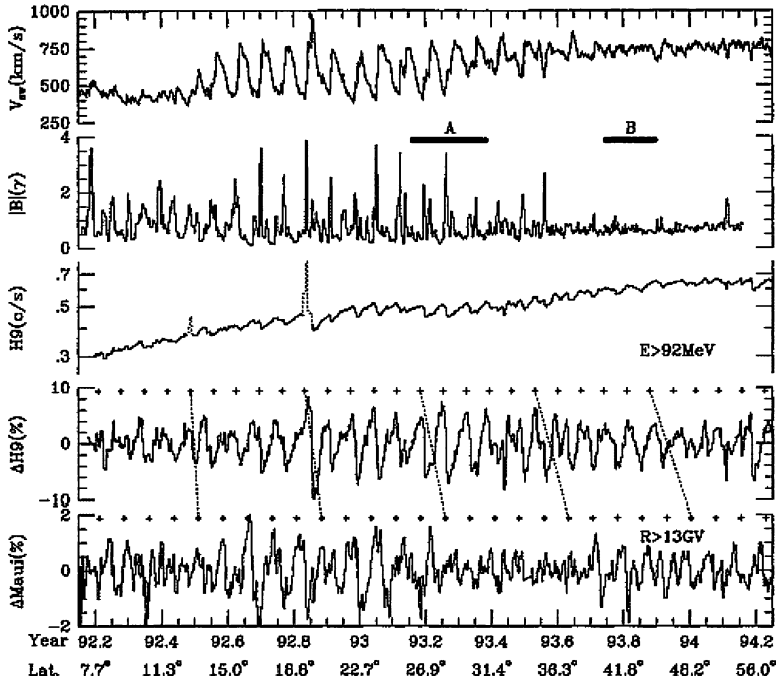

Figure 32. From top to bottom: Solar wind speed, magnetic field strength, count rate of > 92 MeV protons and their long term detrended variation as well as the detrended count rate of the Maui neutron monitor (McKibben *et al.*, 1995). At the bottom, the radial distance and heliographic latitude of Ulysses are shown.

– The northern hemisphere is much quieter than the southern hemisphere. There are only very weak particle increases seen above the streamer belt.
– The peak particle intensity was seen in the southern hemisphere at latitudes around 15°.

From the solar wind speed time profile different regions were identified: From latitudes above 40°S Ulysses had been imbedded in the fast solar wind stream originated from the southern polar coronal hole. As expected corotating forward and reverse shock waves disappeared. In contrast to what had been expected, Figure 32 and 33 show recurrent particle increases and galactic cosmic ray decreases up to polar latitudes. Even more surprising was the fact that the 40–65 keV electrons were delayed from the 0.5–1.0 MeV protons by up to 4 days (Simnett *et al.*, 1994).

Paizis *et al.* (1999), McKibben *et al.* (1995) and Zhang (1997) studied the amplitude evolution of the 26-day recurrent cosmic ray decreases and its rigidity dependence. The amplitude has a maximum around 25°–30° and decreases for both lower and higher latitudes. Although a radial dependency (Keppler, 1998) cannot be a priori excluded, the observations are regarded as a latitude effect. In addition the rigidity dependence of the recurrent cosmic ray decreases on the other hand

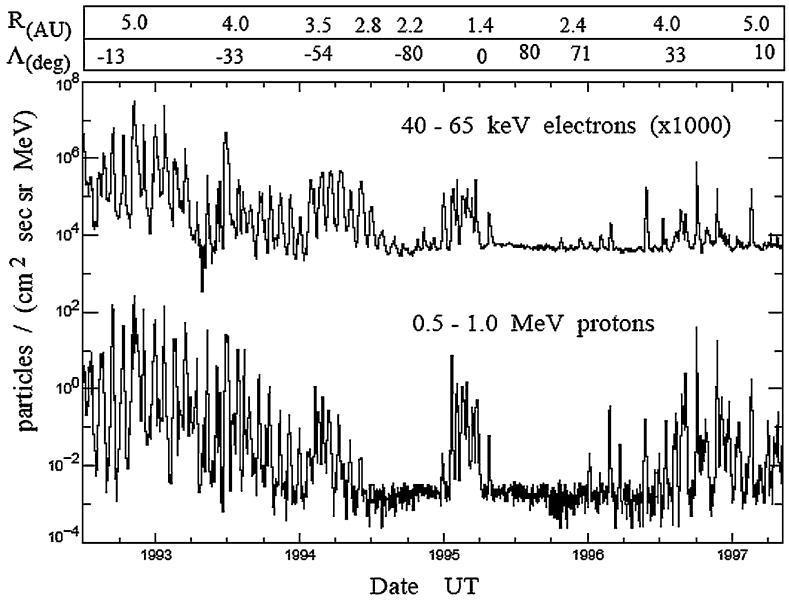

Figure 33. Variations in intensities of 40–65 keV electrons and 0.5–1 MeV protons from the Hi-Scale instrument during Ulysses' first solar minimum orbit (Simnett *et al.*, 1998). At the top, the radial distance and heliographic latitude of Ulysses are shown.

is remarkable similar to the latitudinal gradient discussed in the previous Section (Zhang, 1997; Paizis *et al.*, 1999; Zhang and McDonald, 2001).

Figure 34 shows in comparison to Figure 32 simulated variations of the solar wind speed, magnetic field strength, and the flux of 1 GeV galactic cosmic rays along the trajectory of Ulysses. Recurrent 26-day cosmic ray variations are most prominent at medium latitudes, where corotating interaction regions are present. The passage of corotating interaction regions causes recurrent depressions in the GeV cosmic-ray flux. These extend to high latitudes where the solar wind speed and the magnetic field no longer exhibit recurrent variations. The effect becomes more pronounced if perpendicular diffusion is enhanced latitudinally as proposed by Jokipii (1973) and Jokipii *et al.* (1995). Note, that this model also can explain the delay of the recurrent electron increases with respect to the protons (Kóta and Jokipii, 1998). It can be qualitatively understood in terms of latitudinal diffusion. Ions are slower and are more effectively convected outward by the solar wind. Thus ions reaching Ulysses at high latitudes must have been accelerated close to the Sun. Electrons, on the other hand, are fast and can reach from a considerably larger area, explaining their longer duration in time. The time lag may be interpreted in terms of a velocity shear.

The analysis of the Ulysses magnetic field data showed that the polar heliospheric magnetic field is dominated by strong variations. These observations are not in

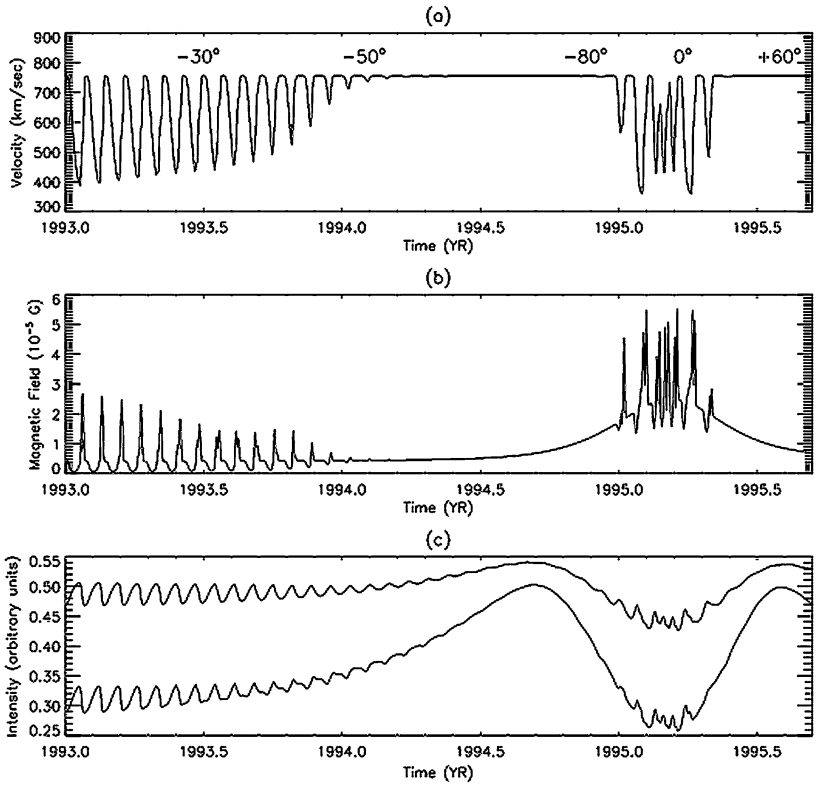

Figure 34. Simulated solar wind speed (top) and magnetic field strength (middle) along the trajectory of Ulysses. A constant tilt angle of 30 was used. The bottom panel shows the simulated variation of 1 GeV proton flux, calculated for larger ($\kappa_\perp/\kappa_| = 0.05$), upper curve) and smaller ($\kappa_\perp/\kappa_| = 0.02$, lower curve) values of perpendicular diffusion. Ulysses' latitude is indicated in the top panel (Kóta and Jokipii, 1998).

agreement with the standard Parker geometry for the magnetic field, as shown in Figure 2 and in the upper right hand panel of Figure 22, where field lines are lying on a cone at a constant latitude (see also Section 3.4). Two competing models are qualitatively able to explain the observation; the one by Jokipii and co-workers (Jokipii and Kóta, 1989) is based on stochastic processes whereas the one by Fisk and co-workers (Fisk, 1996) introduces systematic modification of the heliospheric magnetic field (Fisk and Jokipii, 1999). Jokipii (1966) pointed out that random walk of field lines due to turbulence in the solar magnetic field, e.g. by stochastic movement of super granules, could provide a meridional magnetic field component. In such a field configuration the heliospheric magnetic field lines are no longer bound to a cone, as shown in Figure 22. Since the random walk of field lines occurs on a variety of length scales, it is possible for particles to move from one field line to another.

The heliospheric magnetic field modification proposed by Fisk (1996) is based on the following assumptions: The heliospheric magnetic field is attached to the photosphere that rotates differentially. The high speed solar wind expands non-radially from polar coronal holes. The expansion of the solar wind in the polar coronal holes is around an axis offset from the solar rotation axis and that tends to rotate rigidly at approximately the equatorial rotation rate. The resulting field patterns, as displayed in the lower panel of Figure 22, are rather complicated and may extend to lower latitudes at larger radial distances.

The two modifications of the heliospheric magnetic field are qualitatively able to explain the observation. It can be argued that such modification results in an enhanced component of the diffusion tensor in the polar direction. Of course, the mechanisms are not mutually exclusive, and both may be contributing to the latitudinal transport. (See also Burger and Hitge, 2004).

4.3.4. *Propagation of Jovian Electrons in the Inner Heliosphere*

As mentioned in the introduction Jovian electrons are a handy tool to investigate the particle propagation in the inner heliosphere. The main advantage is that they can be used directly to investigate the diffusion tensor at low rigidities ($<$100 MV), because (1) electrons and positrons suffer less adiabatic energy losses, and (2) for energies below $\sim$100 MeV drift effects become of minor importance (Ferreira *et al.*, 2001c).

At these energies several other sources, like solar energetic, interplanetary and galactic cosmic ray electrons contribute to the MeV electron measurements. While solar electrons and electrons accelerated at shock waves are distinguishable from them, because of softer energy spectra (e.g., Heber *et al.*, 2002a, and references in there), it is not possible to separate Jovian and galactic cosmic electrons by using the spectral information. Therefore, model calculations are essential to determine a reasonable diffusion tensor. Because of Jupiter's position with respect to the heliospheric magnetic field, the intensity of Jovian electrons will not only vary with the spacecraft's radial distance and heliographic latitude but also with its longitude, making a three-dimensional propagation model mandatory. Such models have been developed by Ferreira *et al.* (2001c) and Fichtner *et al.* (2000).

In order to understand the Ulysses MeV electron observations with respect to Jovian electron propagation, it is necessary to view the Ulysses trajectory in an appropriate coordinate system (e.g., Heber *et al.*, 2001b, 2002a). The two panels in Figure 35 display the Ulysses trajectory from launch in 1990 to end of 2002 in a reference frame where the Sun and Jupiter are fixed. Figure 35 A shows the trajectory projected onto the Jovian orbital plane, and Figure 35 B the projection onto the solar meridional plane containing Jupiter. A standard Parker magnetic field line for a solar wind speed of 400 km/s "passing through" Jupiter is also drawn in Figure 35 A. This allows a direct estimate of the magnetic connection between Ulysses and Jupiter for a realistic solar wind speed during times when Ulysses was close to the ecliptic in 1998 and in 2001. Figure 35 (B) reflects Ulysses'

heliographic latitude, which increases after the Jovian fly-by until the pass over the Sun's southern polar region in 1994. In 1994 to 1995 and in 2000 to 2001 the spacecraft performed a complete latitude scan within 11 months and was then heading towards the ecliptic plane. In 1998 Ulysses began its second out-of-ecliptic orbit, and reached a heliographic latitude of 80° in August 2000.

Figure 36 displays 3-day averaged quiet time count rates of 3–10 MeV electrons from 1990 to 1997. The gray curves display the result of two different propagation models used to describe the Jovian electron propagation along the Ulysses

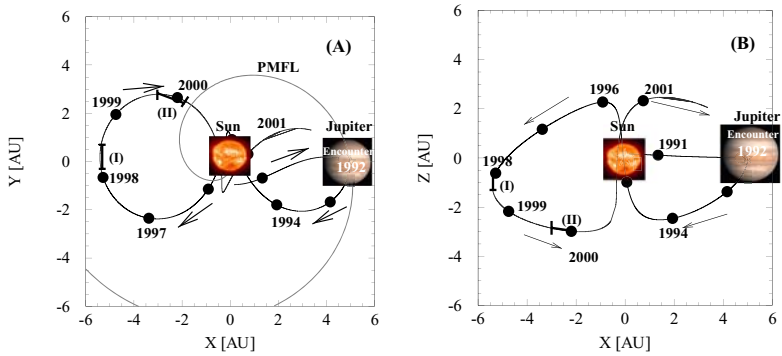

Figure 35. Ulysses trajectory projected onto the Jovian orbital plane (left) and onto the meridional plane in a system where the positions of Jupiter and Sun are fixed. In the left panel, a Parker magnetic field line (PMFL) is shown for a solar wind speed of 400 km/s. (I) and (II) mark two periods discussed here. Open and filled circles are plotted for every 100 days and at the beginning of each year (adapted from Heber *et al.*, 2001b).

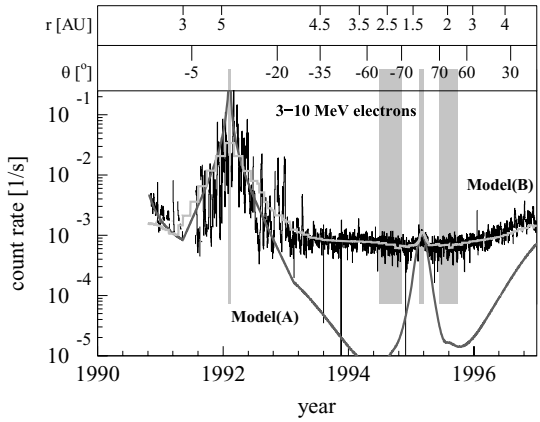

Figure 36. The 3-day averaged quiet time count rates of 3–10 MeV electrons. The superimposed grey curves (A) and (B) display the model results by Ferrando *et al.* (1999) and Ferreira *et al.* (2001a), respectively. Marked by shading are the Jovian flyby in 1992 and the rapid pole-to-pole passages in 1994 to 1995. Ulysses' radial distance to the Sun and its heliographic latitude are shown at the top.

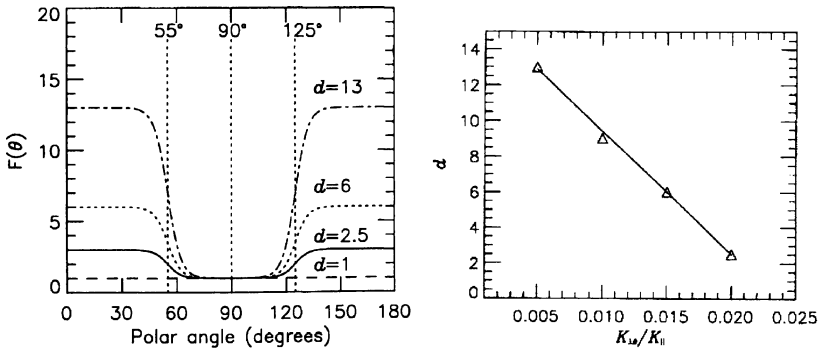

Figure 37. Left: Latitudinal enhancement of $\kappa_{\perp\theta}$ as function of the polar angle (see Equation (14)). At the angle $\theta = 55^\circ$ and $\theta = 125^\circ$ the function rapidly increases from 1 to $d/2$ for four assumed values of d. Right: Magnitude of d as a function of $b = \kappa_{\perp\theta}/\kappa_{\parallel}$ which produces compatibility with the Ulysses observations. (Ferreira *et al.*, 2001c).

trajectory. The first one is a modification of the Conlon model (Conlon, 1978) as described by Rastoin (1995). Rastoin (1995) used a Jupiter-centered coordinate system to determine the magnetic connection of the spacecraft to Jupiter with respect to the heliospheric magnetic field. The heliospheric magnetic field is represented by a Parker spiral for a given solar wind speed. The fit to the 1991 to 1992 data leads to $\kappa_{\parallel} = 1.8^{+7.0}_{-1.2} \cdot 10^{23}\text{cm}^2/\text{s}$, $\kappa_{\perp} = 8^{+9}_{-3.5} \cdot 10^{20}\text{cm}^2/\text{s}$, and $\kappa_Z = 1.7 \pm 1 \cdot 10^{20}\text{cm}^2/\text{s}$. The source strength was found to be 10^{26} electrons/MeV$^{1.5}$ in the 3 to 10 MeV range. Obviously the approximation to the data cannot describe the high latitude Ulysses observations.

In order to fit the Ulysses data as displayed in Figure 36, Ferreira *et al.* (2001c) had to introduce a latitude dependent $\kappa_{\perp\theta}$, given by:

$$\kappa_{\perp\theta}(\theta) = b \cdot \kappa_{\parallel} \cdot f(\theta, d) \tag{14}$$

displayed in Figure 37. Here d is a parameter describing the ratio of $\kappa_{\perp\theta}$ over the poles to that in the ecliptic. This relation is similar to the modification of $\kappa_{\perp\theta}$ to explain the small latitudinal gradients for galactic cosmic ray nuclei (see Figure 27).

The effects on the modulation for the computed electron intensity have been studied for different scenarios for d along the Ulysses trajectory. The model results shown in Figure 36 were obtained with the same model as described by Ferreira *et al.* (2001c) and Ferreira *et al.* (2001b), but with $\kappa_{\perp,r}/\kappa_{\parallel} = 0.005$ and $\kappa_{\perp,\theta}/\kappa_{\parallel} = 0.015$ in the equatorial plane and $\kappa_{\perp,\theta}/\kappa_{\parallel} = 0.09$ over the poles. However, Ferreira *et al.* (2001c) showed that the parameter b and d are not independent from each other (right panel of Figure 37). The best approximation for $b = 2$ is d between 2.5 and 6, while for $b = 0.005$ only $d = 13$ leads to a good fit to the data. It is important to note that, depending on the choice of the parameter, the observed intensities are either dominated by Jovian electrons or by galactic electrons.

5. Ulysses High Heliolatitude Cosmic Ray Observations During Solar Maximum

During its second fast latitude scan, Ulysses explored the latitudinal structure under very different conditions. The Sun was near the maximum in its activity cycle, and the intensity profiles, shown in Figure 24, were dominated by the transient increases produced by energetic solar flares and coronal mass ejections events. Concurrently, the baseline intensity of cosmic rays and anomalous components had decreased. Thus, the Ulysses orbit was ideally suited to investigate the variation in the latitudinal structure of the inner heliosphere between solar minimum and maximum.

5.1. The Modulation Environment During the two Ulysses Fast Latitude Scans

Figure 38 displays six source surface maps from http://quake.stanford.edu/∼wso/. The surface map (A) for May 1994, (B) December 1994, and (C) in July 1995 show the solar magnetic field configuration for the $A > 0$ solar minimum magnetic epoch in the mid-1990's, during the time period of the first fast latitude scan. The black line separating the light (outward polarity) and dark (inward polarity) gray areas indicates the waviness of the current sheet at that time. Obviously, the magnetic field was well organized, with the current sheet having only a small inclination. Source surface fields, as displayed in panels (D) to (F), indicate that the polarity reversal occurred at the north and south solar poles by February and July 2000, respectively. Ulysses' observations near 80° in November 2000 suggested that the reversal had not occurred at that time (Smith *et al.*, 2001). While the result seems surprising, it can be explained when taking into account that the source surface maps were calculated from the measured photospheric magnetic field. The south pole was however tipped away from the Earth during late 2000, significantly affecting the source surface model (Jones *et al.*, 2003). The solar wind speed cannot be characterized as fast or slow in the southern hemisphere, but showed the characteristics of a fast solar wind in the northern hemisphere (McComas *et al.*, 2001).

An indicator for open magnetic field lines at polar latitudes is the existence of polar coronal holes. Figure 39 displays coronal hole maps obtained from ftp://ftp.noao.edu/kpvt/synoptic/choles. Note the different latitude scales when comparing the source surface with the coronal hole maps: In 1994 to 1995 during solar minimum the two polar coronal holes are stable features and extensions of coronal holes are reflected in the corresponding source surface maps. In contrast to solar minimum, no southern polar coronal hole is evident in panels (D) to (F) at solar maximum. A stable northern coronal hole is developing during the Ulysses fast latitude scan. It should also be emphasized that it takes several solar rotations until such a new configuration has been established in the whole inner heliosphere.

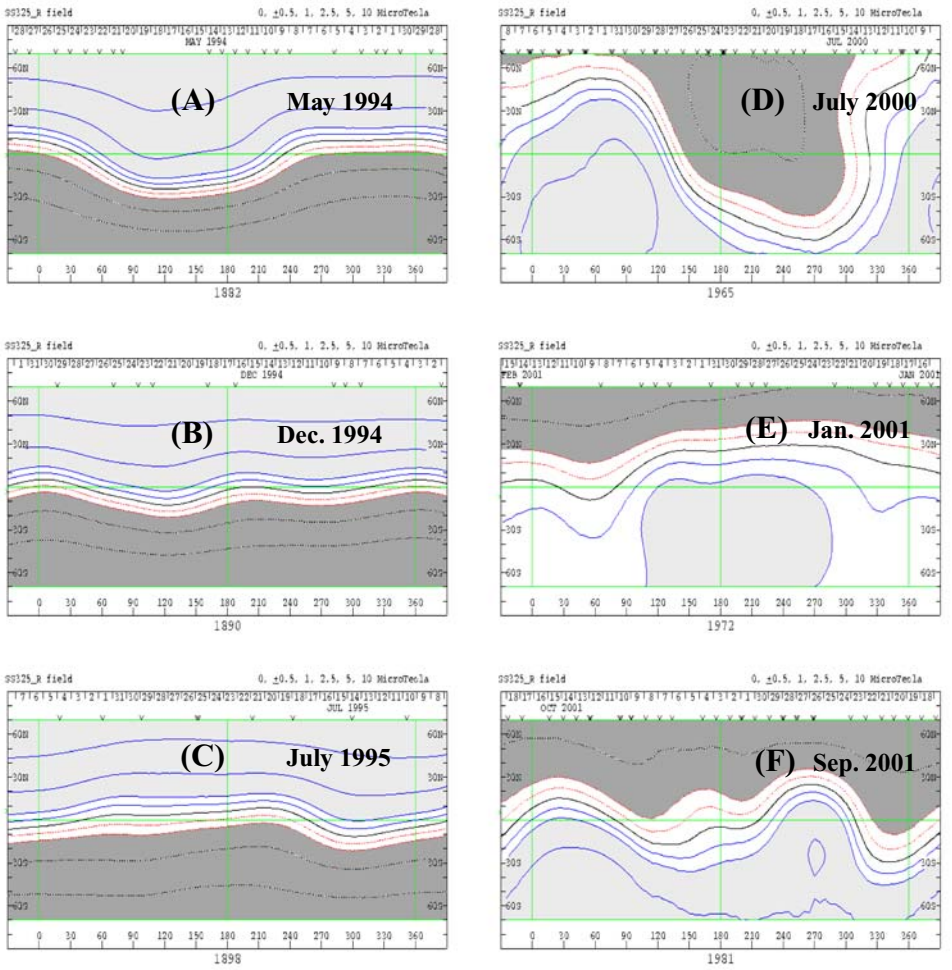

Figure 38. Configuration of the solar magnetic field as calculated by (Hoeksema, 1995) for a source surface at 3.25 solar radii, for the first (left) and second (right) fast latitude scan of Ulysses. (A) displays May 1994, (B) December 1994, (C) July 1995, (D) July 2000, (E) January 2001, and (F) October 2001.

The magnetic field structure during solar maximum has a highly inclined current sheet (Figure 38) that was distorted by coronal mass ejections at all latitudes.

McKibben *et al.* (2003) addressed the following cosmic ray modulation issues concerning this period:

– Would the latitudinal gradient become larger or smaller during solar maximum?
– Would there still be evidence, from solar particle events and Jovian electron observations, for effective propagation of particles between the heliospheric equatorial and polar regions?

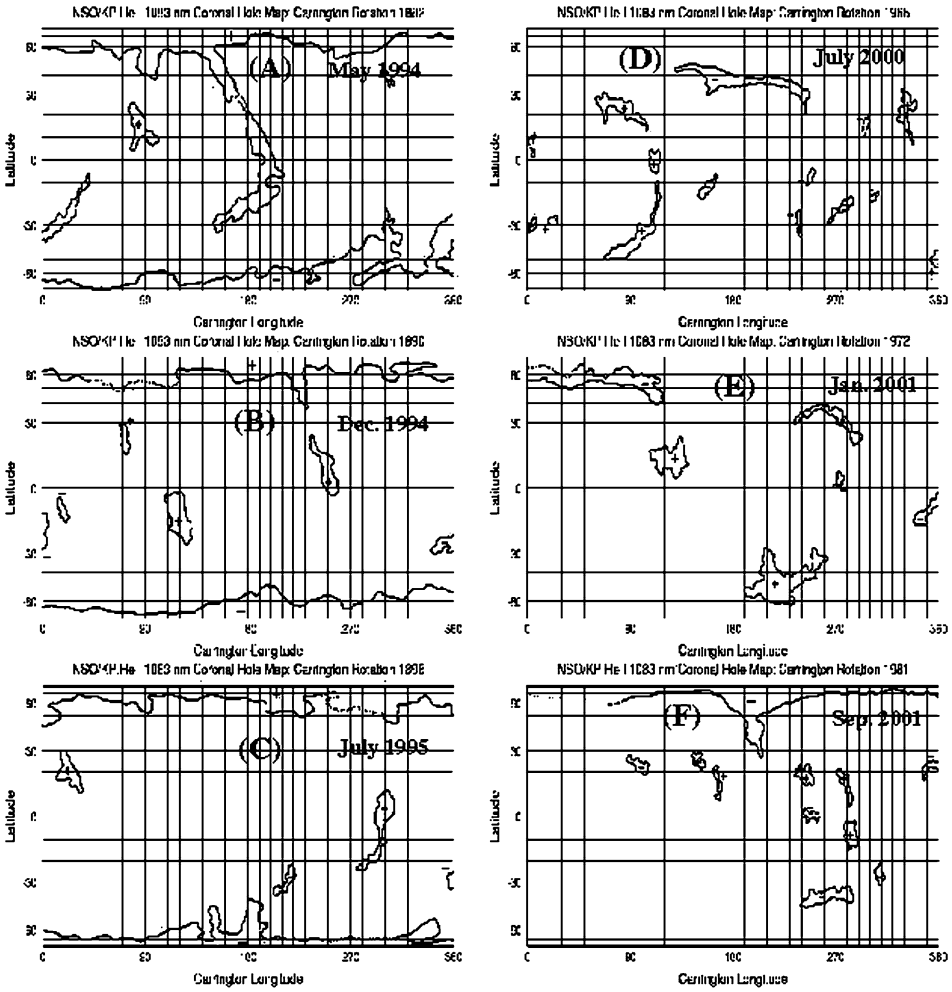

Figure 39. Coronal holes by Carrington rotation number as inferred from 1083 nm He I observations made at Kitt Peak for the first (left) and second (right) fast latitude scan of Ulysses (ftp://ftp.noao.edu/kpvt/synoptic/choles).

– Would there again be evidence of a global magnetic field asymmetry reflected by asymmetries in particle modulation?

5.2. Latitudinal Distribution of Galactic Cosmic Rays

Measurements of the latitude dependence of 35–70 MeV/nucleon and 70–90 MeV/nucleon helium (two top panels) and 70–90 MeV and >100 MeV protons (lower two panels) during solar minimum and solar maximum are shown in Figure 40 from McKibben *et al.* (2003). Temporal variations of these cosmic ray

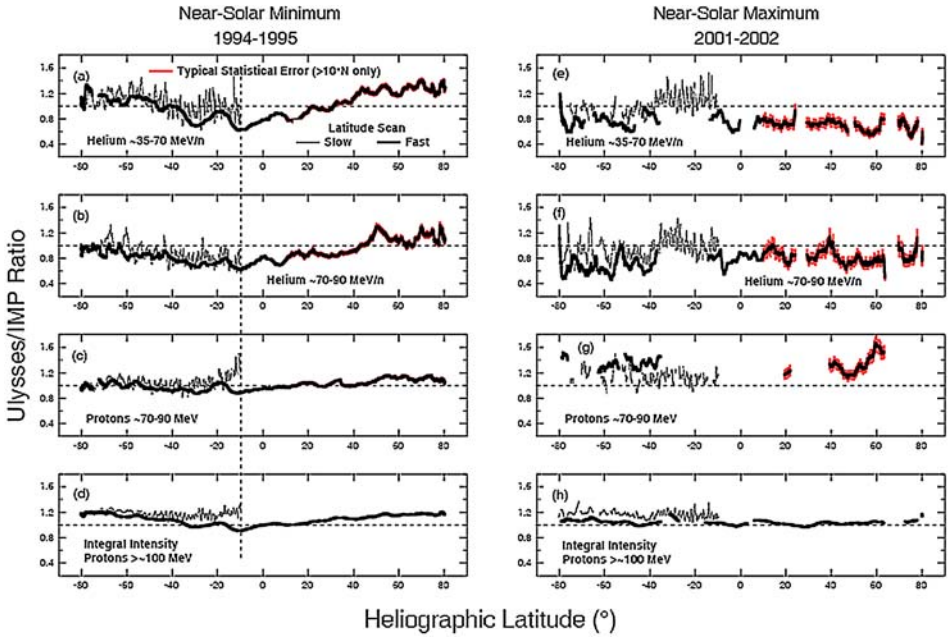

Figure 40. Temporal variations as a function of latitude in the ratios of normalized count rates measured simultaneously at Ulysses by the COSPIN HET and at Earth (IMP 8 instrument), for protons and helium in several energy ranges as noted in the panels. Panels on the left contain observations from Ulysses' first (solar minimum) orbit, and panels on the right contain observations from the second (solar maximum) orbit. The heavy dark lines identify observations taken during the fast latitude scans, which provide the most definitive information concerning cosmic ray latitudinal gradients. Gray lines identify observations made during the climb to high southern latitude from aphelion (light line) and the return to low latitudes (heavy line) following the north polar pass (McKibben *et al.*, 2003).

intensities have been taken into account by using the ratios of the Ulysses to IMP 8 count rates. These ratios are shown as a function of heliographic latitude for the solar minimum first orbit (left panels) and the second orbit, at solar maximum (right panels). While there are significant fluctuations in all panels, it follows that during solar minimum a clear latitude gradient existed for all species during both the slow latitude scans (between Jupiter and the polar regions) and the fast latitude scan (from the south polar region through perihelion and on to the north polar region), as discussed in the previous section. The gradient measurements during solar maximum are displayed in the right panels of Figure 40. The fluctuations were of the order of 2 and larger than during the solar minimum scan. Thus, there is no evidence for a measurable gradient larger than the fluctuations (see also Heber *et al.*, 2002b, 2003 and McKibben *et al.*, 2003). McKibben (2005) attributed the small rise in the Ulysses to IMP ratio, observed as Ulysses returned to the ecliptic near 5 AU, as a radial gradient of the order of 4–8%/AU, consistent with the

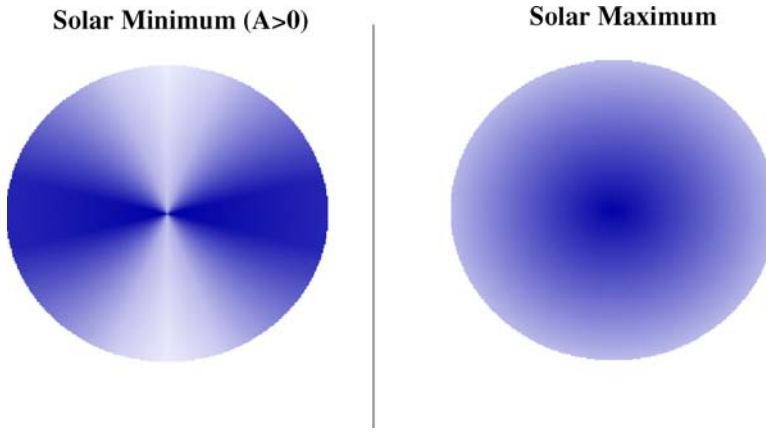

Figure 41. Meridional cut of the >2 GeV protons spatial distribution in a sphere of ∼2 AU radius during solar minimum (a) and solar maximum (b). Thus the two panels show the reconfiguration of the cosmic ray distribution towards spherical symmetry at solar maximum (Belov *et al.*, 2003). Such structures are confirmed by model calculations by Haasbroek and Potgieter (1995b) and Langner and Potgieter (2005).

measurements by Heber *et al.* (2002b) and with previous measurements of the radial gradient in the inner heliosphere as summarized by Webber and Lockwood (1999).

Belov *et al.* (2003) derived radial and latitudinal gradients for >2 GeV/nucleon protons and alpha-particles by using data from the Kiel Electron Telescope, the Chicago instrument on board IMP 8 and the neutron monitor network. To visualize the differences between the mean cosmic ray distribution at solar minimum in 1994 to 1996 and around solar maximum from mid-1999 to mid-2001, Figure 41 displays these distributions within a sphere of 5 AU radius, respectively. To obtain the solar minimum distribution they used $G_r = 0.5\%$/AU, $G_\theta = 0\%$/degree for $|\theta| < 15^\circ$, otherwise $G_\theta = 0.19\%$/degree. To obtain the solar maximum distribution, a constant radial gradient of 4%/AU was applied. In contrast to solar minimum, their analysis indicates a spherically symmetric distribution of cosmic rays around solar maximum, also the conclusion of the modeling work by Ferreira *et al.* (2003) and Ferreira and Potgieter (2004).

Heber *et al.* (2002b), Belov *et al.* (1999), and McDonald *et al.* (2001) showed that the radial gradient was increasing in 1997 to 1998. Thus Belov *et al.* (2003) and Heber *et al.* (2002b) suggested that the transformation from the minimum to the maximum distribution must have occurred around mid-1999, when the spacecraft was well below the heliographic equator, allowing for a good determination of latitudinal effects.

Another important conclusion can be made by the comparison of the spatial distributions displayed in Figure 41. Since latitudinal gradients were positive at solar

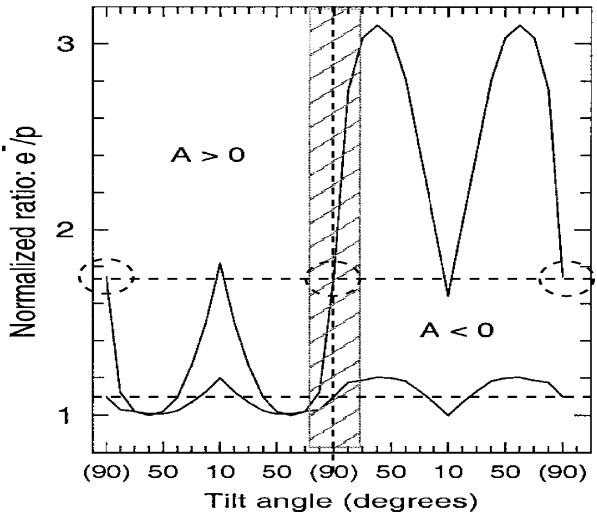

Figure 42. Computed normalized ratio of cosmic ray electron to proton intensities at Earth, for 1 GV (upper line) and 3 GV (bottom line), as a function of tilt angle for the two polarity cycles. Shaded area represents time of maximum modulation with a theoretical tilt angle of 90° (Potgieter *et al.*, 2001).

minimum in the last cycle and vanishing thereafter, the modulation at polar latitudes must have become relatively larger during this transition than in the ecliptic.

5.3. The Electron to Proton Ratio

At each sunspot maximum the solar magnetic dipole reverses its direction. Since particles undergo drifts in the large scale heliospheric magnetic field, the temporal variation of the cosmic ray intensity depends on the current sheet tilt angle. Figure 42 from Potgieter *et al.* (2001) displays the computed variation of the electron to proton ratio as a function of this tilt angle by using a series of steady state model runs. Since they included full drifts such an approach leads to a characteristic variation of the electron to proton ratio over the 22-year (Hale) cycle. Starting at solar maximum in an $A > 0$ solar magnetic epoch the electron to proton ratio is first decreasing and then increasing with decreasing solar activity. Because protons drift primarily into the inner heliosphere over the polar regions they are recovering more quickly than electrons. When the tilt angle is below $\sim 60^\circ$ the recovery of cosmic ray protons to solar minimum values is nearly completed, and only small intensity increases are observed from then on. In contrast the intensity of galactic cosmic ray electrons, drifting in along the heliospheric current sheet, varies little with the tilt angle when it is above $\sim 60^\circ$. Below that value electrons become more sensitive to the variation of the tilt angle, leading to an increase of the electron to proton ratio when the heliosphere approaches solar minimum conditions. With the approach to

solar maximum, the electron intensity is first decreasing stronger than the proton intensity. From tilt angles of above $\sim 60^\circ$, the proton intensity, however, starts to decrease more quickly, leading to a flattening in the electron to proton ratio and an increase again towards solar maximum. With the reversal from an $A > 0$ to an $A < 0$ solar magnetic epoch the drift pattern reverses so that electrons recover more quickly for large tilt angles than protons. When the tilt is small enough protons start to recover while the intensity of the electrons stays high, leading to a M-shaped profile during a whole $A < 0$ epoch until a solar magnetic field reversal is reached at solar maximum. Note that the expected ratio reaches the same value at consecutive solar maxima, independent of the magnetic epoch changing from an $A < 0$ to an $A > 0$ epoch or vice versa. This is indicated by the inserts, ($-$ to $+$) and ($+$ to $-$), in Figure 43.

Such an approximation is appropriate for solar minimum activity periods when the tilt angle only changes slowly with time. Close to solar maximum time dependent effects become more important. However, computations with a time dependent model show qualitatively the same result (Ndiitwani *et al.*, 2005). Therefore, Ulysses observations can be used to determine the time period in which the heliospheric magnetic field switched its polarity.

In Figure 43 the Ulysses radial distance and heliographic latitude are shown together with the solar magnetic field strength observed in northern and southern solar polar regions, the sunspot number and the tilt angle. The solar magnetic field and tilt data are taken from http://quake.Stanford.EDU:80/∼wso/. From the third panel it is obvious that the polarity of the magnetic field switches around solar maximum. As an example the northern (southern) hemisphere changed from a positive (negative) to a negative (positive) magnetic field strength in the first half of 2000, as indicated by the dashed line. Ulysses was launched in the declining phase of solar cycle 22, when the solar magnetic field switched or already had switched from an $A < 0$ to an $A > 0$ epoch. The observation of equal gradient for electrons and protons by Clem *et al.* (2002) supports the assumption that observed variations of the electron to proton ratio is due to temporal changes, although Ulysses moved out to 5 AU within a year (see first panel). In 2000 and 2001 when Ulysses was at polar latitudes the magnetic field switched from an $A > 0$ to an $A < 0$ epoch. From what we discussed in the last paragraph the electron to proton ratio is again expected to be the same as in 1990. Due to the Ulysses trajectory this statement is only valid if the assumptions that the latitudinal gradients were zero for both charge signs was fulfilled. The radial variation of the spacecraft is small during the rapid pole to pole transit, so that minor differences in the radial gradient would not alter the conclusion. Since the latitudinal gradient of nuclei is consistent with zero during that period, a significant electron gradient would reflect the systematic variation of the Ulysses trajectory (second panel of Figure 43).

The grey curve in Figure 44 displays the measured electron to proton ratio at a rigidity of 2.5 GV from Ulysses' launch to the end of 2004. It is evident that the electron to proton ratio was decreasing at the beginning of the mission, and

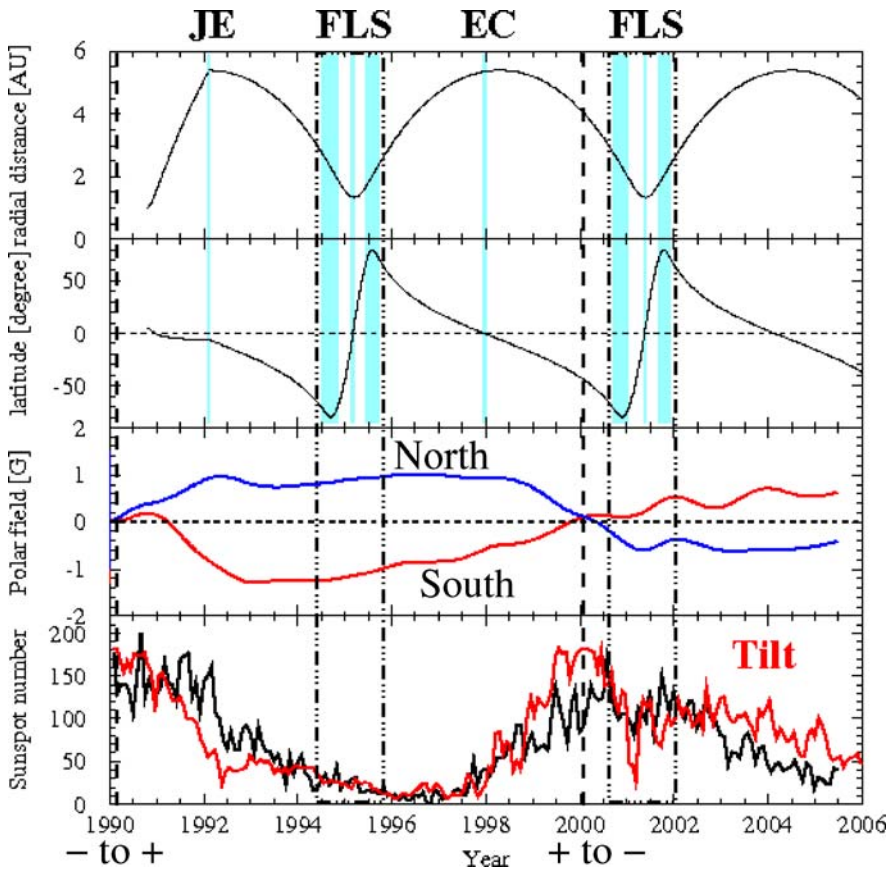

Figure 43. From top to bottom: Ulysses' radial distance and heliographic latitude, the strength of the solar polar magnetic field as derived by the Wilcox Solar Observatory, sunspot number and tilt angle. Marked by shading are the two Ulysses' fast latitude scans and the time of the solar magnetic field reversal derived from the solar polar magnetic field strength.

increasing from mid-1999 onwards. This behavior was expected from the model predictions by Potgieter *et al.* (2001); see also Ferreira and Potgieter (2004) and Ndiitwani *et al.* (2005). The horizontal box is chosen such that it covers the measured range early in the mission. The dashed box indicates the period when the values are again the same as in 1990. Therefore, the earliest possible date for the solar magnetic field reversal would be during the fast latitude scan. This result is consistent with Ulysses magnetic field measurements. Jones *et al.* (2003) reported no clear evidence for the reversal during the southern polar pass of the spacecraft. When the spacecraft was above 70°N in 2001 a uniform magnetic field polarity was measured. The reversal must have been occurred between late-2000 and mid-2001. Unfortunately Ulysses cannot continue into the next solar maximum in 2012, so that galactic

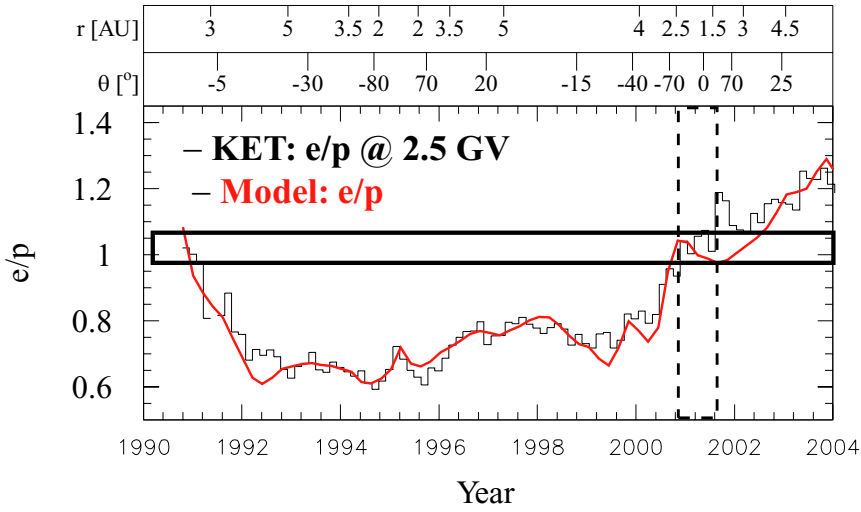

Figure 44. Variation of the electron to proton ratio at 2.5 GV. Marked by the vertical box of ∼1 year is the time period in 2000 when the observed electron to proton ratio was between 0.95 and 1.05. Model results are from Ferreira *et al.* (2003).

cosmic ray observations of both charge signs will be needed from another mission for this ideal tool to investigate the Sun's polarity reversal.

5.4. Solar Energetic Particles

During solar maximum, the dominant feature of the low energy electron and proton time histories is the frequent increases due to the injection of particles at the Sun (Dalla *et al.*, 2003; McKibben *et al.*, 2003; McKibben,2005; Struminsky *et al.*, 2005; Sanderson, 2005). Figure 45 from McKibben *et al.* (2003) displays the intensity of 35–70 MeV and 70–95 MeV protons measured by Ulysses and by IMP 8 close to Earth during the period from the south polar pass of Ulysses in 2000 to the north polar pass in 2001. The bottom panels (c) and (d) show the latitude and longitude (with respect to the central meridian as observed from Earth) of the initiating events on the Sun, together with the positions of the footpoints on the Sun of an ideal Parker spiral field lines through IMP 8 (blue) and Ulysses (red, salmon) for the solar wind velocities indicated (for further details, see McKibben *et al.*, 2003).

Essentially all large events at Earth in Figure 45 also produce comparable intensity increases at Ulysses. Dalla *et al.* (2003) investigated the onset time of 8 selected high latitude events. Also the onset of the events at high latitudes are delayed and the delay is ordered by Ulysses latitude. Struminsky *et al.* (2005) emphasized the similarity of all these 8 events during the first days. McKibben *et al.* (2003) reported on nearly equal particle intensities at Ulysses and close to Earth after 3–4 days.

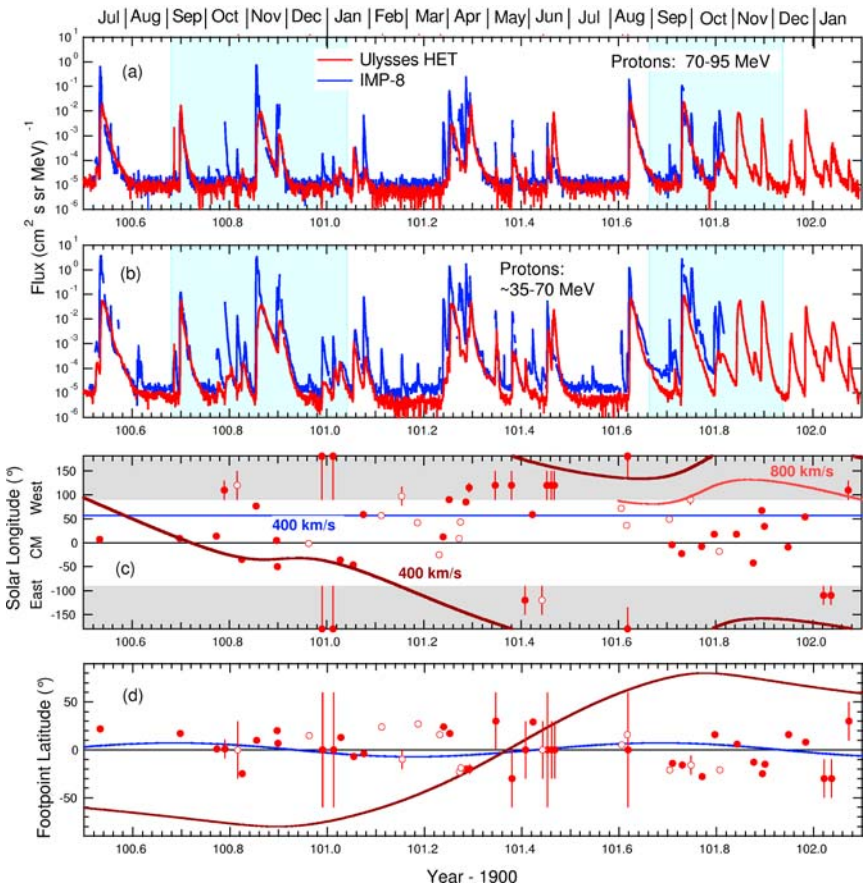

Figure 45. From top to bottom: 70–95 MeV and 35–70 MeV protons measured at IMP 8 (blue) and Ulysses (red) during the solar maximum polar passes and the fast latitude scan. Marked by shading are the periods when Ulysses latitude was above 70°. Panel (c) displays the locations in longitude with respect to central meridian observed from Earth of solar flares associated with solar energetic particle events observed at IMP 8. Solid dots indicate events observed both at Ulysses and IMP 8. Open dots correspond to events producing particle increases observed only at IMP 8. Estimated uncertainties in the position are shown as error bars. Gray shading indicates the invisible hemisphere of the Sun. Flare locations from McKibben *et al.* (2003). Red (or salmon) and blue curves show the location of the footpoints on the Sun of an ideal Parker spiral magnetic field lines through IMP 8 (blue) and Ulysses (red, salmon) for the solar wind velocities indicated (McKibben *et al.*, 2003).

After formation, the apparent 'reservoir' seemed to slowly dissipate as a result of the normal diffusion, convection, adiabatic cooling, and drift mechanisms that govern both the propagation of solar energetic particles and the solar modulation of cosmic rays. A similar 'reservoir' effect had been observed already in the 1970's (McKibben, 1972). It may also be related to the super-events discussed by Dröge *et al.* (1991).

In fact, without knowledge of Ulysses position during the fast latitude scan, it would be very difficult to distinguish between the high-latitude and low-latitude measurements. Thus McKibben *et al.* (2003) concluded that either an acceleration front for energetic particles in large events extended over a broad range in latitude and longitude, or that mechanisms existed to transport particles efficiently along and across the mean magnetic field. The observation of the 'reservoir' effect favors, however, the existence of effective cross-field transport.

5.5. Jovian Electrons

As discussed above, the studies of Jovian electron propagation at solar minimum provided new insights on the radial and latitudinal transport coefficients at solar minimum. For the periods from 1991 to 1998 no time-dependent changes in the transport parameters were necessary to compute realistic electron modulation. Figure 46 from Ferreira *et al.* (2003) displays in the first panel the measured 3–10 MeV electron intensity time profile together with calculations using the set of parameters found by Ferreira *et al.* (2001c). The lower two panels show the relative contribution of

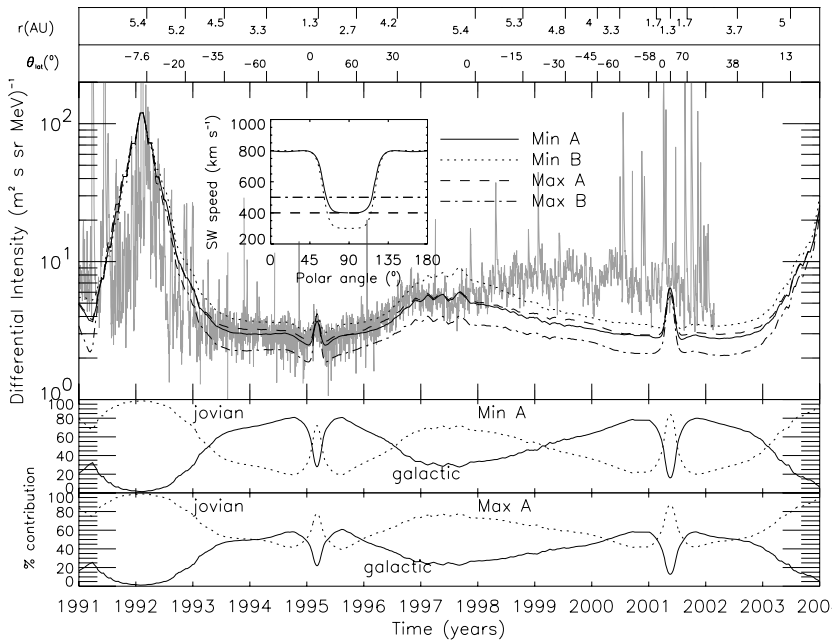

Figure 46. From top to bottom: Ulysses distance from the Sun and its heliographic latitude. Measured 3–10 MeV electrons together with different model computations corresponding to four different assumed scenarios for the solar wind speed V, displayed in the insert. The relative contribution of the Jovian (dotted line) and galactic electrons (solid line) to the total electron intensity for the Min A and Max A scenarios are calculated (Ferreira *et al.*, 2003).

Jovian and galactic cosmic ray electrons to the model calculations. From the figure it is evident that the computed intensities are considerably lower than what was observed onboard Ulysses at solar maximum periods, e.g., after 1998 (see also Heber *et al.*, 2002a). This discrepancy initiated the studies by Ferreira *et al.* (2003), Ferreira *et al.* (2004b) and Moeketsi *et al.* (2005). They investigated and reported on the following modulation issues as discussed below:

- What is the influence of realistic solar wind profiles consistent with the observations on the 3–10 MeV electron flux at solar maximum?
- Does an increase of the Jovian source strength with the solar cycle describe the Ulysses observations?
- How must the diffusion tensor be changed with increasing solar activity, in particular $\kappa_{\perp\theta}$, in order to describe the Ulysses observations at solar maximum?

5.5.1. *Influence of the Solar Wind*

The calculated effects of different solar wind scenarios on the modulation of these electrons along the Ulysses trajectory are shown and compared to the actual Ulysses measurements in Figure 46. Two of the four different scenarios, shown in the insert, are applicable to solar maximum and to solar minimum conditions respectively and are motivated by the Ulysses observations (McComas *et al.*, 2001; Richardson *et al.*, 2001): The Min A and Min B scenarios correspond to the assumption that V increases from 300 km/s and from 400 km/s in the equatorial plane to 800 km/s at the poles. The transition from the slow to the fast solar wind is taken at 60° and 120° colatitude. In contrast, the Max A and Max B scenarios correspond to solar maximum conditions with V on average 400 km/s and 500 km/s at all latitudes, respectively. Comparing the Min A and Max A computations with each other no large differences can be found, and good compatibility with the data is evident up to ∼1998. The intensities using the Min B and Max B parameters result in computed intensities higher and lower than the two A scenarios. Since the Max B results in too small computed intensities for both solar minimum and solar maximum conditions this scenario is less suitable than the other cases. However, none of the computed electron intensities fit the Ulysses observations after ∼1998, illustrating that improved V profiles alone cannot explain the observations around solar maximum; see also Moeketsi *et al.* (2005).

5.5.2. *Effects of a Stronger Jovian Electron Source*

The finding of Morioka *et al.* (1997) that due to the changes in the solar wind pressure at Jupiter, higher Jovian electron intensities could be expected around solar maximum was used by Ferreira *et al.* (2003) and Moeketsi *et al.* (2005) to investigate the consequence of such a stronger source, with consequent intensity increases, on the Ulysses 3–10 MeV intensity-time profile from 1998 to 2002. A realistic increase of a factor of 2 was incorporated in the model. However, they found that in order to describe the observations from 1998 to the end of 1999 a

gradual increase of the source strength by a factor of four was needed but using such a value led to three times larger intensities than observed during Ulysses' ecliptic plane crossing in 2001. Ferreira *et al.* (2003) and Moeketsi *et al.* (2005) concluded that using a large increase in the variation of the Jovian source strength alone could not explain the Kiel Electron Telescope measurements towards solar maximum.

5.5.3. *Temporal Variation of the Diffusion Tensor*

Ferreira *et al.* (2004a) showed that in addition to changes in the solar wind speed and the source strength, a reduction in the enhancement of perpendicular transport, $\kappa_{\perp\theta}$, towards the poles was required for solar maximum periods to explain the Ulysses observations shown in the upper panel of Figure 47. The computed results are displayed using a ratio of $b = \kappa_{\parallel}/\kappa_{\perp\theta} = 0.04$ in the ecliptic plane and different values for the increase d towards the poles. The best fit to the data is obtained for $d = 1$, which means no latitude dependence of $\kappa_{\perp\theta}$. The two lower panels of the figure display the variation of the Jovian and galactic cosmic ray component, respectively. For $b = 0.04$ in Equation (14), the computed intensity along the Ulysses trajectory was almost always Jovian dominated, except for a few months when the spacecraft was at polar latitudes. This indicates that this scenario may be more feasible in explaining the observation of quiet time electron increase observed by Ulysses at $\sim 40°$N. (Heber *et al.*, 2002a) and is more consistent to diffusion coefficients simulations done by, e.g., Giacalone and Jokipii (1999). Ferreira *et al.* (2004a) concluded therefore that in order to explain the Kiel Electron Telescope observations of low-energy electrons after 1998, the vanishing galactic cosmic ray gradients and some properties of solar particle events at polar latitudes, little enhancement of $\kappa_{\perp\theta}$ with increasing solar activity is required in the model and can be associated to the disappearance of the fast solar wind and/or the vanishing of a heliospheric magnetic field with a meridional component.

6. Summary and New Insights from Ulysses

The main scientific goal of the joint ESA-NASA Ulysses deep-space mission was to make the first-ever measurements of the unexplored region of space above the solar poles. The Ulysses scientific investigations encompass studies of the heliospheric magnetic field, heliospheric radio and plasma waves, the solar wind plasma including its minor heavy ion constituents, solar and interplanetary energetic particles, galactic cosmic rays and the anomalous cosmic ray component. Here we concentrated on observations which are relevant for the understanding of cosmic ray measurements in the polar regions in relation to the solar wind and the magnetic field investigations.

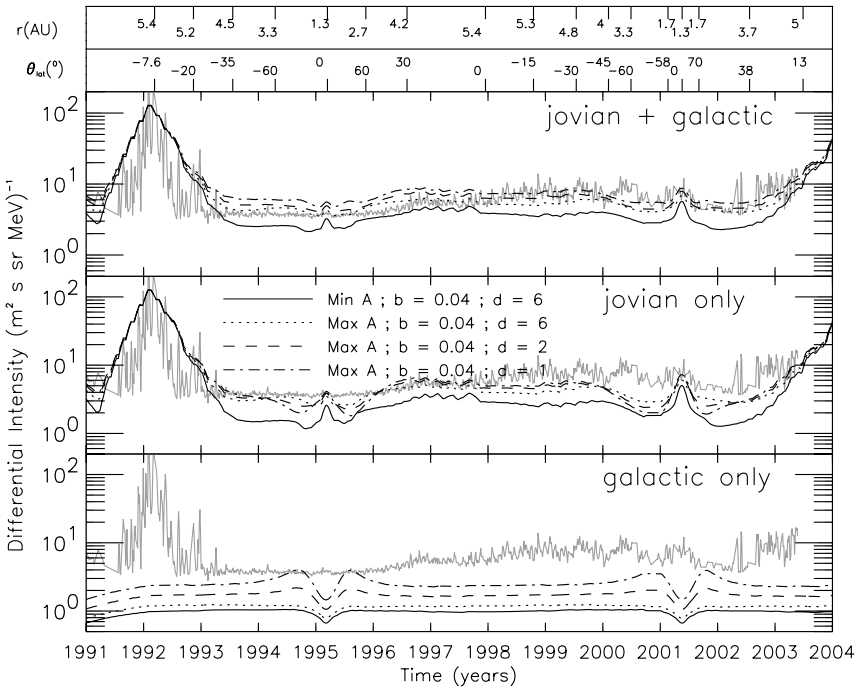

Figure 47. Measured and computed ∼7 MeV Jovian and galactic electron intensities along the Ulysses trajectory (Ferreira *et al.*, 2004a). The middle and lower panels display the Jovian and galactic intensities, respectively. The computed curves represent four different scenarios for $\kappa_{\perp\theta}$. For details see the associated text.

6.1. Solar Wind and the Heliospheric Magnetic Field

The Ulysses mission firmly established with in-situ observations that at solar minimum the solar wind is not uniform. Always directed away from the Sun, it changes speed and carries with it disturbances and interacting regions. The speed is high (800 km/s) above coronal holes and low (300 km/s) above the streamer belt. During most of the solar cycle, the solar wind at high latitudes is almost uniformly fast, while at lower latitudes the speed may vary. The magnetic field is uniformly directed in and outwards over the southern and northern hemisphere, respectively, during the $A > 0$ solar magnetic minimum epoch. Another unexpected observation from the magnetic field investigation was the measurement of long-lasting Alfvén waves in the fast solar wind regime.

At solar maximum, the solar wind exhibits a remarkably different and complicated structure than during solar minimum. The polar wind speed is then slower and gustier than at other times. The magnetic field around solar maximum could not be explained by a highly tilted dipole only.

6.2. Highlights of Cosmic Rays at High Heliolatitudes

Ulysses observations during solar minimum are ideally suited to investigate the spatial structure and its consequences for our understanding of particle propagation in the inner heliosphere. In what follows we summarize first the observations for solar minimum:

Spatial gradients and the local interstellar spectra: A particular motivation of Ulysses mission was to explore the possibility of observing cosmic ray intensities close to the local interstellar values over the solar poles in an $A > 0$ solar magnetic epoch. Especially protons below several 100 MeV should have had large positive latitudinal gradients and their intensity should have increased by an order of magnitude. Electrons on the other hand were expected to show negative latitudinal gradients. But in contrast to this expectation the proton spectrum was highly modulated and Ulysses did not observe the local interstellar spectra at polar latitudes. The variation of the electron intensities was dominated by temporal changes and not by an intensity change correlated with Ulysses latitude. Thus the latitudinal gradient of electrons is consistent with zero. The observed latitudinal gradient of cosmic ray protons in the inner heliosphere at solar minimum is small and shows a maximum at $\sim$2 GV. These observations had a significant impact on our understanding of particle transport in the heliospheric magnetic field. Especially, it was found that the two elements of the diffusion tensor perpendicular to the mean magnetic field scale differently from each other. This was not expected and is still not very well understood from a turbulence theory approach. It makes the modeling of cosmic rays much more demanding but also more interesting.

Jovian electrons at high heliolatitudes: Since Jupiter is a non central source of electrons with respect to the heliospheric magnetic field, Jovian electrons provide a handy tool to investigate the particle propagation properties in the inner heliosphere. Using the Ulysses electron observations the diffusion tensor at low rigidities ($<$100 MV) could be investigated in great detail. A major result of this analysis is the different particle propagation properties in the two solar wind regimes. Especially the large anisotropy of the two perpendicular components still awaits its microphysical explanation.

Recurrent events and cosmic ray decreases at high heliolatitudes: Since measurements with space probes in interplanetary space became available it has been known that recurrent variations in the energetic particle intensities are observed in association with the occurrence of recurrent fast and slow solar wind streams. Normally, the passage of corotating interaction regions causes recurrent depressions in the cosmic ray flux and MeV/n nuclei and keV electron intensity increases centered around the forward and reverse shock. From latitudes above 40° Ulysses had been embedded in the fast solar

wind stream originated from the southern polar coronal hole. As expected corotating forward and reverse shock waves disappeared. But in contrast to what had been expected, recurrent particle increases and galactic cosmic ray decreases were observed up to polar latitudes. Even more surprising was the fact that the 40–65 keV electrons were delayed from the 0.5-1.0 MeV protons by up to 4 days. To explain this observations two competing proposals have been put forward:

1. One explanation is that because of enhanced latitudinal diffusion the temporal variation at high heliolatitudes is determined by the interaction regions at low latitudes. The delay is than explained by the details of the diffusion process, especially perpendicular diffusion.

2. The second explanation relies on the analysis of the Ulysses magnetic field data which showed that the polar magnetic field was dominated by strong variations. Systematic modifications of the standard Parker theory of the heliospheric magnetic field would then cause a meridional field component along which particles may move easily to polar latitudes.

Since both proposals explain the observations equally well, only magnetic field measurements in the distant, high latitude heliosphere where the systematic effects will be larger than the statistical variation may prove which one is correct.

The North-South-asymmetry and its consequences: A real surprise of the Ulysses mission was the observation that the galactic cosmic ray flux was not symmetric to the heliographic equator. Neither the solar wind experiments nor the magnetic field investigations reported this asymmetry. Only five years later magnetic field investigations from 1 AU measurements confirmed a deficit of the magnetic flux in the southern hemisphere. It remains an open question whether this observation was an occurrence of events that pertained during the rapid pole to pole passage of Ulysses or is correlated to a permanent magnetic flux deposit in the southern heliosphere.

The Ulysses orbit is ideally suited to investigate the variation in the latitudinal dependence of charged particles in the inner heliosphere at solar minimum and at solar maximum. The heliospheric magnetic structure during solar maximum is characterized by a highly inclined current sheet that was distorted by coronal mass ejections at all latitudes. In what follows we summarize the observations around solar maximum activity:

Gradients and charge sign dependence at solar maximum: Gradient measurements during solar maximum exhibited fluctuations of the order of 2 and larger so that no unambiguous evidence could be found for latitudinal cosmic ray gradients. In contrast to solar minimum conditions, the cosmic ray distribution was almost spherically symmetric around solar maximum, consistent with model computations. From this the important conclusion was

made that since the latitudinal gradients were positive at solar minimum, the total modulation is relatively higher at polar latitudes than in the ecliptic.

Model computations predicted the electron to proton ratio to have a W-shape in $A > 0$ epochs and a M-shape during $A < 0$ epochs, with the ratio always decreasing from large values to small values during solar maximum in a $A < 0$ to $A > 0$ transition, but increasing from a $A > 0$ to $A < 0$ transition. The ratio should however return to the same values during every reversal. This was confirmed by the Ulysses observations. It was concluded that less than 10% drifts was required at extreme solar maximum to explain the observations when the magnetic field reversed. The proton to electron intensity ratios turned out to be an excellent indicator of when the magnetic field actually reversed. It was found that the reversal must have occurred between late 2000 and mid-2001.

Particle events and the reservoir effect: It was found for 35–70 MeV and 70–95 MeV protons that essentially all large events at Earth also produce comparable intensity increases at Ulysses during the period from Ulysses south polar pass in 2000 to the north polar pass in 2001. The onset of the events at high latitudes are delayed and the delay is ordered by Ulysses' latitude emphasized the similarity of all studied events during the first days of this part of the Ulysses trajectory. Nearly equal particle intensities at Ulysses and close to Earth occurred after 3–4 days. After formation, this 'reservoir' slowly dissipates as a combined result of normal modulation processes. A similar 'reservoir' effect was observed in the 1970's. Without Ulysses' fast latitude scan, it would have been very difficult to distinguish between these high-latitude and low-latitude measurements. Thus it was concluded that either an acceleration front for energetic particles in large events extends over a broad range in latitude and longitude, or that mechanisms exist to transport particles efficiently across the mean magnetic field close to the Sun.

In what follows we further focus on the new insights on particle propagation and its correlation with a turbulent astrophysical plasma.

6.3. Insights on Particle Propagation

The Ulysses mission to high heliolatitudes led to several insights concerning propagation and modulation theory in particular the relative importance of the various diffusion coefficients. It was concluded that in order to obtain agreement between current modulation models and Ulysses observations, enhancing $\kappa_{\perp\theta}$ latitudinally and changing the rigidity dependence of $\kappa_{\perp\theta}$ differently from $\kappa_{\parallel}$ was essential. The latitudinal enhancement is related to the different solar wind regimes observed around solar minimum.

The observed electron to proton ratios (implicitly also containing the radial and latitudinal gradients) indicated that large particle drifts were occurring during solar

minimum but diminished significantly toward solar maximum when less than 10% drifts were required in models to explain the observed values.

These combined observational and modeling studies initiated new projects concerning diffusion and turbulence theories which have become known as the 'ab initio' approach to modulation theory and modeling, with exceptional progress being made the past few years.

6.4. Cosmic Ray Modulation Surprises from Ulysses

From the Ulysses cosmic ray observations and corresponding modulation modeling it is evident that cosmic rays studies have led to new and surprising insights from large scale phenomena like the global magnetic field to microphysical processes like the wave particle interaction. In what follows we conclude with listing the most important cosmic ray modulation surprises according to the scale they operate in the heliosphere:

Large scale

- A North-South-asymmetry in cosmic ray modulation with respect to the heliospheric equator.
- Small latitudinal gradients, implying that the local interstellar spectra cannot be observed in the inner polar regions of the heliosphere.
- Essentially no latitudinal gradients and little drifts at solar maximum.

Intermediate scale

- Recurrent particles events at high heliolatitudes without direct corresponding evidence in the solar wind and magnetic field.
- Jovian electrons at high heliolatitudes and the consequently implied effective latitudinal transport.

Micro scale

- The latitudinal enhancement of perpendicular diffusion in the polar direction.
- The difference in the rigidity dependence of latitudinal and radial perpendicular diffusion.

The above mentioned topics will become even more important, for comparative reasons, when the spacecraft will perform its third rapid pole to pole passage in 2007 and 2008.

Acknowledgements

This work was partially funded within the framework of the bi-lateral collaboration programme between South Africa and Germany by the Deutsche Forschungsgemeinschaft (DFG) and the South African Research Foundation (NRF). The ULYSSES/KET project is supported under grant No. 50 ON 9103 by the German Bundesminister für Wirtschaft through the Deutsches Zentrum für Luft- und Raumfahrt. We thank Gerd Wibberenz, Horst Fichtner, Klaus Scherer, Adri Burger, Stefan Ferreira, and Ulrich Langner for many discussions and insights. We thank Christian Steigies for reading the manuscript carefully and making useful suggestions. We gratefully acknowledge the support of the International Space Science Institute (ISSI) in Bern, Switzerland, where a large part of this review was written during visits in 2005 and 2006.

References

Ahluwalia, H. S. and Kamide, Y.: 2005, *Adv. Space Res.* **35**, 2119–2123.

Balogh, A., Beek, T., Forsyth, R., Hedgecock, P., Marquedant, R., Smith, E., *et al.*: 1992, *Astron. Astrophys. Suppl.* **92**(2), 221–236.

Balogh, A., Smith, E. J., Tsurutani, B. T., Southwood, D. J., Forsyth, R. J., and Horbury, T. S.: 1995, *Science* **268**, 1007–1010.

Bame, S., McComas, D., Barraclough, B., Phillips, J., Sofaly, K., Chavez, J., *et al.*: 1992, *Astron. Astrophys. Suppl.* **92**(2), 237–265.

Belov, A. V., Eroshenko, E. A., Heber, B., Yanke, V. G., Raviart, A., Röhrs, K., *et al.*: 2003, *Ann. Geophys.* **21**, 1295–1302.

Belov, A. V., Eroshenko, E. A., Heber, B., Ynake, V. G., Ferrando, P., Raviart, A., *et al.*: 1999, *Adv. Space Res.* **23**(3), 443–447.

Bieber, J. W. and Matthaeus, W. H.: 1997, *Astrophys. J.* **485**, 655.

Bieber, J. W., Matthaeus, W. H., Smith, C. W., Wanner, W., Kallenrode, M., and Wibberenz, G.: 1994, *Astrophys. J.* **420**, 294–306.

Borrmann, T. and Fichtner, H.: 2005, *Adv. Space Res.* **35**, 2091–2101.

Bryant, D., Cline, T., Desai, U., and McDonald, F.: 1963, *Phys. Res. Lett.* **11**, 144.

Burger, R. A.: 2000, in *AIP Conference Proceedings 516: 26th International Cosmic Ray Conference, ICRC XXVI*, p. 83.

Burger, R. A.: 2005, *Adv. Space Res.* **35**, 636–642.

Burger, R. A. and Hattingh, M.: 1998, *Astrophys. J.* **505**, 244–251.

Burger, R. A. and Hattingh, M.: 2001, in *Proceedings of the 27th International Cosmic Ray Conference*, Vol. 9, pp. 3698–3701.

Burger, R. A. and Hitge, M.: 2004, *Astrophys. J.* **617**, L73–L76.

Burger, R. A. and Potgieter, M. S.: 1989, *Astrophys. J.* **339**, 501–511.

Burger, R. A., Potgieter, M. S., and Heber, B.: 2000, *J. Geophys. Res.* **105**, 27447–27456.

Burger, R. A., van Niekerk, Y., and Potgieter, M. S.: 2001, *Space Sci. Rev.* **97**, 331–335.

Burlaga, L. F., Ness, N. F., Acuña, M. H., Lepping, R. P., Connerney, J. E. P., Stone, E. C., *et al.*: 2005, *Science* **309**, 2027–2029.

Burlaga, L. F., Perko, J., and Pirraglia, J.: 1993, *Astrophys. J.* **407**, 347–358.

Caballero-Lopez, R. A. and Moraal, H.: 2004, *J. Geophys. Res. (Space Phys.)* **109**(A18), 1101.

Cane, H. and Lario, D.: 2005, *Space Sci. Rev.* in press.
Cane, H. V.: 2000, *Space Sci. Rev.* **93**, 55–77.
Chenette, D. L., Conlon, T. F., and Simpson, J. A.: 1974, *J. Geophys. Res.* **79**, 3551.
Clem, J., Evenson, P., and Heber, B.: 2002, *Geophys. Res. Lett.* **29**, doi: 10.1029/2002G.
Conlon, T. F.: 1978, *J. Geophys. Res.* **83**, 541–552.
Conlon, T. F. and Simpson, J. A.: 1977, *Astrophys. J.* **211**, L45–L49.
Crooker, N. U., Siscoe, G. L., Shodhan, S., Webb, D. F., Gosling, J. T., and Smith, E. J.: 1993, *J. Geophys. Res.* **98**(17), 9371–9381.
Cummings, A. C., Stone, E. C., and Webber, W. R.: 1987, *Geophys. Res. Lett.* **14**, 174–177.
Dalla, S., Balogh, A., Krucker, S., Posner, A., Müller-Mellin, R., Anglin, J. D., *et al.*: 2003, *Ann. Geophys.* **21**, 1359–1366.
Decker, R. B., Krimigis, S. M., Roelof, E. C., Hill, M. E., Armstrong, T. P., Gloeckler, G., *et al.*: 2005, *Science* **309**, 2020–2024.
Denskat, K. U., Beinroth, H. J., and Neubauer, F. M.: 1983, *J. Geophys.-Zeitschrift fuer Geophysik (ISSN 0340-062X)* **54**, 60–67.
Desai, M. I., Mason, G. M., Dwyer, J. R., Mazur, J. E., Gold, R. E., Krimigis, S. M., *et al.*: 2003, *Astrophys. J.* **588**, 1149–1162.
Dröge, W.: 2000, *Astrophys. J.* **537**, 1073–1079.
Dröge, W.: 2003, *Astrophys. J.* **589**, 1027–1039.
Dröge, W.: 1994, Technical report, Institut für Reine und Angewandte Kernphysik, Christian-Albrechts-Universität, Kiel. Habilitationsschrift.
Dröge, W.: 2005, *Adv. Space Res.* **35**, 532–542.
Dröge, W., Müller-Mellin, R., and Cliver, E.: 1991, in *Proceedings of the 22nd International Cosmic Ray Conference*, Dublin, Ireland, Vol. 3, pp. 300–303.
Fahr, H.-J.: 2004, *Adv. Space Res.* **34**, 3–13.
Fahr, H. J., Kausch, T., and Scherer, H.: 2000, *Astron. Astrophys.* **357**, 268–282.
Fan, C. Y., Gloeckler, G., and Simpson, J. A.: 1965, in *Proceedings of the 9th International Cosmic Ray Conference*, London, GB, Vol. 1, p. 109.
Ferrando, P., Raviart, A., Haasbroek, L. J., Potgieter, M. S., Dröge, W., Heber, B., *et al.*: 1996, *Astron. Astrophys.* **316**(2), 528–537.
Ferrando, P., Raviart, A., Heber, B., Bothmer, V., Kunow, H., Müller-Mellin, R., *et al.*: 1999, in *Proceedings of the 26th International Cosmic Ray Conference*, Vol. 7, pp. 17–25.
Ferreira, S., Potgieter, M., Heber, B., Fichtner, H., and Burger, R.: 2001a, in *Proceedings of the 27th ICRC*, pp. 3702–3705.
Ferreira, S. E., Potgieter, M. S., Burger, R. A., Heber, B., and Fichtner, H.: 2001b, *J. Geophys. Res.* **106**, 29313–29322.
Ferreira, S. E. S. and Potgieter, M. S.: 2004, *Astrophys. J.* **603**, 744–752.
Ferreira, S. E. S., Potgieter, M. S., Burger, R. A., Heber, B., and Fichtner, H.: 2001c, *J. Geophys. Res.* **106**(A11), 24979–24988.
Ferreira, S. E. S., Potgieter, M. S., and Heber, B.: 2003, *Adv. Space Res.* **32**, 645–650.
Ferreira, S. E. S., Potgieter, M. S., Heber, B., Fichtner, H., and Kissmann, R.: 2003, *Adv. Space Res.* **32**, 669–674.
Ferreira, S. E. S., Potgieter, M. S., Heber, B., Fichtner, H., and Wibberenz, G.: 2004a, *J. Geophys. Res. (Space Phys.)* **109**(A18), 2115.
Ferreira, S. E. S., Potgieter, M. S., and Scherer, K.: 2004b, *Astrophys. J.* **607**, 1014–1023.
Fichtner, H.: 2001, *Space Sci. Rev.* **95**, 639–754.
Fichtner, H.: 2005, *Adv. Space Res.* **35**, 512–517.
Fichtner, H., Potgieter, M., Ferreira, S., and Burger, A.: 2000, *Geophys. Res. Lett.* **27**, 1611.
Fichtner, H., Potgieter, M., Ferreira, S., Heber, B., and Burger, R. : 2001, in *Proceedings of the 27th ICRC*, p. 3666.

Fichtner, H., Sreenivasan, S. R., and Fahr, H. J.: 1996, *Astron. Astrophys.* **308**, 248–260.
Fisk, L. A.: 1976, *J. Geophys. Res.* **81**(.10), 4646–4650.
Fisk, L. A.: 1979, in *AIP Conference Proceedings 56: Particle Acceleration Mechanisms in Astrophysics*, pp. 63–79.
Fisk, L. A.: 1996, *J. Geophys. Res.* **101**, 15547–15554.
Fisk, L. A.: 1999, *Adv. Space Res.* **23**, 415–423.
Fisk, L. A. and Jokipii, J. R.: 1999, *Space Sci. Rev.* **89**, 115–124.
Florinski, V., Zank, G. P., and Pogorelov, N. V.: 2003, *J. Geophys. Res. (Space Phys.)* **108**, 1.
Forbush, S. E.: 1946, *Phys. Rev.* **70**, 771.
Forman, M. A., Jokipii, J. R., and Owens, A. J.: 1974, *Astrophys. J.* **192**, 535–540.
Forsyth, R. J., Balogh, A., Horbury, T. S., Erdoes, G., Smith, E. J., and Burton, M. E.: 1996, *Astron. Astrophys.* **316**, 287–295.
Forsyth, R. J., Balogh, A., and Smith, E. J.: 2002, *J. Geophys. Res. (Space Phys.)* (A11), 19.
Fujii, Z. and McDonald, F. B.: 2001, *Adv. Space Res.* **27**, 559–564.
Garcia-Munoz, M., Mason, G. M., and Simpson, J. A.: 1973, *Astrophys. J.* **182**, L81.
Giacalone, J. and Jokipii, J. R.: 1999, *Astrophys. J.* **520**, 204–214.
Gleeson, L. J. and Axford, W. I.: 1967, *Astrophys. J.* **149**, L115.
Gloeckler, G., Geiss, J., Balsiger, H., Fisk, L. A., Galvin, A. B., Ipavich, F. M., *et al.*: 1993, *Science* **261**, 70–73.
Haasbroek, L. J. and Potgieter, M. S.: 1995a, *Space Sci. Rev.* **72**, 385.
Haasbroek, L. J. and Potgieter, M. S.: 1995b, *Space Sci. Rev.* **72**, 385.
Hamilton, D. C. and Simpson, J.: 1979, *Astrophys. J.* **228**, L123–L127.
Hattingh, M.: 1998, Ph.D. thesis, Potchefstroom University, South Africa.
Hattingh, M. and Burger, R. A.: 1995, *Adv. Space Res.* **16**, 213.
Hattingh, M., Burger, R. A., Potgieter, M. S., and Haasbroek, L. J.: 1997, *Adv. Space Res.* **19**, 893–896.
Heber, B.: 2001a, *Adv. Space Res.* **27**, 451–460.
Heber, B.: 2001b, in R. Schlickeiser (ed.), *27th International Cosmic Ray Conference. Invited, Rapporteur, and Highlight Papers*, p. 118.
Heber, B., Blake, J. B., Paizis, C., Bothmer, V., Kunow, H., Müller-Mellin, R., *et al.*: 2000, in R. A., Mewaldt, J. R., Jocipii, M. A., Lee, E., Moebius and T. Zurbuchen, (eds.), *Acceleration and Transport of Energetic Particles Observed in the Heliosphere*, pp. 357–360.
Heber, B., Bothmer, V., Dröge, W., Ferrando, P., Haasbroek, L., Kunow, H., *et al.*: 1998, *J. Geophys. Res.* **103**, 4809–4816.
Heber, B. and Burger, R.: 1999, *Space Sci. Rev.* **89**, 125–140.
Heber, B., Dröge, W., Ferrando, P., Haasbroek, L., Kunow, H., Müller-Mellin, R., *et al.*: 1996a, *Astron. Astrophys.* **316**, 538–546.
Heber, B., Dröge, W., Kunow, H., Müller-Mellin, R., Wibberenz, G., Ferrando, P., *et al.*: 1996b, *Geophys. Res. Lett.* **23**, 1513–1516.
Heber, B., Ferrando, P., Paizis, C., Müller-Mellin, R., Kunow, H., Potgieter, M. S., *et al.*: 2001a, in K., Scherer, H., Fichtner, H. J., Fahr and E. Marsch (eds.), *The Outer Heliosphere: The Next Frontiers*, p. 191.
Heber, B., Ferrando, P., Raviart, A., Paizis, A., Posner, C., Wibberenz, G., *et al.*: 2002a, *Astrophys. J.* **579**, 888–894.
Heber, B., Ferrando, P., Raviart, A., Paizis, C., Müller-Mellin, R., and Kunow, H.: 2001b, *Adv. Space Res.* **27**, 547–552.
Heber, B., Ferrando, P., Raviart, A., Wibberenz, G., Müller-Mellin, R., Kunow, H., *et al.*: 1999, *Geophys. Res. Lett.* **26**(14), 2133–2136.
Heber, B., Ferrando, P., Raviart, A., Wibberenz, G., Müller-Mellin, R., Kunow, H., *et al.*: 1999, *Geophys. Res. Lett.* **26**(14), 2133–2136.

Heber, B., Keppler, Marsden, E. R. G., Tranquille, C., Blake, B., and Fränz, M.: 2001c, *Space Sci. Rev.* **97**, 363–366.
Heber, B. and Marsden, R. G.: 2001, *Space Sci. Rev.* **97**, 309–319.
Heber, B., Potgieter, M., and Ferrando, P.: 1997, *Adv. Space Res.* **19**(5), 795–804.
Heber, B. and Potgieter, M. S.: 2000, *Adv. Space Res.* **26**(5), 839–852.
Heber, B., Sanderson, T. R., and Zhang, M.: 1999, *Adv. Space Res.* **23**(3), 567–579.
Heber, B., Sarri, C., Paizis, G., Ferrando, P., Raviart, A., Posner, A., *et al.*: 2003, *Ann. Geophys.* **21**, 1275–1288.
Heber, B., Wibberenz, G., Potgieter, M. S., Burger, R. A., Ferreira, S. E. S., Müller-Mellin, R., *et al.*: 2002b, *J. Geophys. Res.* **107**, doi: 10.10.1029/200.
Hoeksema, J.: 1995, *Space Sci. Rev.* **72**, 137–148.
Jokipii, J. and Kóta, J.: 1989, *Geophys. Res. Lett.* **16**, 1–4.
Jokipii, J. R.: 1966, *Astrophys. J.* **146**, 480.
Jokipii, J. R.: 1973, *Astrophys. J.* **182**, 585–600.
Jokipii, J. R.: 1986, *J. Geophys. Res.* **91**(.10), 2929–2932.
Jokipii, J. R.: 1989, *Adv. Space Res.* **9**, 105–119.
Jokipii, J. R. and Kóta, J.: 2000, *Astron. Astrophys. Suppl.* **274**, 77–96.
Jokipii, J. R. and Kopriva, D. A.: 1979, *Astrophys. J.* **234**, 384–392.
Jokipii, J. R., Kóta, J., Giacalone, J., Horbury, T. S., and Smith, E. J.: 1995, *Geophys. Res. Lett.* **22**, 3385–3388.
Jokipii, J. R. and Parker, E. N.: 1969, *Astrophys. J.* **155**, 799.
Jokipii, J. R. and Thomas, B. T.: 1981, *Astrophys. J.* **243**, 1115–1122.
Jones, G. H., Balogh, A., and Smith, E. J.: 2003, *Geophys. Res. Lett.* **30**, 2.
Kóta, J. and Jokipii, J. R.: 1998, *Space Sci. Rev.* **83**, 137–145.
Kóta, J. and Jokipii, J. R.: 2001a, *Adv. Space Res.* **27**, 529–534.
Kóta, J. and Jokipii, J. R.: 2001b, *Space Sci. Rev.* **97**, 327–330.
Keppler, E.: 1998, *Ann. Geophys.* **16**, 1552–1556.
Keppler, E., Blake, J. B., Hovestadt, D., Korth, A., Quenby, J., Umlauft, G., *et al.*: 1992, *Astron. Astrophys. Suppl.* **92**, 317–331.
Keppler, E., Drolias, B., Fraenz, M., Korth, A., Reuss, M. K., Blake, B., *et al.*: 1996, *Astron. Astrophys.* **316**, 464–480.
Kóta, J. and Jokipii, J. R.: 1983, *Astrophys. J.* **265**, 573–581.
Kota, J. and Jokipii, J. R.: 1991, *Geophys. Res. Lett.* **18**, 1797–1800.
Krimigis, S. M., Decker, R. B., Hill, M. E., Armstrong, T. P., Gloeckler, G., Hamilton, D. C., *et al.*: 2003, *Nature* **426**, 45–48.
Kunow, H., Lee, M. A., Fisk, L. A., Forsyth, R. J., Heber, B., Horbury, T. S., Keppler, E., *et al.*: 1999, *Space Sci. Rev.* **89**, 221–268.
Kunow, H., Wibberenz, G., Green, G., Müller-Mellin, R., and Kallenrode, M.-B.: 1991, in R. Schwenn, and E. Marsch (eds.), *Physics of the Inner Heliosphere*, Vol. 2. Springer-Verlag, Berlin, pp. 243–342.
Langner, U. W., de Jager, O. C., and Potgieter, M. S.: 2001, *Adv. Space Res.* **27**, 517–522.
Langner, U. W. and Potgieter, M. S.: 2004, *J. Geophys. Res. (Space Phys.)* **109**(A18), 1103.
Langner, U. W. and Potgieter, M. S.: 2005, *Astrophys. J.* **630**, 1114–1124.
Langner, U. W., Potgieter, M. S., Fichtner, H., and Borrmann, T.: 2006, *J. Geophys. Res. (Space Phys.)* **111**(A10), 1106.
Langner, U. W., Potgieter, M. S., and Webber, W. R.: 2003, *J. Geophys. Res. (Space Phys.)* (A10), 14.
Langner, U. W., Potgieter, M. S., and Webber, W. R.: 2004, *Adv. Space Res.* **34**, 138–143.
Lanzerotti, J., Gold, R., Anderson, K., Armstrong, T., Lin, R., Krimigis, S., *et al.*: 1992, *Astron. Astrophys., Suppl.* **92**(2), 349–363.

le Roux, J. A.: 2001, in *The Outer Heliosphere: The Next Frontiers, Edited by Klaus Scherer, Horst Fichtner, Hans Jörg Fahr, and Eckart Marsch COSPAR Colloquiua Series*, 11. Pergamon Press, Amsterdam, p. 163.
le Roux, J. A. and Potgieter, M. S.: 1995, *Astrophys. J.* **442**, 847–851.
Lee, M. A. and Fisk, L. A.: 1982, *Space Sci. Rev.* **32**, 205–228.
Leipold, M., Fichtner, H., Heber, B., Groepper, P., Lascar, S., Burger, F., *et al.*: 2003, in *ESA SP-542: Low-Cost Planetary Missions*, pp. 367–375.
Lerche, I. and Schlickeiser, R.: 2001, *Astron. Astrophys.* **378**, 279–294.
L'Heureux, J., Fan, C., and Meyer, P.: 1972, *Astrophys. J.* pp. 363–372.
Lopate, C.: 1991, in *Proceedings of the 22nd ICRC*, p. 415.
Mace, R. L., Matthaeus, W. H., and Bieber, J. W.: 2000, *Astrophys. J.* **538**, 192–202.
Malama, Y. G., Izmodenov, V. V., and Chalov, S. V.: 2006, *Astron. Astrophys.* **445**, 693–701.
Matthaeus, W. H., Qin, G., Bieber, J. W., and Zank, G. P.: 2003, *Astrophys. J.* **590**, L53–L56.
McComas, D. J., Barraclough, B. L., Funsten, H. O., Gosling, J. T., Santiago-Muñoz, E., Skoug, R. M., *et al.*: 2000, *J. Geophys. Res.* **105**(.14), 10419–10434.
McComas, D. J., Elliott, H. A., Gosling, J. T., Reisenfeld, D. B., Skoug, R. M., Goldstein, B. E., *et al.*: 2002, *Geophys. Res. Lett.* **29**, 4–1.
McComas, D. J., Goldstein, R., Gosling, J. T., and Skoug, R. M.: 2001, *Space Sci. Rev.* **97**, 99–103.
McDonald, F., Ferrando, P., Raviart, A., Heber, B., Kunow, H., McGuire, R., *et al.*: 1997, *J. Geophys. Res.* **102**, 4643–4651.
McDonald, F., Fujii, Z., Ferrando, P., Heber, B., Raviart, A., Kunow, H., *et al.*: 2001, in *Proceedings of the 27th ICRC*, p. 3906.
McDonald, F. B.: 1998, *Space Sci. Rev.* **83**, 33–50.
McDonald, F. B., Cline, T. L., and Simnett, G. M.: 1972, *J. Geophys. Res.* **77**, 2213–2231.
McDonald, F. B., Fujii, Z., Heikkila, B., and Lal, N.: 2003, *Adv. Space Res.* **32**, 633–638.
McKibben, R., Heber, R. B. B., McDonald, J. J. F., and Potgieter, M. : 1998, *Space Sci. Rev.* **83**, 188–194.
McKibben, R. B.: 1972, *Bull. Am. Astron. Soc.* **4**, 387.
McKibben, R. B.: 2005, *Adv. Space Res.* **35**, 518–531.
McKibben, R. B., Connell, J. J., Lopate, C., Anglin, J. D., Balogh, A., Dalla, S., *et al.*: 2003, *Ann. Geophys.* **21**, 1217–1228.
McKibben, R. B., Jokipii, J. R., Burger, R. A., Heber, B., Kóta, J., McDonald, F. B., *et al.*: 1999, *Space Sci. Rev.* **89**, 307–326.
McKibben, R. B., O'Gallagher, J. J., Simpson, J. A., and Tuzzolino, A. J.: 1973, *Astrophys. J.* **181**, L9.
McKibben, R. B., Simpson, J. A., Zhang, M., Bame, S., and Balogh, A.: 1995, *Space Sci. Rev.* **72**, 403.
Mewaldt, R. A. and Liewer, P. C.: 2001, in *The Outer Heliosphere: The Next Frontiers*, p. 451.
Minnie, J., Burger, R. A., Parhi, S., Bieber, J. W., and Matthaeus, W. H.: 2003, *Adv. Space Res.* **32**, 567–572.
Minnie, J., Burger, R. A., Parhi, S., Matthaeus, W. H., and Bieber, J. W.: 2005, *Adv. Space Res.* **35**, 543–546.
Möbius, E., Hovestadt, D., Klecker, B., Scholer, M., and Gloeckler, G.: 1985, *Nature* **318**, 426–429.
Moeketsi, D. M., Potgieter, M. S., Ferreira, S. E. S., Heber, B., Fichtner, H., and Henize, V. K.: 2005, *Adv. Space Res.* **35**, 597–604.
Moraal, H.: 2001, in *The Outer Heliosphere: The Next Frontiers, Edited by Klaus Scherer, Horst Fichtner, Hans Jörg Fahr, and Eckart Marsch COSPAR Colloquiua Series*, 11. Pergamon Press, Amsterdam, p. 147.
Moraal, H., Gleeson, L. J., and Webb, G. M.: 1979, in *Proceedings of the 16th ICRC*, Vol. 3. pp. 1–4.
Morioka, A., Tsuchiya, F., and Misawa, H.: 1997, *Adv. Space Res.* **20**, 205–208.

Moskalenko, I. V., Strong, A. W., Ormes, J. F., and Potgieter, M. S.: 2002, *Astrophys. J.* **565**, 280–296.
Ndiitwani, D. C., Ferreira, S. E. S., Potgieter, M. S., and Heber, B.: 2005, *Ann. Geophys.* **23**, 1061–1070.
Paizis, C., Heber, B., Ferrando, P., Raviart, A., Falconi, B., Marzolla, S., *et al.*: 1999, *J. Geophys. Res.* **104**(A12), 28241.
Paizis, C., Raviart, A., Heber, B., Falconi, B., Ferrando, P., Kunow, H., *et al.*: 2001, *Space Sci. Rev.* **97**, 349–354.
Palmer, I. D.: 1982, *Rev. Geophys. Space Phys.* **20**, 335–351.
Parhi, S., Bieber, J. W., Matthaeus, W. H., and Burger, R. A.: 2003, *Astrophys. J.* **585**, 502–515.
Parker, E. N.: 1958, *Astrophys. J.* **128**, 664.
Parker, E. N.: 1963, *Interplanetary Dynamical Processes*, Wiley and Sons, New York.
Parker, E. N.: 1965, *Planet Space Sci.* **13**, 9–49.
Perko, J. S. and Fisk, L. A.: 1983, *J. Geophys. Res.* **88**(.17), 9033–9036.
Pesses, M. E., Eichler, D., and Jokippi, J. R.: 1981, *Astrophys. J.* **246**, L85–L88.
Phillips, J. L., Bame, S. J., Barnes, A., Barraclough, B. L., Feldman, W. C., Goldstein, B. E., *et al.*: 1995, *Geophys. Res. Lett.* **22**, 3301–3304.
Pogorelov, N. V., Zank, G. P., and Ogino, T.: 2006, *Astrophys. J.* **644**, 1299–1316.
Potgieter, M., Ferreira, S. E. S., and Burger, R. A.: 2001, *Space Sci. Rev.* **97**, 295–307.
Potgieter, M., Haasbroek, L., Ferrando, P., and Heber, B.: 1997, *Adv. Space Res.* **19**(6), 917–920.
Potgieter, M. S.: 1989, *Adv. Space Res.* **9**, 21–24.
Potgieter, M. S.: 1998, *Space Sci. Rev.* **83**, 147–158.
Potgieter, M. S., Burger, R. A., and Ferreira, S. E. S.: 2001a, *Space Sci. Rev.* **97**, 295–307.
Potgieter, M. S., Ferreira, S. E. S., Ferrando, P., and Heber, B.: 1999, *Adv. Space Res.* **23**(3), 467–470.
Potgieter, M. S. and Langner, U. W.: 2003, *Adv. Space Res.* **32**, 687–692.
Potgieter, M. S. and Langner, U. W.: 2004, *Adv. Space Res.* **34**, 132–137.
Potgieter, M. S., Langner, U. W., and Ferreira, S. E. S.: 2001b, *Adv. Space Res.* **27**, 523–528.
Potgieter, M. S. and le Roux, J. A.: 1992, *Astrophys. J.* **386**, 336–346.
Potgieter, M. S., Le Roux, J. A., and Burger, R. A.: 1989, *J. Geophys. Res.* **94**, 2323–2332.
Potgieter, M. S. and Moraal, H.: 1985, *Astrophys. J.* **294**, 425–440.
Potgieter, M. S. and Moraal, H.: 1988, *Astrophys. J.* **330**, 445–455.
Quenby, J. J., Drolias, B., Keppler, E., Reuss, M. K., and Blake, J. B.: 1996, *Solar Phys.* **163**, 397–403.
Rastoin, C.: 1995, Ph.D. thesis, Saclay.
Reames, D. V.: 1999, *Space Sci. Rev.* **90**, 413–491.
Richardson, I. G.: 1997, *Using Energetic Particles to Probe the Magnetic Topology of Ejecta*, Vol. 99, pp. 189–198. AGU Geophysical Monograph.
Richardson, I. V.: 2004, *Space Sci. Rev.* **111**, 267–376.
Richardson, J. D., Wang, C., and Paularena, K. I.: 2001, *Adv. Space Res.* **27**, 471–479.
Sanderson, T. R.: 2005, in K. Dere, J. Wang, and Y. Yan (eds.): *IAU Symposium*, pp. 350–360.
Sanderson, T. R., Bothmer, V., Marsden, R. G., Trattner, K. J., Wenzel, K.-P., Balogh, A., *et al.*: 1995, *Geophys. Res. Lett.* **22**, 3357–3360.
Scherer, K. and Fahr, H. J.: 2003, *Geophys. Res. Lett.* **30**, 17.
Scherer, K. and Ferreira, S. E. S.: 2005, *Astrophys. Space Sci. Trans.* **1**, 17–27.
Scherer, K., Fichtner, H., and Stawicki, O.: 2001, in *The Outer Heliosphere: The Next Frontiers, Edited by Klaus Scherer, Horst Fichtner, Hans Jörg Fahr, and Eckart Marsch COSPAR Colloquiua Series*, 11. Pergamon Press, Amsterdam, p. 493.
Scherer, K., Fichtner, H., and Stawicki, O.: 2002, *J. Atmos. Terr. Phys.* **64**, 795–804.
Schlickeiser, R.: 2002, *Cosmic Ray Astrophysics*, Springer, Berlin, London.
Scholer, M., Mann, G., Chalov, S., Desai, M. I., Fisk, L. A., Jokipii, J. R., *et al.*: 1999, *Space Sci. Rev.* **89**, 369–399.

Schwenn, R.: 1990, in R. Schwenn and E. Marsch (eds.), *Physics of the Inner Heliosphere*, Chapt. 3. Springer, Berlin, pp. 99–183.
Shalchi, A., Bieber, J. W., and Matthaeus, W. H.: 2004a, *Astrophys. J.* **604**, 675–686.
Shalchi, A., Bieber, J. W., and Matthaeus, W. H.: 2004b, *Astrophys. J.* **615**, 805–812.
Shalchi, A., Bieber, J. W., Matthaeus, W. H., and Qin, G.: 2004c, *Astrophys. J.* **616**, 617–629.
Shalchi, A. and Schlickeiser, R.: 2004, *Astron. Astrophys.* **420**, 821–832.
Shikaze, Y., Abe, K., and Anraku, K.: 2003, in *International Cosmic Ray Conference*. p. 4027.
Simnett, G. M., Kunow, H., Flückiger, E., Heber, B., Horbury, T., Kóta, J., *et al.*: 1998, *Space Sci. Rev.* **83**, 215–258.
Simnett, G. M., Sayle, K., Roelof, E. C., and Tappin, S. J.: 1994, *Geophys. Res. Lett.* **21**, 1561–1564.
Simpson, J., Anglin, J., Barlogh, A., Bercovitch, M., Bouman, J., Budzinski, E., *et al.*: 1992, *Astron. Astrophys. Suppl.* **92**(2), 365–399.
Simpson, J. A.: 1974, *EOS Trans.* (55), 556.
Simpson, J. A.: 1998, *Space Sci. Rev.* **83**, 7–19.
Simpson, J. A.: 2000, *Space Sci. Rev.* **93**, 11–32.
Simpson, J. A., Hamilton, D., Lentz, G., McKibben, R. B., Mogro-Campero, A., Perkins, M., *et al.*: 1974, *Science* **183**, 306–309.
Simpson, J. A., Zhang, M., and Bame, S.: 1996, *Astrophys. J.* **465**, L69.
Smith, E. J.: 2001, *J. Geophys. Res.* **106**(.15), 15819–15832.
Smith, E. J., Balogh, A., Forsyth, R. J., and McComas, D. J.: 2001, *Geophys. Res. Lett.* **28**, 4159.
Smith, E. J., Jokipii, J. R., Kóta, J., Lepping, R. P., and Szabo, A.: 2000, *Astrophys. J.* **533**, 1084–1089.
Snyder, C. W. and Neugebauer, M.: 1963, *Solar Particles and Sun-Earth Relations. Proceedings from the 8th International Cosmic Ray Conference*, Vol. 1, p. 210.
Steenberg, C. D. and Moraal, H.: 1996, *Astrophys. J.* **463**, 776.
Steenberg, C. D. and Moraal, H.: 1999, *J. Geophys. Res.* **104**, 24879–24884.
Stone, E. C., Cummings, A. C., McDonald, F. B., Heikkila, B. C., Lal, N., and Webber, W. R.: 2005, *Science* **309**, 2017–2020.
Strong, A. W., Moskalenko, I. V., and Reimer, O.: 2000, *Astrophys. J.* **541**, 1109–1109.
Struminsky, A., Heber, B., Kallenrode, M., Müller-Mellin, R., Klassen, A., and Kunow, H.: 2005, *Adv. Space Res.* in press.
Teegarden, B. J., McDonald, F., Trainor, J. H., Webber, W. R., and Roelof, E.: 1974, *J. Geophys. Res.* **79**, 3615–3622.
Teegarden, B. J., McDonald, F. B., Trainor, J. H., Roelof, E. C., and Webber, W. R.: 1973, *Astrophys. J.* **185**, L155.
Thomas, B. T. and Smith, E. J.: 1981, *J. Geophys. Res.* **86**(15), 11105–11110.
Trattner, K. J., Marsden, R. G., Bothmer, V., Sanderson, T. R., Wenzel, K.-P., Klecker, B., *et al.*: 1995, *Geophys. Res. Lett.* **22**, 3349–3352.
Trattner, K. J., Marsden, R. G., Bothmer, V., Sanderson, T. R., Wenzel, K.-P., Klecker, B., *et al.*: 1996, *Astron. Astrophys.* **316**, 519–527.
Trattner, K. J., Marsden, R. G., and Sanderson, T. R.: 1997, *Geophys. Res. Lett.* **24**, 1719–1722.
Van Allen, J. A. (ed.): 1998, *Cosmic Rays, the Sun and Geomagnetism: The Works of Scott E. Forbush*. American Geophys. Union.
Vasyliunas, V. M. and Siscoe, G. L.: 1976, *J. Geophys. Res.* **81**, 1247–1252.
Washimi, H. and Tanaka, T.: 1996, *Space Sci. Rev.* **78**, 85–94.
Webber, W. R. and Lockwood, J. A.: 1999, *J. Geophys. Res.* **104**, 2487–2498.
Wimmer-Schweingruber, R. F., Von Steiger, R., and Paerli, R.: 1997, *J. Geophys. Res.* **102**, 117407.
Witte, M., Rosenbauer, H., Banaszkiewicz, M., and Fahr, H.: 1993, *Adv. Space Res.* **13**, 121–130.
Zank, G. P.: 1999, *Space Sci. Rev.* **89**, 413–688.
Zank, G. P. and Müller, H.-R.: 2003, *J. Geophys. Res. (Space Phys.)* (A6), 7.
Zank, G. P. and Pauls, H. L.: 1996, *Space Sci. Rev.* **78**, 95–106.

Zhang, M.: 1997, *Astrophys. J.* **488**, 841.
Zhang, M.: 1999, *Astrophys. J.* **513**, 409–420.
Zhang, M. and McDonald, F. B.: 2001, in *Proceedings of the 27th ICRC*, p. 3902.
Zurbuchen, T. H., Schwadron, N. A., and Fisk, L. A.: 1997, *J. Geophys. Res.* **102**(11), 24175–24182.